https://doi.org/10.5194/egusphere-2026-2450
Preprint. Discussion started: 26 June 2026

Aerobic and anaerobic contributions to carbon dioxide and methane emissions in a 1D peatland model: Peatland-VU v3.0

Tan J.R. Lippmann[1,2], Jacobus van Huissteden[2], Ype van der Velde[2], Veronique E. N. Boon[2], and Merit van den Berg[2,3]

[1]Earth Systems and Global Change Group, Wageningen University, 6708 PB Wageningen, the Netherlands
[2]Department of Earth Sciences, VU Amsterdam, Boelelaan 1085, 1081 HV Amsterdam, the Netherlands
[3]UK Centre for Ecology and Hydrology, Wallingford, United Kingdom

Correspondence: Tan J.R. Lippmann (tan.lippmann@wur.nl)

Abstract. Accurate modelling of peatland carbon dynamics is essential for understanding their role in the global carbon cycle and predicting greenhouse gas (GHG) fluxes under changing environmental and management conditions. We present Peatland-VU v3.0, an updated 1D process-based model with new representations of key above- and below-ground processes controlling peatland carbon exchange. Developments include improved vegetation phenology (leaf area index and growing degree days), alternative formulations for the temperature sensitivity of soil organic matter (SOM) decomposition, and explicit representation of anaerobic SOM mineralisation.

Model behaviour and sensitivity were evaluated at two contrasting peatland sites in the Netherlands: a restored fen marshland (the Weerribben site) and a drained peat pasture (the Assendelft site) where model performance was evaluated against in situ flux measurements. Using ensembles of targeted perturbation experiments, we quantified sensitivity to internal parameters and environmental drivers and identified the processes and parameters that most strongly control variability in simulated CO_2 and CH_4 fluxes across contrasting peatland types. Beyond presenting new developments, this study provides a complete and consolidated sensitivity assessment of all processes and modules, not only newly implemented processes. The comprehensive evaluation provides a clear reference for future model developments, parametrisation and application to new sites.

1 Introduction

Peatlands play a critical role in the global carbon cycle. Despite covering less than 3% of the global land surface (Xu et al., 2018), peatlands store approximately 25% of the planet's soil carbon (Yu et al., 2010), equivalent to twice the carbon stored in the world's forests (Pan et al., 2011). Peatlands functions as both a major long-term carbon sink and a potential source of carbon to the Earth's atmosphere. The stored carbon in peatlands is released primarily as carbon dioxide (CO_2) and methane (CH_4), the two most abundant anthropogenic greenhouse gases (GHG).

Peatland management plays a critical role in the mitigation of climate change because peatland drainage, due to the intensification of agriculture, leads to enhanced CO_2 and N_2O emissions (Hu et al., 2017). On the other hand, reflooded peatlands, for the purposes of restoration, can lead to elevated CH_4 emissions (Hemes et al., 2018). With approximately 20% of European peatlands currently threatened by climate change and drainage (van der Velde et al., 2021), careful management of both drained

https://doi.org/10.5194/egusphere-2026-2450
Preprint. Discussion started: 26 June 2026

and natural systems is critical to prevent additional carbon releases to the atmosphere and mitigate climate warming (Loisel et al., 2021).

The development of process based models is a critical step towards introducing peatland carbon dynamics into both global land surface and Earth System Models (Loisel et al., 2021) where peatlands are not yet typically represented (Helbig et al., 2020). However, peatlands are not yet included in the Coupled Model Intercomparison Project (CMIP) version of any global land surface model which is testimony to the obstacles that must be overcome for accurate representation of peatland carbon cycle processes (Apers et al., 2022). Lack of peatland representation contributes to inaccurate estimates of organic soil mass and CH_4 emissions (Loisel et al., 2021). The increasing complexity and computational cost of global models limits rapid process development and testing (Fisher and Koven, 2020). Plot-scale models are accompanied by minimal computing requirements, and by reducing confounding geospatial feedbacks by focusing on individual sites, model development and testing of small scale processes can be expedited (Nungesser, 2003; Metzger et al., 2016; Raivonen et al., 2015; Clymo et al., 1998; Silva et al., 2024). Whilst the role of plot-scale models is often overlooked in the land surface modelling community, development and representation of peatland dynamics in plot-scale process-based models remains a powerful catalyst to the development of all types of peatland models. Estimating peatland carbon fluxes using process-based models is a critical step towards improved projections of future climate change (Silva et al., 2024).

The Peatland-VU model is plot-scale process-based model developed to simulate CO_2 and CH_4 fluxes as functions of site-specific environmental drivers, including water table position, soil and air temperature, and vegetation type (van Huissteden et al., 2006; Mi et al., 2014). Various versions of the model have been described, and applied in several studies across the temperate, boreal, and arctic region (Hendriks et al., 2007; Petrescu et al., 2008; van Huissteden et al., 2009; Petrescu et al., 2010; Budishchev et al., 2014; Mi et al., 2014; Lippmann et al., 2023). Early versions of the model paid particular attention to the representation of below-ground biogeochemistry using seven soil organic matter (SOM) pools to represent peat, humus, microbial biomass, litter and dead roots, root exudates, liquid manure, and solid manure, each vertically distributed across soil layers. Vegetation is represented in the model as a driver of both carbon inputs, plays a central role in below-ground carbon storage and soil-atmosphere carbon exchange. In this study, we present Peatland-VU v3.0, which introduces new representations of key above- and below-ground processes governing peatland carbon dynamics.

Peatland-VU v3.0 includes new representations of key plant physiological processes, including leaf area index (LAI), growing degree days (GDD), and leaf senescence. Below-ground dynamics are enhanced through the addition of temperature-sensitive Q10 SOM decomposition, explicit representation of anaerobic mineralisation in saturated soil layers, allowing improved representation of vertical respiration dynamics, and management-related disturbances such as biomass harvest. Two new harvest pools have been introduced to estimate emissions from fast- and slow-decomposing harvested biomass. The aim of this study is to describe new model developments, evaluate the new model at two peatland sites, and assess the sensitivity of both new and existing model functions.

https://doi.org/10.5194/egusphere-2026-2450
Preprint. Discussion started: 26 June 2026

2 Peatland-VU model

This study is structured as follows: (1) a brief outline of the model history and structure (Table 1 and Sect. 2), (2) a description of new developments (Sect. 3) and existing biogeochemical processes (Sect. S2), (3) validation at two peatland sites (Sect. 5.1) and (4) a comprehensive sensitivity analysis of all model modules (Sect. 5.2). The methods for model validation and sensitivity assessment are outlined in Sect. 4.

2.1 History of Peatland-VU model developments

Since the original version of the Peatland-VU model was published in 2006, considerable efforts have been made to improve the stability, functionality, and usability of the model (Table 1). The original version of the model, Peatland-VU V1.0 (van Huissteden et al., 2006) included the 7 SOM pools, SOM decomposition sensitive to environmental conditions, the CH_4 modules taken from (Walter and Heimann, 2000), where CO_2 and CH_4 were the primary model outputs. Further efforts were made to improve the parametrisation process and understand the sensitivity of Peatland-VU v1.0 (van Huissteden et al., 2009; Petrescu et al., 2008).

Peatland-VU v2.0 introduced two new net primary production (NPP) modules (Shaver et al., 2007; Haxeltine and Prentice, 1996) to improve the reproducibility of CH_4 emissions (Mi et al., 2014). Whilst Peatland-VU v1.0 was initially used to simulate managed peatlands (van Huissteden et al., 2006; Hendriks et al., 2007), the capacity of Peatland-VU v2.0 to simulate Arctic peatlands was tested (Budishchev et al., 2014). Efforts were made to offline couple Peatland-VU v2.0 with the global hydrological model, PCR-GLOBWB, to estimate wetland CH_4 emissions from boreal, Arctic and subarctic wetlands (Petrescu et al., 2010). Adopting dynamic Plant Functional Types (PFT) and other components of the NUCOM-bog model (Heijmans et al., 2008) into the Peatland-VU v2.0 framework, led to the development of the Peatland-VU-NUCOM (PVN) model (Lippmann et al., 2023).

2.2 Overview of model structure

The Peatland-VU model is designed to simulate both pristine and managed peatlands. The Peatland-VU model simulates photosynthesis, autotrophic respiration, above- and below-ground biomass, basic plant phenology, SOM decomposition, and CH_4 production, oxidation, and transport. Each timestep, the model follows the following production and decomposition processes. There are two possible available modules to estimate gross primary production (GPP), plant autotrophic respiration, and NPP - adapted from either Shaver et al. (2007) or the BIOME3 model (Haxeltine and Prentice, 1996). After above- and below-ground growth is calculated, SOM accumulation and decomposition occurs. Finally, CH_4 production, oxidation and transport take place. The primary model outputs are net ecosystem exchange (NEE), GPP, plant and heterotrophic respiration, and CH_4 fluxes between the land surface and the atmosphere.

The Peatland-VU model is a site specific model which means that climate (Table A1), land management (Table A2), and soil (Table A3) forcing inputs must be prepared for each site simulation.

https://doi.org/10.5194/egusphere-2026-2450
Preprint. Discussion started: 26 June 2026

Table 1. Peatland-VU model functionality and development.

Process	PV v1.0 (van Huissteden et al., 2006)	PV v2.0 (Mi et al., 2014)	PVN (Lippmann et al., 2023)	PV v3.0 (this publication)
Photosynthesis	1. Sinusoidal seasonal, 2. cloudiness	1. Sinusoidal seasonal, 2. cloudiness, 3. Shaver, 4. BIOME3	Shaver and BIOME3 dependent on PFT traits	As in PV v2.0 but with harvest correction
Autotrophic respiration	Ratio of GPP	Shaver or BIOME3, or ratio of GPP	Shaver or BIOME3, dependent on PFT traits	As in PV v2.0
Phenology	Prescribed day of year	As in PV v1.0	As in PV v1.0	GDD function modified
LAI	-	Constant for evergreen, function of GDD for deciduous	Function of SLA and aboveground biomass, dependent on PFT traits	GDD function modified
Allocation	Above- and below-ground biomass as prescribed ratio of NPP	As in PV v1.0	As in PV v1.0, dependent on PFT traits	As in PV v1.0
Plant functional Types	-	-	Short and tall grasses, *Sphagnum*, brown mosses, *Typha*, sedges	-
Dynamic vegetation	-	-	Competition as function of shading, air temperature and water level	-
Soil temperature	1. Simple sinusoidal, 2. classical heat transport as a function of TA	as in PV v1.0	as in PV v1.0	1. Simple sinusoidal, 2. classical heat transport, 3. analytical heat diffusion as a function of surface TA or TS
Water table	1. Time series input, 2. function of precipitation and evapotranspiration	As in PV v1.0	As in PV v1.0	As in PV v1.0
Harvest	Prescribed day of year, biomass fraction	As in PV v1.0	Prescribed day of year & harvest height	Prescribed calendar dates & biomass fractions. Decomposition of fast and slow harvest pools
Grazing	Prescribed days of year, biomass removed, manure added	As in PV v1.0	As in PV v1.0	As in PV v1.0
Manure	Prescribed days of year, manure added	As in PV v1.0	As in PV v1.0	As in PV v1.0

https://doi.org/10.5194/egusphere-2026-2450
Preprint. Discussion started: 26 June 2026

Table 1. Table 1 continued.

Process	PV v1.0 (van Huissteden et al., 2006)	PV v2.0 (Mi et al., 2014)	PVN (Lippmann et al., 2023)	PV v3.0 (this publication)
Biomass senescence	Prescribed seasonal ratio of biomass	As in PV v1.0	As in PV v1.0, dependent on PFT traits	As in PV v1.0
Peat surface height	-	-	Function of moss density	-
Heterotrophic respiration	Litter, aerobic decomposition, methanogenesis	As in PV v1.0	As in PV v1.0	Litter, aerobic and anaerobic decomposition, methanogenesis
Litter decomposition	Function of Arrhenius temperature	As in PV v1.0	As in PV v1.0, dependent on PFT traits	Function of Arrhenius or Q10 temperature
Root senescence	Ratio of root mass	As in PV v1.0	As in PV v1.0, dependent on PFT traits	As in PV v1.0
SOM pools	Peat, humus, root and litter mass, root exudates, microbial biomass, manure solids and liquids	As in PV v1.0	SOM pools in PV v1.0 allocated to each PFT	As in PV v1.0
Temperature sensitivity of R_h	Arrhenius temperature function of total SOM pool	As in PV v1.0	As in PV v1.0	Function of Q10 or Arrhenius, per SOM pool
Aerobic SOM decomposition	Function of decomposition constant, temperature, pH, priming, soil moisture age, C/N ratio	As in PV v1.0	As in PV v1.0	As in PV v1.0 with modified C/N sensitivity
Anaerobic SOM decomposition	-	-	-	Function of Arrhenius or Q10
Methane	Production, oxidation, diffusion, ebullition, plant transport	As in PV v1.0	As in PV v1.0, plant transport dependent on PFT traits	As in PV v1.0 and also aceticlastic vs hydrogenotrophic methanogenesis parameterisation
Carbon mass balance check	-	-	-	Daily check

https://doi.org/10.5194/egusphere-2026-2450
Preprint. Discussion started: 26 June 2026

3 Model developments

We begin by introducing the model's complete carbon budget. The terms included in the carbon budget provide an overview of the biophysical and biochemical processes represented within the model and therefore, whilst introducing the model's carbon budget, we also take the opportunity to outline the recent model developments introduced in Peatland-VU v3.0 (Table 1). All variables for NEE, LAI, and GDD modules are defined in Table 2. The carbon budget is the balance between the carbon change in the carbon pools (left) and the carbon fluxes entering or leaving the system (right):

$$\frac{\Delta\left(M_{\mathrm{plant}}(t)+M_{\mathrm{lit}}(t)+M_{\mathrm{som}}(t)+M_{\mathrm{harv}}(t)\right)}{\Delta t}=NEE_{\mathrm{CO_2}}(t)+NEE_{\mathrm{CH_4}}(t)+F^{\mathrm{harv}}(t) \tag{1}$$

Where M_{plant} [kg C m^{-2}], M_{lit} [kg C m^{-2}], and M_{som} [kg C m^{-2}] represent the mass of the above- and below-ground living biomass, litter, and SOM at time, t. M_{harv} [kg C m^{-2}] represents the harvested biomass. $\mathrm{NEE_{CO_2}}$ [kg C m^{-2} day^{-1}] and $\mathrm{NEE_{CH_4}}$ [kg C m^{-2} day^{-1}] represent the net ecosystem exchange of CO_2 and CH_4 at the surface. F^{harv} [kg C m^{-2} day^{-1}] represents the offsite decomposition of harvested biomass.

3.1 Net Ecosystem Exchange

$\mathrm{NEE_{CO_2}}$ is defined as the balance of CO_2 uptake by gross primary production (GPP), and CO_2 release by ecosystem respiration (RECO):

$$\mathrm{NEE_{CO_2}}(t)=\mathrm{GPP}(t)-\mathrm{RECO}(t) \tag{2}$$

$$\mathrm{RECO}(t)=R_{\mathrm{a}}(t)+R_{\mathrm{h}}(t) \tag{3}$$

$$R_{\mathrm{h}}(t)=R_{\mathrm{lit}}(t)+\sum_{z=1}^{Z}\left(R_{\mathrm{h}}^{\mathrm{ae}}(t,z)+R_{\mathrm{h}}^{\mathrm{an}}(t,z)+R_{\mathrm{ox}}(t,z)+R_{\mathrm{ac}}(t,z)\right) \tag{4}$$

In Eq. 2, GPP [kg C m^{-2} day^{-1}] denotes gross primary production, while RECO [kg C m^{-2} day^{-1}] is the total ecosystem respiration. RECO is composed of both R_{a} [kg C m^{-2} day^{-1}], autotrophic (plant) respiration, and R_{h} [kg C m^{-2} day^{-1}], heterotrophic (soil and litter) respiration. The heterotrophic component is comprised of the CO_2 produced by litter decomposition (R_{lit} [kg C m^{-2} day^{-1}]), aerobic SOM decomposition ($R_{\mathrm{h}}^{\mathrm{ae}}$ [kg C m^{-2} day^{-1}]), anaerobic SOM decomposition ($R_{\mathrm{h}}^{\mathrm{an}}$ [kg C m^{-2} day^{-1}]), the CO_2 production associated with CH_4 oxidation (R_{ox} [kg C m^{-2} day^{-1}]), and the CO_2 production associated with acetoclastic methanogenesisis (R_{ac} [kg C m^{-2} day^{-1}]), at depth z.

Relative to previous versions, Peatland-VU v3.0 now includes several updates to processes contributing to $\mathrm{NEE_{CO_2}}$. In Peatland-VU v3.0, GPP has been modified to mimic plant stress following harvest events where LAI is now simultaneously reduced (Sect. 3.3). LAI (Sect. 3.5) and GDD (Sect. 3.4) have also both been further improved. Heterotrophic respiration now includes contributions from both aerobic and anaerobic SOM decomposition (Sect. 3.6), where decomposition is estimated using either Arrhenius or Q10 temperature dependencies (Sect. 3.6.3). Methane-related CO_2 production now accounts for both methanotrophy and acetoclastic methanogenesis, with explicit partitioning between acetoclastic and hydrogenotrophic pathways (Sect. 3.7).

https://doi.org/10.5194/egusphere-2026-2450
Preprint. Discussion started: 26 June 2026

3.2 Photosynthesis and autotrophic respiration

Here we describe the two modules that can be used to estimate NPP, GPP and autotrophic respiration in Peatland-VU v3.0 (Shaver et al., 2007; Haxeltine and Prentice, 1996). In the NPP module adapted from the BIOME3 model (Haxeltine and Prentice, 1996), the amount of carbon fixation is influenced by the quantity of photosynthetically active radiation (PAR) captured by the plant as mediated by stomatal conductance (Sect. SB1).The BIOME3 module provides a mechanistic representation of C3 photosynthesis in which gross primary production (GPP) and leaf respiration are linked to the activity of Rubisco and other photosynthetic enzymes within the chloroplast. Previous applications and evaluations of BIOME3 have focused predominantly on forest ecosystems. In contrast, peatland vegetation is highly heterogeneous and often contains a large proportion of non-vascular species, including *Sphagnum* and other brown mosses, which differ substantially from the vegetation types for which the model was originally developed and tested. For this reason, the Peatland-VU model also includes an NPP module which was originally developed and tested on Arctic tundra ecosystems (hereafter the Shaver model) adapted from Shaver et al. (2007). NPP is calculated as:

$$\mathrm{NPP}(t) = \mathrm{GPP}(t) - R_{\mathrm{a}}(t) \tag{5}$$

where GPP and R_{a} can be calculated using either the Shaver or BIOME3 module. In the Shaver module, GPP is a function of PAR, and LAI:

$$\mathrm{GPP}(t) = \frac{P_{\mathrm{maxL}}}{Kb} \cdot \ln\left(\frac{P_{\mathrm{maxL}} + \mathrm{PAR}(t) \cdot E_0}{P_{\mathrm{maxL}} + \mathrm{PAR}(t) \cdot E_0 \cdot e^{-Kb \cdot \mathrm{LAI}(t)}}\right) \tag{6}$$

where P_{maxL} [μ mol m^{-2} leaf day^{-1}] represents the light-saturated photosynthetic rate per unit leaf area, Kb [m^2 ground m^{-2} leaf^{-1}] represents the Beer-Lambert light extinction coefficient, $E0$ [μ mol CO_2 μ mol^{-1} photons] represents the initial slope of the light response curve, and PAR [μ mol photons m^{-2} ground day^{-1}] represents photosynthetically active radiation at the top of the canopy. LAI [m^2 m^{-2}] represents leaf area index of the entire canopy.

In the autotrophic respiration module adapted from Shaver et al. (2007), temperature and LAI are the dominant drivers of autotrophic respiration.

$$R_{\mathrm{a}}(t) = R_0 \cdot \mathrm{LAI}(t) \cdot e^{\beta \cdot \mathrm{TA}(t)} \tag{7}$$

where, R_0 [μ mol m^{-2} leaf day^{-1}] represents the amount of leaf respiration at 0°C, β [°C] is a temperature sensitivity factor for autotrophic respiration, and TA [°C] represents daily air temperature. In the adapted BIOME3 module, autotrophic respiration is dependent on leaf growth and maintenance respiration coefficients and the maximum daily rate of net photosynthesis (Sect. SB1). After NPP is calculated, the allocation of root and shoot growth is calculated and above- and below-ground growth occurs (Sect. SB2 and Sect. SB3).

https://doi.org/10.5194/egusphere-2026-2450
Preprint. Discussion started: 26 June 2026

Table 2. Variable descriptions for NEE, NPP, and phenology modules and labels used in sensitivity testing, if applicable.

Module	Symbol in text	Sensitivity testing	Unit	Description
NEE	NEE_{CO_2}	-	kg C m^{-2} day^{-1}	Net ecosystem exchange
	GPP	GPP	kg C m^{-2} day^{-1}	Gross primary productivity
	R_a	Ra	kg C m^{-2} day^{-1}	Autotrophic respiration
	R_h	R_h	kg C m^{-2} day^{-1}	Total heterotrophic respiration
	R_h^{ae}	-	kg C m^{-2} day^{-1}	CO_2 production from aerobic SOM decomposition per soil layer
	R_h^{an}	-	kg C m^{-2} day^{-1}	CO_2 production from anaerobic SOM decomposition per soil layer
	R_{ac}	-	kg C m^{-2} day^{-1}	CO_2 produced during acetoclastic methanogenesis
	R_{ox}	-	kg C m^{-2} day^{-1}	CO_2 produced during methanotrophic mineralisation
	R_{lit}	-	kg C m^{-2} day^{-1}	CO_2 production from litter decomposition
NPP	NPP	-	kg C m^{-2} day^{-1}	Net primary production
	P_{maxL}	Pmax	μ mol m^{-2} leaf day^{-1}	Light-saturated photosynthetic rate per unit leaf area
	PAR	PAR	μ mol photons m^{-2} ground day^{-1}	Photosynthetically active radiation at the top of the canopy
	E_0	Pslope	μ mol CO_2 μ mol^{-1} photons	Initial slope of the light response curve
	Kb	KBeer	m^2 ground m^{-2} $leaf^{-1}$	Beer-Lambert light extinction coefficient
	LAI	LAI	m^2 m^{-2}	Leaf area index
	H_c	HarC	-	Correction factor defining the minimum photosynthetic capacity immediately after harvest
	H_d	-	days	Elapsed days since the most recent harvest event
	H_r	RecovT	days	Days required for vegetation to regain full photosynthetic capacity
	R_0	PlantResp0	μ mol m^{-2} leaf day^{-1}	Leaf respiration at 0°C
	β	RespBeta	-	Temperature sensitivity constant for leaf respiration
	TA	TA	°C	Daily air temperature
Phenology	GDD	-	°C	Growing degree days (GDD)
	TA_b	BaseT	°C	GDD base temperature
	GDD_{max}	GDD_max	°C	Maximum GDD
	t_a	AutumnStart	day of year	Start of autumn
	t_{gs}	GS_start	day of year	Start of the growing season
	SF	ShootsFactor	-	Fraction of NPP allocated to above-ground biomass
	LAI_{max}	LAI_max	m^2 m^{-2}	maximum LAI
	LAI_{min}	LAI_min	m^2 m^{-2}	minimum LAI
	ΔLAI_{NPP}	-	m^2 m^{-2}	Change in LAI due to NPP
	LAI_{GDD}	-	m^2 m^{-2}	Potential LAI due to GDD
	LAI_c	LAICarbonFraction	kg C m^{-2} leaf	LAI to carbon biomass constant

https://doi.org/10.5194/egusphere-2026-2450
Preprint. Discussion started: 26 June 2026

3.3 Stress due to harvest

To account for the physiological effects of cutting on vegetation, the model applies a temporary reduction in photosynthetic capacity after harvest, which is particularly relevant for agricultural and other managed peatlands (Knox et al., 2015; Evans et al., 2021). Harvest events can be prescribed either by fixed dates (Lippmann et al., 2023) or by day-of-year values (van Huissteden et al., 2006). At each event, above-ground biomass is reduced according to the user-defined harvest fraction. When the harvest scheme is activated, vegetation is harvested (mowed) either on the prescribed date or according to the specified day-of-year values modified from Lippmann et al. (2023) and (van Huissteden et al., 2006). Above-ground biomass is removed from the above-ground biomass pool according to the specified harvest fraction. Following a harvest event, removed biomass is partitioned between fast- and slow-decomposing pools using a prescribed fraction. Following harvest, LAI is recalculated, and a fraction of the harvested biomass is assumed to remain uncollected in the field and is added to the litter layer. After harvest, photosynthetic capacity is temporarily reduced:

$$\mathrm{GPP}(t) = \mathrm{GPP}(t) \cdot \left(H_\mathrm{c} + \frac{H_\mathrm{d}(t) \cdot (1 - H_\mathrm{c})}{H_\mathrm{r}} \right) \tag{8}$$

where, H_c [-] is the harvest reduction factor of photosynthetic capacity immediately after harvest, H_r [days] is the number of days required for vegetation to regain full photosynthetic capacity, and H_d [days] is the number of elapsed days since the most recent harvest event.

3.4 Phenology and growing degree days

Seasonal changes in biomass production and leaf area development are important drivers of carbon fluxes (Köster et al., 2023; Campioli et al., 2015). During the growing season, a constant turnover of biomass is calculated, representing senescence due to age or damage (Sect. SB4). Phenology in Peatland-VU controls the seasonal development of LAI which regulates GPP, R_a, and the capacity of plant-mediated CH_4 transport. In Peatland-VU, the phenological driver referred to as growing degree days (GDD) functions as a seasonally bounded thermal state variable. Unlike classical GDD formulations, which accumulate only positive temperature deviations, this implementation allows thermal forcing to both increase and decrease depending on seasonal context. During the growing season, positive temperature deviations promote thermal accumulation and leaf development. Whereas during autumn, GDD declines under negative thermal forcing, allowing cold periods to accelerate senescence while warm autumn conditions may delay it. This bidirectional formulation provides a simple empirical representation of temperature-driven leaf expansion and decay that is consistent with grassland and tundra phenology schemes (Höglind et al., 2016).

Peatland-VU v3.0 distinguishes between two phenological strategies: evergreen and summergreen vegetation. Evergreen vegetation (e.g. mosses such as *Sphagnum* and trees such as pine or spruce) maintains a constant LAI throughout the year. Summergreen vegetation, such as grasses (e.g. $Pragmites$, $Loliumperenne$) or shrubs (e.g. $Betulanana$), grow leaves during the growing season and undergo leaf senescence during autumn and winter.

https://doi.org/10.5194/egusphere-2026-2450
Preprint. Discussion started: 26 June 2026

For summergreen vegetation, GDD are calculated as:

$$\mathrm{GDD}(t) = \begin{cases} 0 & \text{if } \mathrm{DOY}(t) = t_{\mathrm{gs}}, \\ \mathrm{GDD}(t-1) + \Delta\mathrm{GDD}(t) & \text{if growing season and } \Delta\mathrm{GDD}(t) > 0, \\ \mathrm{GDD}_{\max} & \text{if } \mathrm{DOY}(t) = t_{\mathrm{a}}, \\ \max(\mathrm{GDD}(t-1) + \Delta\mathrm{GDD}(t), 0) & \text{if autumn and } \Delta\mathrm{GDD}(t) < 0, \\ \mathrm{GDD}(t-1), & \text{otherwise.} \end{cases} \tag{9}$$

Where

$$\Delta\mathrm{GDD}(t) = \Delta t \left(\mathrm{TA}(t) - \mathrm{TA}_b\right) \tag{10}$$

Where t_{gs} is the start of the growing season and t_{a} the start of autumn. The growing season is defined as $t_{\mathrm{gs}} \leq \mathrm{DOY}(t) < t_{\mathrm{a}}$. The autumn period is defined as $\mathrm{DOY}(t) \geq t_{\mathrm{a}}$ or $\mathrm{DOY}(t) < t_{\mathrm{gs}}$. GDD [°C] represents the cumulative growing degree days. TA_b [°C] is the base temperature below which no thermal accumulation occurs. The daily thermal increment $\Delta\mathrm{GDD}(t)$ is calculated as the temperature surplus above the base temperature.

At the start of the growing season ($\mathrm{DOY}(t) = t_{\mathrm{gs}}$), GDD is reset to zero. During the growing season, GDD increases if $\Delta\mathrm{GDD}(t) > 0$, and otherwise remains unchanged.

At the onset of autumn ($\mathrm{DOY}(t) = t_{\mathrm{a}}$), GDD is set to $\mathrm{GDD}_{\max}$. During autumn, GDD may decrease when $\Delta\mathrm{GDD}(t) < 0$, representing cooling conditions and progression of senescence. If $\Delta\mathrm{GDD}(t) > 0$, GDD remains unchanged, and further senescence is delayed. Leaf senescence is therefore driven by declining GDD during the autumn period, while warm conditions during autumn can temporarily halt the progression of senescence.

3.5 Leaf Area Index

Leaf area index is an important indication of the biophysical state of vegetation because leaf surface area affects both the absorption of atmospheric carbon through photosynthesis and the emission of water into the atmosphere via transpiration (Raivonen et al., 2015; Kala et al., 2014). In the model, LAI impacts the amount of R_{a}, GPP, plant-transported CH_4, and leaf senescence. Senescence of the above-ground living biomass is added to the litter layer (Sect. SB5). In Peatland-VU, LAI development is controlled by two competing processes: temperature-driven phenological progression and limitation of foliage growth due to carbon availability. At each time-step, the dominant process determines the increase in LAI. This concept is based on the LINGRA and BASGRA grassland models (Schapendonk et al., 1998; Höglind et al., 2016) with the reasoning that leaf growth is driven by either temperature or carbon availability.

https://doi.org/10.5194/egusphere-2026-2450
Preprint. Discussion started: 26 June 2026

LAI is calculated as:

$$\mathrm{LAI}(t) = \begin{cases} \mathrm{LAI}_{\min}, & \text{if } DOY(t) = t_{gs} \\ \min\left(\mathrm{LAI}(t-1) + \Delta\mathrm{LAI}_{\mathrm{NPP}}(t), \mathrm{LAI}_{\max}\right) & \text{if } \mathrm{LAI}(t-1) < \mathrm{LAI}_{\mathrm{GDD}}(t-1) \\ & \text{or if } \Delta\mathrm{LAI}_{\mathrm{GDD}}(t) < \Delta\mathrm{LAI}_{\mathrm{NPP}}(t) \\ \mathrm{LAI}_{\mathrm{GDD}}(t), & \text{otherwise} \end{cases} \tag{11}$$

where, $\mathrm{LAI}_{\max}$ [$\mathrm{m}^2\ \mathrm{m}^{-2}$] and $\mathrm{LAI}_{\min}$ [$\mathrm{m}^2\ \mathrm{m}^{-2}$] represent the maximum and minimum LAI, respectively. $\Delta\mathrm{LAI}_{\mathrm{NPP}}$ [$\mathrm{m}^2\ \mathrm{m}^{-2}$] represents the incremental increase in LAI due to NPP, $\mathrm{LAI}_{\mathrm{GDD}}$ [$\mathrm{m}^2\ \mathrm{m}^{-2}$] represents the thermally driven LAI estimate. In the case that LAI is driven by temperature change, $\mathrm{LAI}_{\mathrm{GDD}}$ [$\mathrm{m}^2\ \mathrm{m}^{-2}$], varies according to GDD:

$$\mathrm{LAI}_{\mathrm{GDD}}(t) = \begin{cases} \mathrm{LAI}_{\max}, & \text{if } \mathrm{GDD}(t) > \mathrm{GDD}_{\max} \\ \mathrm{LAI}_{\min} + (\mathrm{LAI}_{\max} - \mathrm{LAI}_{\min}) \cdot \frac{\mathrm{GDD}(t)}{\mathrm{GDD}_{\max}}, & \text{otherwise.} \end{cases} \tag{12}$$

$$\Delta\mathrm{LAI}_{\mathrm{GDD}}(t) = \mathrm{LAI}_{\mathrm{GDD}}(t) - \mathrm{LAI}_{\mathrm{GDD}}(t-1) \tag{13}$$

In the case that LAI is limited by carbon availability, $\Delta\mathrm{LAI}_{\mathrm{NPP}}$ is calculated:

$$\Delta\mathrm{LAI}_{\mathrm{NPP}}(t) = \frac{\mathrm{NPP}(t) \cdot SF}{\mathrm{LAI}_C} \tag{14}$$

$$\tag{15}$$

where, SF [-] represents the above to belowground growth ratio, and LAI_C [kg C m^{-2} leaf] represents a LAI to carbon constant. This approach differs from formulations that prescribe LAI directly as a function of temperature or biomass alone, but provides a flexible representation of phenological and productivity controls on canopy development.

3.6 SOM decomposition

In drained peatlands, exposure of previously saturated organic matter to aerobic conditions enhances decomposition and heterotrophic respiration, whereas in saturated systems the extent of aerobic decomposition is reduced. Across both drained and saturated peatlands, SOM comprises compounds at different stages of decomposition.

In Peatland-VU v3.0, the pH, soil aeration, soil moisture, and NPP priming sensitivity corrections remain consistent with Peatland-VU v1.0 (van Huissteden et al., 2006). New developments include flexible C/N sensitivity, an alternative Q10 temperature sensitivity formulation, and explicit representation of anaerobic SOM decomposition. The mass of each SOM pool is updated dynamically throughout the simulation, while the number of soil layers and their thicknesses remain fixed. During decomposition, organic carbon is mineralised and may subsequently be transferred among pools and recycled within the soil system (Basile-Doelsch et al., 2020). As a result, turnover rates differ substantially between pools, with microbial biomass, litter, dead roots, and root exudates decomposing relatively rapidly, whereas humus and peat are characterised by much slower

https://doi.org/10.5194/egusphere-2026-2450
Preprint. Discussion started: 26 June 2026

turnover. Carbon fluxes associated with SOM decomposition are mass-conserving across all SOM pools. All variables associated with the SOM decomposition modules are defined in Table 3.

The CO_2 lost through SOM decomposition is calculated as:

$$R_h^{\mathrm{ae}}(t) = \sum_z \sum_s \left(D_{\mathrm{ae}}(t,z,s) - T_{ae}^{\mathrm{microb}} - T_{ae}^{\mathrm{humus}} \right) \tag{16}$$

$$R_h^{\mathrm{an}}(t) = \sum_z \sum_s \left(D_{\mathrm{an}}(t,z,s) - T_{an}^{\mathrm{microb}} - T_{an}^{\mathrm{humus}} \right) \tag{17}$$

where

$$D_x(t,z,s) = \lambda_x(t,z)\, M(t,z,s) \left(1 - e^{-ke_x(t,z,s)}\right) \tag{18}$$

where $x \in \{\mathrm{ae}, \mathrm{an}\}$. D is the carbon lost from the decomposition of each SOM pool (s) in soil layer z. λ_{ae} [-] represents the fraction of the layer above the water table and λ_{an} [-] represents the fraction of the layer below the water table. M is the carbon mass of SOM pool s at timestep t and soil layer z. ke_x is the environmental adjusted decomposition rate constant. T^{microb} [kg C m^{-2} day^{-1}] and T^{humus} [kg C m^{-2} day^{-1}] represents the carbon mineralised and reincorporated into microbial biomass and humus SOM pools, respectively.

During decomposition,, carbon originating from the decomposition of litter and dead roots, root exudates, and peat is redistributed to the microbial biomass and humus pools as follows:

$$T_x^{microb}(t,z,s) = \frac{D_x(t,z,s)}{1 + ad_x} \tag{19}$$

$$T_x^{humus}(t,z,s) = ah \cdot D_x(t,z,s) \tag{20}$$

where, ad_{ae} [-] and ad_{an} represents the constants used to calculate the fractions of decomposed SOM to be transferred to the microbial SOM pool in aerobic and anaerobic conditions, respectively. ah represents fraction of decomposed SOM that is transferred to the humus SOM pool.

The environmentally adjusted aerobic SOM decomposition rate constants are estimated:

$$ke_{ae}(t,z,s) = \frac{k_{ae}(s)}{t_{yr}} \cdot fT_{ae}(t,z,s) \cdot fp(t,z) \cdot fCN(z,s) \cdot fd(t,z) \cdot fm(t,z) \cdot fpH(z) \tag{21}$$

where, the decomposition rate constant of each SOM pool in aerobic conditions, k_{ae} [year^{-1}] are defined in Table SB1. t_{yr} [year^{-}1] represents the number of timesteps in a year. fT [-] represents the correction factor for soil temperature (Sect. 3.6.3), fp [-] represents the correction factor for priming due to the addition of fresh organic matter due to changing rates of NPP (Sect. SB5.1), fCN [-] represents the effects of changing C/N ratios on SOM decomposition (Sect. 3.6.2), fd [-] represents a correction factor for soil dryness (Sect. SB5.2), fm [-] represents a correction factor for soil moisture limitation (Sect. SB5.3), fpH [-] represents a correction factor for soil pH (Sect. SB5.4).

While surface layers are a dominant source of heterotrophic respiration due to high oxygen availability and continuous input of labile carbon, recent findings indicate that deep soil layers also produce substantial CO_2 fluxes, attributed to large,

https://doi.org/10.5194/egusphere-2026-2450
Preprint. Discussion started: 26 June 2026

active microbial communities in saturated environments (Tolunay et al., 2024; Pärn et al., 2025). Previous versions of the model have estimated CO_2 emissions derived from mineralisation in oxygenated soil layers only. In this new version of the model, anaerobic decomposition is impacted by localised soil temperatures but not other environmental factors, as in the calculation of aerobic decomposition, reflecting the limited empirical constraints on anaerobic process modifiers relative to aerobic decomposition.

Anaerobic SOM decomposition is calculated as:

$$ke_{an}(t,z,s) = \frac{k_{an}(s)}{t_{yr}} \cdot fT_{an}(t,z,s) \tag{22}$$

where, k_{an} [-] are the anaerobic SOM decomposition rate constants, and fT_{an} [-] represents the sensitivity of anaerobic SOM decomposition to changing soil temperatures. If the Q10 method is being used, fT_{an} is calculated using the Q10 relationship (Eq. 26). If the Arrhenius method is being used, fT_{an} is calculated using the Arrhenius equation (Eq. 27).

3.6.1 Decomposition of mowed or harvested biomass

Many drained peatlands are converted to croplands whilst some rewetted peatlands are being used for wet agriculture (Qiu et al., 2021). In these instances, atmospheric CO_2 is sequestered in vegetation that is harvested and removed offsite. Comparing land management efforts requires comprehensive accounting of removed biomass. Therefore, the offsite decomposition of harvested biomass pools can be calculated using first order decay principles:

$$F^{\text{harv}}(t) = F^{\text{harv}}_{\text{fast}}(t) + F^{\text{harv}}_{\text{slow}}(t) \tag{23}$$

$$F^{\text{harv}}_{i}(t) = M^{\text{harv}}_{i}(t)\left(1 - e^{-k^{\text{harv}}_{i}\Delta t}\right) \tag{24}$$

where $i \in \{\text{fast}, \text{slow}\}$. F^{harv} [kg C m^{-2} day^{-1}] is the carbon lost to the atmosphere through the decomposition of the total, fast, and slow, harvest pools respectively. M^{harv}_{i} [kg C] is the size of the harvested biomass pool, and k^{harv}_{i} [time^{-1}] is the corresponding decomposition rate constant for pool i.

3.6.2 C/N ratio sensitivity for peat decomposition

C/N ratios are a function of their input in litter and previous decomposition pathways and intensity (Moore et al., 2018; Leifeld et al., 2020) as well as agricultural input of fertilizers or the occurence of grazing. For different peat types C/N ratios differ, where the C/N ratio correlate with the potential relative decomposition rate. In previous model versions a fixed relation was used, leading to a decrease in decomposition rate constant with increasing C/N ratio based on the relation with botanic origin. In Peatland-VU v3.0, there is more flexibility in the dependency by creating limiting input parameters CN_s and CN_r:

$$fCN(z,s) = 1.0 + CN_s(s) \cdot \left(CN_r - CN(z)\right) \tag{25}$$

where, CN_r [-] refers to the reference C/N ratio, CN [-] refers to the C/N ratio, and CN_s [-] is the slope of the relative decrease. If the C/N ratio is very low or high, C/N values are constrained, $CN_{\min} \leq CN \leq CN_{\max}$.

https://doi.org/10.5194/egusphere-2026-2450
Preprint. Discussion started: 26 June 2026

Table 3. Variable descriptions for SOM decomposition module as well as labels used in sensitivity testing, if applicable.

Module	Symbol in text	Sensitivity	Unit	Description
	M	-	kg C m^{-2}	Carbon mass of each SOM pool, per layer
	D	-	kg C m^{-2} day^{-1}	Carbon lost from decomposition of each SOM pool
	T^{microb}	-	kg C m^{-2} day^{-1}	SOM transferred to the microbial SOM pool
	T^{humus}	-	kg C m^{-2} day^{-1}	SOM transferred to the humus SOM pool
	ke_{ae}	-	day^{-1}	Decomposition rate for each SOM pool, adjusted by an environmental correction factor
	ke_{an}	-	day^{-1}	Anaerobic decomposition rates considering localised soil temperatures
	ad_{ae}	DissimAssimRatio	-	Fraction of decomposed SOM transferred to microbial SOM pool in aerobic layers
	ad_{an}	AnaerobicDARatio	-	Fraction of decomposed SOM transferred to microbial SOM pool in anaerobic layers
	ah	ResistFrac	-	Fraction of decomposed SOM transferred to resistant SOM
	λ_{ae}	-	-	Fraction of soil layer above water table
	λ_{an}	-	-	Fraction of soil layer below water table
Rh	k_{ae}	Kdecay	$year^{-1}$	Aerobic decomposition rate constants
	k_{an}	KAnaerobic	$year^{-1}$	Anaerobic SOM decomposition rate constants
	fT_{ae}	-	-	Temperature correction factor for aerobic SOM decomposition
	fT_{an}	-	-	Temperature correction factor for anaerobic SOM decomposition
	fp	priming	-	Correction factor for priming due to the addition of fresh SOM
	fCN	-	-	Effects of changing C/N ratios on SOM decomposition
	fd	-	-	Correction factor for soil aeration
	fm	-	-	Correction factor for soil moisture
	fpH	-	-	Correction factor for soil pH
	t_{yr}	-	days	Convert from yearly to daily
	CN_s	KPeatCN1	-	The slope of the relative decrease
	CN_r	KPeatCN1	-	Reference C/N ratio
	CN	CNRatio	-	C/N ratio for each soil horizon
	$CNmax$	-	-	Maximum C/N ratio
	$CNmin$	-	-	Minimum C/N ratio
	$Q10_{ae}$	AerobicQ10	-	Q10 value for aerobic soil layer
	$Q10_{an}$	Q10_or_MolAct_Anaerobic	-	Q10 value for anaerobic soil layers
	TS	TS profile	°C or K	Daily soil temperature for each soil layer
	TS_r	T_ref	°C or K	Reference temperature
	Ea	MolAct	J mol^{-1}	Molecular activation energy required for the reaction in aerobic conditions
	R	-	J K^{-1} mol^{-1}	Universal gas constant
	Ea_an	Q10_or_MolAct_Anaerobic	J mol^{-1}	Molecular activation energy required for the reaction in anaerobic conditions
	F^{harv}	decomposed_harvest_fast, decomposed_harvest_slow	kg C m^{-2} day^{-1}	Carbon lost through decomposition of harvest biomass
	k^{harv}	k_harvest_fast, k_harvest_slow	$year^{-1}$	Decomposition rate constants of the slow and fast harvest pools

https://doi.org/10.5194/egusphere-2026-2450
Preprint. Discussion started: 26 June 2026

3.6.3 SOM decomposition sensitivity to temperature

Temperature sensitivity of SOM decomposition is a major source of uncertainty when modelling GHG exchange in peatlands. To reflect heterogeneity in substrate quality and microbial processes, Peatland-VU v3.0 allows temperature sensitivity to be specified independently for each SOM pool using either Q10-based or Arrhenius formulations.

Previous versions of the Peatland-VU model included an Arrhenius-based formulation for temperature dependence of decomposition processes. In this version, we introduce an alternative Q10-based approach, widely used by empirical (Bond-Lamberty and Thomson, 2010) and modelling (Huntzinger et al., 2020) studies. This enables direct comparison with a broad range of observational datasets and modelling studies.

$$fT_x(t,z,s) = Q10_x(s)^{\frac{TS(t,z)-TS_r}{10}} \tag{26}$$

where $Q10$ [-] is the prescribed Q10 value, and TS_r [°C] is the reference temperature.

If estimating the temperature sensitivity using the Arrhenius equation, we calculate the microbial activity required for aerobic SOM decomposition, dependent on soil temperature according to the Arrhenius relationship:

$$fT_x(t,z,s) = e^{\frac{Ea_x(s)}{R}\cdot\left(\frac{1}{TS(t,z)}-\frac{1}{TS_r}\right)} \tag{27}$$

Where Ea [J mol^{-1}] represents the molecular activation energy of the reaction, R [J K^{-1} mol^{-1}] represents the universal gas constant, TS_r^{arh} [K] is the reference temperature.

3.7 Methane

The processes governing net surface CH_4 emissions operate across multiple spatial and temporal scales and are influenced by hydrology, vegetation composition, and soil temperature (Knox et al., 2021). Substrate availability, air pressure, nutrient status, and snow cover can further modulate emissions depending on site-specific conditions (Knox et al., 2021; Wang et al., 2024). Changes in vegetation and climate are therefore expected to influence peatland CH_4 emissions and potentially amplify climate feedbacks (Müller and Joos, 2021).

In Peatland-VU v3.0, CH_4 production and its coupling to SOM decomposition have been revised, including an effective partitioning of methanogenic carbon between CO_2 and CH_4, representing the net outcome of acetoclastic and hydrogenotrophic pathways. Consistent with previous model versions, the concentration of CH_4 in each soil layer (Eq. 29) is dependent on the amount of plant transported CH_4 (Sect. SB6.2), CH_4 production (methanogenesis, Sect. 3.7.1), CH_4 oxidation (methanotrophy, Sect. SB6.1), ebullition (Sect. SB6.4), and diffusion (Sect. SB6.3) adapted from Walter and Heimann (2000); Walter et al. (2001).

After the calculation of the CH_4 concentration in each soil layer, the transport mechanisms are summed to obtain the CH_4 flux at the surface (variables are defined in Table 4):

$$\mathrm{NEE}_{\mathrm{CH_4}}(t) = F_{pl}(t) + F_{diff}(t,z=0) + F_{eb}(t) \tag{28}$$

https://doi.org/10.5194/egusphere-2026-2450
Preprint. Discussion started: 26 June 2026

Here, F_{pl} [μM m^{-2} day^{-1}] is the CH_4 flux transported via aerenchyma-containing vegetation, F_{diff} [μM m^{-2} day^{-1}] is the diffusive exchange at the soil/water-atmosphere interface ($z = 0$), and F_{eb} [μM m^{-2} day^{-1}] is the CH_4 flux released through ebullition.

$$\frac{\partial}{\partial t}C_{CH_4}(t,z) = R_{pr}(t,z) - Q_{pl}(t,z) - \frac{\partial}{\partial z}Q_{diff}(t,z) - Q_{eb}(t,z) - R_{ox}(t,z) \tag{29}$$

where, C_{CH_4} [μM m^{-3}] represents the CH_4 concentration. R_{pr} [μM m^{-3} day^{-1}] is the production of CH_4. Q_{pl} [μM m^{-3} day^{-1}] is the CH_4 flux by plant roots. Q_{eb} [μM m^{-3} day^{-1}] represents ebullition of CH_4. R_{ox} [μM m^{-3} day^{-1}] represents methanotrophic oxidation of CH_4. The diffusive flux, Q_{diff} [μM m^{-3} day^{-1}] is calculated using Fick's first law.

3.7.1 Methane production

Methane production in Peatland-VU occurs exclusively in anaerobic soil layers and is controlled by soil temperature and the availability of decomposable organic substrate:

$$R_C(t,z) = R_0(z)\, f_{in}(t)\, f_{TS}(t,z)\, Q10_{CH_4}^{\frac{TS(t,z)-MTS_r}{10}} \sum_{s=1}^{S} f_{org}(s) \cdot M(t,z,s) \tag{30}$$

where R_C [μM m^{-3} day^{-1}] is the total methanogenic carbon production. R_0 [day^{-1}] is a rate constant, f_{org} [-] is the fraction of organic substrate available for microbial mineralisation, f_{TS} [-] is a parameter to signal freezing (f_{TS} = 0 when $TS_z(t) <$ 0 and f_{TS} = 1, otherwise), $Q10_{CH_4}$ [-] refers to the extent that CH_4 production is dependent on soil temperature, and MTS_r [°C] refers to the reference temperature. f_{in} [-] is a lag factor that reduces production after re-saturation.

Two main pathways dominate CH_4 production in anaerobic environments: acetoclastic and hydrogenotrophic methanogenesis. Acetoclastic methanogenesis produces CH_4 and CO_2 in a 1:1 ratio from acetate ($CH_3COOH \longrightarrow CH_4 + CO_2$), whereas hydrogenotrophic methanogenesis produces CH_4 through the reduction of CO_2 ($CO_2 + 4H_2 \longrightarrow CH_4 + 2H_2O$) (Conrad, 2020). Only acetoclastic methanogenesis contributes directly to CO_2 production. Therefore, produced carbon (R_C) is split between CO_2 and CH_4:

$$R_{\mathrm{ac}}(t,z) = r_{\mathrm{CO_2:CH_4}}\, R_C(t,z), \tag{31}$$

$$R_{pr}(t,z) = \left(1 - r_{\mathrm{CO_2:CH_4}}\right) R_C(t,z). \tag{32}$$

where $r_{\mathrm{CO_2:CH_4}} \in [0,1]$ is the fraction of methanogenic carbon released as CO_2.

3.8 Soil temperature profile with time-lagged surface forcing

In previous versions of the model, soil temperature was calculated as either a seasonal sinusoidal relationship or a full thermal transport module accounting for the thermal capacity of water. Here, we introduce a new alternative module where soil temperature is estimated using an analytical approximation of heat diffusion, where the observed surface temperature (TS or TA) is prescribed as the upper boundary condition and propagated downward with depth-dependent damping and temporal lag. The

https://doi.org/10.5194/egusphere-2026-2450
Preprint. Discussion started: 26 June 2026

soil temperature profile is calculated as (variables are defined in Table 3):

$$TS(z,t) = \overline{TS} + \left(TS(t-\tau(z)) - \overline{TS}\right) \cdot e^{-\frac{z}{d_m}} \tag{33}$$

where $\overline{TS}$ [°C] is the long-term mean surface temperature, d_m [m] is the dampening depth, $\tau(z)$ [days] is the depth-dependent time lag. d_m and $\tau(z)$ are calculated by:

$$d_m = \sqrt{\frac{2\kappa}{\omega}} \tag{34}$$

$$\omega = \frac{2\pi}{t_{\mathrm{yr}}} \tag{35}$$

$$\tau(z) = \frac{z}{d_m} \cdot \frac{t_{\mathrm{yr}}}{2\pi} \tag{36}$$

where κ [m^2 day^{-1}] is the thermal diffusivity, ω [$days^{-1}$] is the angular frequency of the annual temperature cycle. The time lag is discretised to the nearest model time step. At the beginning of the simulation, where $t-\tau(z)$ precedes the available forcing data, the surface temperature from the first available time step is used.

Table 4. Variable descriptions for CH_4 and time-lagged soil temperature profile module, as well as labels used in the sensitivity testing, if applicable.

Module	Symbol in text	Sensitivity	Unit	Description
Methane	F_{pl}	Plant-transported	μM m^{-2} day^{-1}	Plant transported CH_4 flux at the surface
	F_{diff}	Diffusion	μM m^{-2} day^{-1}	Diffusive flux at the surface
	F_{eb}	Ebullition	μM m^{-2} day^{-1}	Ebullitive flux at the surface
	R_C	-	μM m^{-3} day^{-1}	Total methanogenic CH_4 production
	C_{CH_4}	-	μM m^{-3}	CH_4 concentration per soil layer
	Q_{pl}	-	μM m^{-3} day^{-1}	CH_4 transported or oxidised by plant roots
	Q_{diff}	-	μM m^{-3} day^{-1}	Diffusive flux per layer
	Q_{eb}	-	μM m^{-3} day^{-1}	CH_4 ebullition per layer
	R_{pr}	-	μM m^{-3} day^{-1}	Net CH_4 production per soil layer
	R_{ox}	-	μM m^{-3} day^{-1}	Methanotrophic oxidation of CH_4 per layer
	R_0	MethaneR0	day^{-1}	pH dependent CH_4 production constant
	f_{org}	MethaneReservoirs	-	Fraction of organic substrate available for microbial mineralisation
	f_{in}	-	-	Lag factor that reduces production after re-saturation
	$r_{CO_2:CH_4}$	-	-	Fraction of methanogenic carbon released as CO_2
	f_{TS}	-	-	Constant to indicate if $TS_z(t) \leq 0$
	$Q10_{CH_4}$	MethaneQ10	-	Q10 temperature sensitvity for CH_4 production
	MTS_r	MethaneTRef	°C	Reference temperature
TS profile	$\overline{TS}$	-	°C	Long-term mean surface temperature
	d_m	ThermDamp_lag	m	Dampening depth
	$\tau(z)$	ThermTime_lag	days	Depth-dependent time lag
	κ	-	m^2 s^{-1}	Thermal diffusivity
	ω	-	s^{-1}	Angular frequency of the annual temperature cycle

https://doi.org/10.5194/egusphere-2026-2450
Preprint. Discussion started: 26 June 2026

3.9 New model forcings

Peatland-VU v3.0 allows PAR to be prescribed directly as an input rather than calculated from global radiation as in Peatland-VU v1.0 and v2.0. It is now possible, in Peatland-VU v3.0, to provide the model with both soil (surface layer) and air temperature input (Table A1). Previously (in Peatland-VU v1.0 and v2.0), the temperature of the surface layer of the soil was assumed to be equivalent to the air temperature forcings. A thermodynamic module calculates the temperature of all soil layers derived from the surface soil temperature. While air temperature is used to drive autotrophic respiration and GDD, soil temperature is used to calculate the soil temperature profile with depth, influencing CH_4 production and SOM decomposition.

3.10 Carbon balance

In this model version, substantial efforts have been made to establish a daily accounting of the carbon mass balance to ensure that the carbon balance is closed throughout the simulation. For each time step all the carbon fluxes and carbon storage changes (in SOM pools, CH_4 and biomass) are recorded and summed. An output file is generated for this.

4 Testing the model

Here, we outline the model set-up used in this paper (Sect. 4.1.1), including the model parameterisation (Sect. 4.1.2), spin-up process (Sect. 4.1.4), the methodology used to validate the model (Sect. 4.1.3), and assess the sensitivity of the model (Sect. 4.2).

4.1 Simulating the Weerribben and Assendelft peatland sites

4.1.1 Site descriptions

We applied the model at two peatland sites in the Netherlands. The Assendelft site (52.48N, 4.74E) is a drained and managed agricultural site with fen peat soils whereas the Weerribben site (52.77N, 5.93E) is a restored fen site. We compare simulated model estimates against automatic chamber measurements at the Assendelft site (Boonman et al., 2024) and eddy covariance measurements at the Weerribben site (Buzacott et al., 2024). For extensive descriptions on the measurement processes please refer to Boonman et al. (2024) and Buzacott et al. (2024), respectively.

Both site datasets were comprised of half hourly values. As Peatland-VU operates using a daily time step, half-hourly observations were averaged to daily values, where at least 60% of the half-hourly records were available. Days not meeting this data availability threshold were treated as missing and excluded from analysis. The 60% threshold was selected after evaluating cutoffs between 50 and 80%, as stricter criteria markedly reduced usable CH_4 days with little additional gain in daily mean stability. At the Weerribben site, only 22% of days within the measurement period met the quality-control criteria for $\mathrm{NEE}_{\mathrm{CH_4}}$ fluxes, whereas $\mathrm{NEE}_{\mathrm{CO_2}}$, GPP, and RECO fluxes were available for 100% of days. At the Assendelft site, $\mathrm{NEE}_{\mathrm{CO_2}}$, GPP, and RECO were available for 85%, 85%, and 86% of days. The lower data availability for CH_4 reflects the sensitivity of

https://doi.org/10.5194/egusphere-2026-2450
Preprint. Discussion started: 26 June 2026

eddy covariance CH_4 measurements to environmental conditions, including precipitation, cloud cover, and periods of weak turbulence, which can reduce measurement quality.

Table 5. Overview of each site: latitude, longitude, peat layer depth [m], and dominant vegetation.

Site	Latitude	Longitude	Peat depth	Vegetation
Weerribben	52.8	6.0	0 - 2.3	*P. australis*, *Sphagnum spp*
Assendelft	52.5	4.7	0.3 - 2.3	Grass (*Lolium perenne*)

The Assendelft site is a drained peatland site located in Noord-Holland, the Netherlands. The top 50 cm of the site is an amorphous clay whereas the deeper layers (beyond 30 cm below the surface) are formed of reed/sedge peat. The site is exposed to livestock grazing and subsequent manure fertilisation, harvesting, and synthetic fertiliser. Approximately 250 kg N of synthetic fertiliser is applied to the site each year and approximately 14 tonne dry weight of biomass is harvested per hectare per year. Synthetic fertiliser was applied to the site, however this is not accounted for in the model.

The Weerribben site is a Natura2000 restored peatland site in the Province Overijssel, the Netherlands. A great amount of peat was mined from the site in the period 800 to 1950 and as a relic of the mining, a large amount of surface height variation remains. Whilst parts of the site were protected as nature conservation areas from the 1930's, the Weerribben site, as it is known today, was established as a protected nature reserve in 1992. The site is now one of the largest fen marshlands in Western Europe hosting a substantial *Sphagnum* community (Faber et al., 2016).

Environmental inputs to drive both site simulations include site air temperature (TA), soil temperature (TS), water table depth (WTD), photosynthetically activate radiation (PAR), fraction of harvested standing biomass, harvest dates (at Assendelft site), harvest day of year (at Weerribben site) and soil properties. In situ TA, TS, WTD, and PAR were used as model inputs where available. Forcing data for the spin-up period and in situ data gaps used TA and radiation from nearby KNMI weather stations (Marknesse for Weerribben and Schiphol for Assendelft) for TA and PAR, respectively. TS data for the spin-up and in situ data gaps was generated using the TA input data. We applied a 5-day moving average to reduce short-term variability, followed by a linear correction based on the relationship between smoothed TA and observed TS. WTD data for the spin-up and in situ data gaps was constructed with output from the HYDRUS model (Boonman et al., 2022). Assendelft Harvest amounts and dates were obtained as described in (Boonman et al., 2024). The model inputs for TA, TS, WTD, and PAR are plotted (Fig. 1).

Soil samples were obtained on site and properties such as dry bulk density (DBD), organic matter (OM) content, pF values, soil profile description were further analysed in the lab (Boonman et al., 2024; Buzacott et al., 2024).

This application of the model used the NPP module adapted from Shaver et al. (2007). Five SOM pools were simulated: peat, humus, root and litter mass, root exudates, microbial biomass. Whilst it is possible to include liquid and soil manure as two separate SOM pools, these sites were not fertilised with manure and therefore, these pools were bypassed in the model. SOM decomposition in aerobic layers was estimated using the Arrhenius equation, rather than the Q10 relationship. These simulations include the representation of anaerobic SOM decomposition which is optional in the model. The CH_4 cycle was validated at the Weerribben site only because CH_4 measurements were unavailable at Assendelft. However, past studies mea-

https://doi.org/10.5194/egusphere-2026-2450
Preprint. Discussion started: 26 June 2026

suring CH_4 emissions at the Assendelft site show very low (or no) CH_4 emissions (Gremmen et al., 2022; van den Berg et al., 2024).

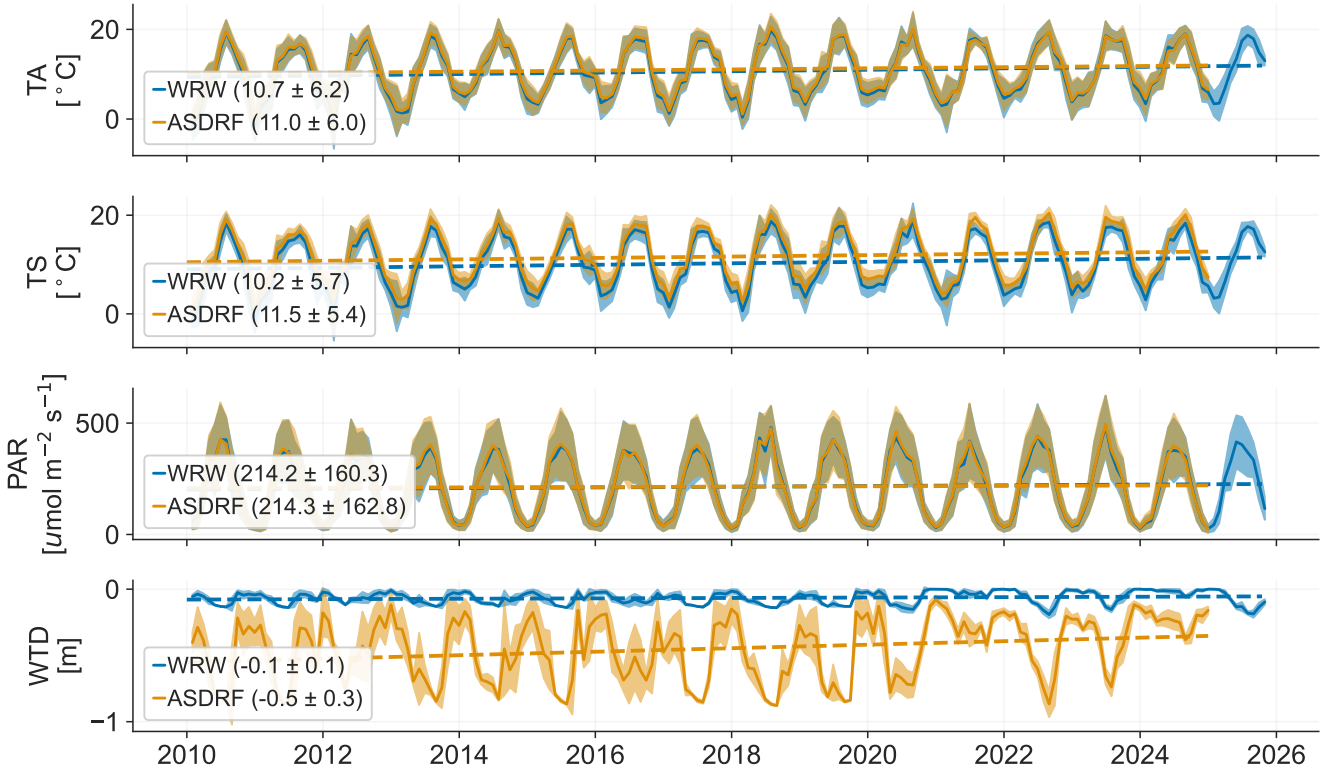

Figure 1. Environmental forcings at the Weerribben (WRW) and Assendelft (ASDRF) sites. Mean weekly air temperature (TA), soil temperature (TS), PAR, and WTD used as model input. Standard deviation calculated using daily values are shaded. Mean ± standard deviation calculated over the entire time period is shown in brackets. Trends (dotted lines) are calculated using Python's Ordinary Least Squares library.

4.1.2 Parameter optimisation

Initial choices of parameters were based on previously used values and parameters (van Huissteden et al., 2009; Mi et al., 2014). For both site simulations, model parameters were optimised using the particle swarm optimalisation (PSO) method (Clerc, 2011), which is available as an R-package hydroPSO ('spo2011'). A swarm size of 70 was chosen and a maximum number of iterations of 800. For the Assendelft site simulation, model parameters were optimised against in situ observational data measured between April 2020 and October 2023 and parameter values were chosen based on simulated estimates of Reco, GPP, NEE_{CO_2}, and harvested biomass. For Weerribben site simulations, model parameters were optimised against in situ observational data measured between August 2021 and December 2023 and parameter values were chosen based on simulated estimates of Reco, GPP, NEE_{CO_2} and NEE_{CH_4}. Model performance of these variables was determined using the lowest normalised mean absolute deviation (MAD).

https://doi.org/10.5194/egusphere-2026-2450
Preprint. Discussion started: 26 June 2026

4.1.3 Model validation

We evaluated model performance by comparing simulated and observed fluxes using the root mean square error (RMSE) and the normalised mean absolute deviation (MAD). Analyses were restricted to days with available measurements, covering periods after October 2023 at the Assendelft site and after December 2023 at the Weerribben site.

4.1.4 Spin-up

A spin up period of 10 years was used to stabilise the SOM carbon pools (Fig. SC3). The length of the spin-up period was determined by the amount of time needed for the pools to approach equilibrium. The resulting SOM carbon stocks reflect site conditions, with the Assendelft site representing carbon stored in a degraded peatland and the Weerribben site representing carbon stocks of a restored peatland.

4.2 Sensitivity and functionality testing

We assessed model sensitivity to both internal parameters and external environmental drivers using both site-specific simulation set-ups. Parameter sensitivity was evaluated by systematically altering model parameter values and analysing the resulting changes in simulated processes. Sensitivity to environmental forcing was examined through a series of simulations with modified input data. We tested parameters related to new developments (Table 2, Table 3, Table 4) as well as existing biogeochemical processes (Table 6, Table 7, Table 8).

Input parameters (for example, the maintenance respiration coefficient or air temperature) were varied one at a time across all relevant modules. For example, sensitivity to the NPP-relevant input parameters and environmental forcings were assessed using both the BIOME3 and Shaver NPP modules. This allows us to explore the sensitivities for all modules and functions. Sensitivity to all modules (including the CH_4, manure, and grazing modules et al) were tested at both sites and therefore, the inputs and parameters used could not always match those used for the model validation. The parameter set used to evaluate the sensitivity of of the Shaver NPP, Arrhenius, phenology, CH_4, and SOM decomposition modules, as well as the soil profile produced results consistent with observations (Fig. SC1). Similarly, the parameter set used to evaluate the sensitivity of the BIOME3 NPP, Q10, CH_4, and management practices produced results in agreement with observations (Fig. SC2).

For each parameter or forcing, we generated an ensemble of ten model simulations by perturbing parameter values or environmental forcings. Parameter values were evenly spaced within $\pm 20\%$ of the calibrated value for each site, while all other parameters were held constant. Similarly, environmental forcings were perturbed by uniformly scaling the original time series using ten evenly spaced multipliers spanning $\pm 20\%$ of the baseline forcing, while all other inputs were held constant. This design allowed us to isolate the model response to individual perturbations.

Sensitivities were calculated separately for the ensemble mean and standard deviation of model outputs, allowing the influence of parameters on both magnitude and variability to be assessed. To enable comparison of sensitivities across parameters and environmental drivers with different units, magnitudes, and ranges of variability, we expressed both parameter perturbations and model responses as normalised changes relative to the ensemble mean. This approach identifies which parameters

https://doi.org/10.5194/egusphere-2026-2450
Preprint. Discussion started: 26 June 2026

and forcings exert the strongest influence on model outputs within the explored parameter space, while remaining independent of absolute units. For example, a normalised sensitivity of one indicates that a change in a parameter leads to a response equal in magnitude to the ensemble mean of the model output.

Table 6. Descriptions of parameters relating to existing NPP, biomass, and management modules used in the sensitivity analysis.

Module	Parameter	Unit	Description
NPP	GrResp	-	Growth respiration constant
	MaintResp	-	Maintenance respiration constant
	SatCorr	-	Saturation correction constant
	Latitude	○	Site latitude
Biomass	SpringCorrection	-	Correction for stronger exudation in spring
	ExudateFactor	-	Mass fraction of of below-ground production that consists of exudates
	MaxRootDepth	m	Root depth
	RootLambda	-	Slope of root density profile
	RootSenescence	-	Fraction of roots that die in each time step
	InitRoots	kg C m^{-2}	Initial root mass in each soil layer
	MinBiomass	kg C m^{-2}	Minimum aboveground biomass
	BioMassSenescence	-	Fraction of aboveground biomass that dies in each time step
	LitFrac	-	Fraction of aboveground biomass that dies in each time step during Autumn
	BioMass	kg C m^{-2}	Initial biomass
Management	HarvestDay	calendar date or day of year	Harvest occurs on this day.
	HarvFrac	-	Fraction of aboveground biomass harvested
	HarvestLitter	-	Fraction of harvested biomass that is lost to litter during harvest.
	Manure (doy)	day of year	Manure is added on this day.
	Manure (kg)	kg	Amount of manure added to site.
	Grazing (start)	day of year	Start of grazing period.
	Grazing (end)	day of year	End of grazing period.
	Grazed_Frac	-	Fraction of biomass that is lost to grazing each day during grazing period.
	ManurefromGrazing	kg	Amount of manure secreted is to site each day during grazing period

https://doi.org/10.5194/egusphere-2026-2450
Preprint. Discussion started: 26 June 2026

Table 7. Descriptions of parameters relating to existing heterotrophic respiration and CH_4 modules.

Module	Parameter	Unit	Description
Rh	Cfrac	kg kg^{-1}	Carbon fraction of each SOM pool
	HalfSatPoint	-	Decomposition correction for partially saturated soils in layers above the WTD
	RootAeration	-	Root mass dependent correction for decomposition
	PrimingCorrection	-	Priming correction for decomposition
	MaxNPP	kg C m^{-2} day^{-1}	Maximum NPP used to calculate priming correction
	MinNPP	kg C m^{-2} day^{-1}	Minimum NPP used to calculate priming correction
	MatricPotThres1	-	Threshold to correct for soil dryness
	MatricPotThres2	-	Threshold to correct for soil dryness
	DrynessCorrection1	-	Constant to correct for soil dryness
	DrynessCorrection2	-	Constant to correct for soil dryness
	LitterLayer	kg C m^{-2}	Initial weight of litter layer
	LitterConversion	-	Fraction of litter converted from litter layer to litter SOM pool
	KLitter	year^{-1}	Litter decomposition rate constant
CH_4	GrowFuncConst	year^{-1}	Scales either NPP or LAI when calculating plant transported CH_4
	MethanePType	-	Vegetation constant for gas transport through plants
	MethanePlantOx	-	Fraction of CH_4 oxidised during plant transport
	MethanePRateC	hour^{-1}	Rate of gas transport through plants
	MethanepHCorr	-	Correction of CH_4 production rate (MethaneR0) for pH
	PartialAnaerobe	-	Fraction of soil layers above the WTD assumed to be anaerobic for methanogenesis
	MethaneKm	μ mol	Michaelis-Menten constant for CH_4 oxidation
	MethaneOxQ10	-	Temperature sensitivity constant for CH_4 oxidation
	MethaneVmax	μ mol hr^{-1}	Michaelis-Menten constant for CH_4 oxidation
	MethaneMaxConc	μ mol m^{-2}	Threshold to trigger ebullition
	MethaneERateC	hour^{-1}	Ebullition rate constant
	MethaneAir	ppb	Atmospheric CH_4 concentration
	InitMethane	μ mol m^{-2}	Initial CH_4 concentration per soil layer

https://doi.org/10.5194/egusphere-2026-2450
Preprint. Discussion started: 26 June 2026

Table 8. Descriptions of parameters relating to existing water table (WTD), soil temperature profile, and soil profile modules.

Module	Parameter	Unit	Description
	MinGW	m	Constrains groundwater depth
	PR	m	Precipitation
	ET	m	Evaporation
	EvapCorrection	-	Correction constant to reduce evapotranspiration when WTD is within soil column (not above surface)
WTD	RunoffThreshold	m	Threshold above which pooled water is converted to runoff
	OpenWaterFactor	-	Evaporation correction constant for pooled water
	CropFactor	-	Makkink evaporation correction constant for vegetation
	WatertableInit	m	Initialises WTD
	DrainageDist	m	Distance to drainage canal
	Ksat	m day^{-1}	Capacity of soil to transport of water, to or from the drainage canal
	DrainLevel	m	Water level in drainage canal
	Tdepth	°C	Depths of initial temperature profile
	SoilTemp	°C	Temperatures of initial temperature profile
	VegTScalingFactor	-	Correction constant for surface soil temperature
	MaxDepthHeat	m	Depth of soil temperature profile
TS profile	TStepHeat	$days^{-1}$	Time step of soil temperature profile
	ThermDiff	m^{-2} day^{-1}	Thermal Diffusivity
	DayMaxSnowdepth	day of year	Day of deepest snow layer
	MaxSnowdepth	m	Deepest snow layer
	SnowMeltrate	°C day^{-1}	Rate of snow melt
	DBD	kg m^{-3}	Dry bulk density of each soil horizon
	PercOrg	%	Percent SOM of each soil horizon
	Layer_pH	pH	pH value of each soil horizon
	ClayFraction	-	Clay fraction of each soil horizon
	SandFraction	-	Sand fraction of each soil horizon
Soil profile	theta_r_pF	L^3 L^{-3}	Van Genuchten parameter for each soil horizon
	theta_s_pF	L^3 L^{-3}	Van Genuchten parameter for each soil horizon
	alpha_pF	cm	Van Genuchten parameter for each soil horizon
	n_pF	-	Van Genuchten parameter for each soil horizon
	l_pF	L	Van Genuchten parameter for each soil horizon
	pFVal	-	pF pressure head (soil suction) values for each pF curve
	InitRes	-	Initial fraction of SOM in each soil horizon
	FreezingCurve	-	Constant for each soil horizon, to determine unfrozen water content curve when temperatures are below freezing

https://doi.org/10.5194/egusphere-2026-2450
Preprint. Discussion started: 26 June 2026

For each ensemble of ten simulations within an ensemble, both the parameter values and the resulting model outputs were normalised using the ensemble mean (Eq. 37). Ensembles were constructed of mean daily model output from the post-spin-up period (after 2020). Sensitivities were quantified by comparing deviations in the mean and standard deviation of model outputs relative to their ensemble means. This transformation places all parameters and outputs on a common, unitless scale, allowing effects on both the magnitude and variability to be compared across parameters.

$$S_i = \frac{x_i - \overline{x}}{\overline{x}}, \quad i = 1, \ldots, 10 \tag{37}$$

where x_i is the parameter value or summary statistic (mean or standard deviation of model output) from simulation i, and $\overline{x}$ is the corresponding ensemble mean calculated from post-spin-up model output.

To quantify the overall behaviour of the perturbed parameter/input forcing on the ensemble results, we fitted a linear regression to the standardised parameter-output pairs of each model ensemble using a Theil-Sen estimator, which provides a robust estimate of slope that is less sensitive to outliers and non-linear responses than simple linear regression, particularly for small ensembles. The resulting slope represents the standardised sensitivity and the extent to which variation in a given parameter contributes to the magnitude and variability of model output within the explored parameter range.

Finally, the regression slopes were visualised as heatmaps to provide an overview of parameter sensitivity across model components and sites.

5 Results and discussion

Here, we evaluate the model's performance against in situ fluxes at the Weerribben and Assendelft peatland sites (Sect. 5.1). We investigate the sensitivity of the model to modified input parameters (Sect. 5.2) by investigating the functioning of the NPP modules (Sect. 5.2.1), plant growth and senescence (Sect. 5.2.2), SOM decomposition (Sect. 5.2.3), the temperature sensitivity of SOM decomposition (Sect. 5.2.4), CH_4 cycling (Sect. 5.2.5), land use management (Sect. 5.2.6), soil profile (Sect. 5.2.7), soil thermal profile (Sect. 5.2.8), and water table modules (Sect. 5.2.9).

5.1 Model validation: estimating emissions at two peatland sites

Overall, the model reproduces the magnitude and seasonal variability of observed fluxes, as well as multi-year trends (Fig. 2). However, mismatches in the timing of peak summer fluxes remain and likely contribute to reduced statistical performance (Fig. 3). The model performed well estimating daily GPP fluxes, where the MAD (0.3 g CO_2 m^{-2} day^{-1}) was low at both the Weerribben and Assendelft sites and the RMSE (6.7 and 9.0 g CO_2 m^{-2} day^{-1}) was equivalent to half of the mean daily observed GPP flux at the Weerribben and Assendelft sites. The model had a tendency to underestimate GPP at the Assendelft site, where GPP showed much more variability. Performance estimating GPP fluxes at the Assendelft site may be due to the impacts of synthetic nitrogen fertilisation where nitrogen effects are not captured by the model or due to the automated chamber technique used to measure fluxes. Chamber measurements can be sensitive to micro-climates and ecosystems, and often increase the heterogeneity of observational measurements.

https://doi.org/10.5194/egusphere-2026-2450
Preprint. Discussion started: 26 June 2026

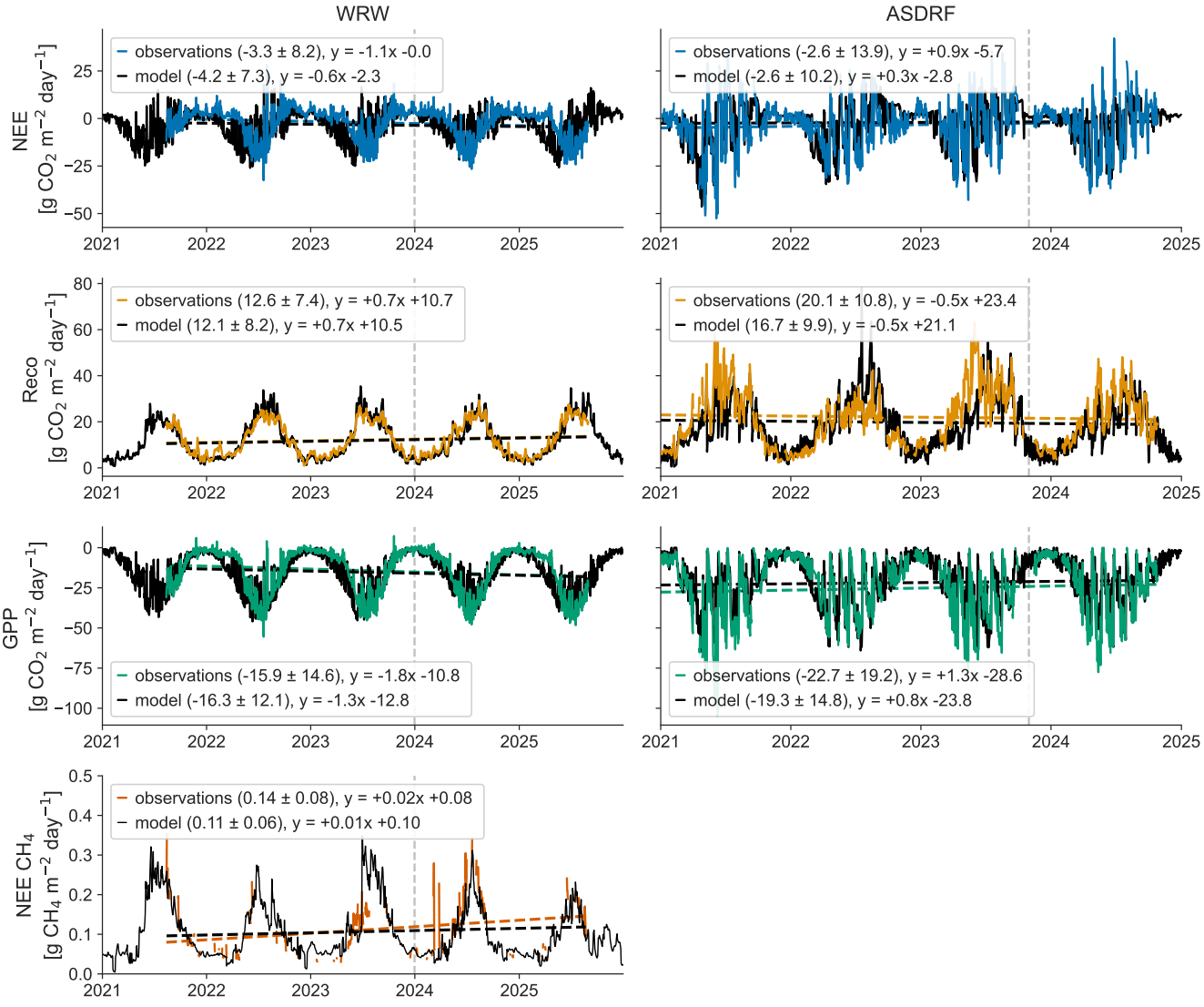

Figure 2. The model reproduces daily and seasonal observed fluxes over time. The dotted vertical line shows divides the data used for calibration and validation. Means and standard deviations are calculated for validation-period days where observational data are available. Trend lines are calculated using all days that measurements were available.

The model performed well estimating dailyRECOfluxes, where the MAD ($\leq$0.2 g CO_2 m^{-2} day^{-1}) was low at both sites and the RMSE (3 - 11 g CO_2 m^{-2} day^{-1}) was equivalent to one third of the mean observed daily flux. Several recent model developments have impacted the representation of heterotrophic respiration in the model. Particularly, the representation of anaerobic respiration has been introduced into the model, allowing more accurate simulation of winter time soil respiration, when WTD is typically high.

https://doi.org/10.5194/egusphere-2026-2450
Preprint. Discussion started: 26 June 2026

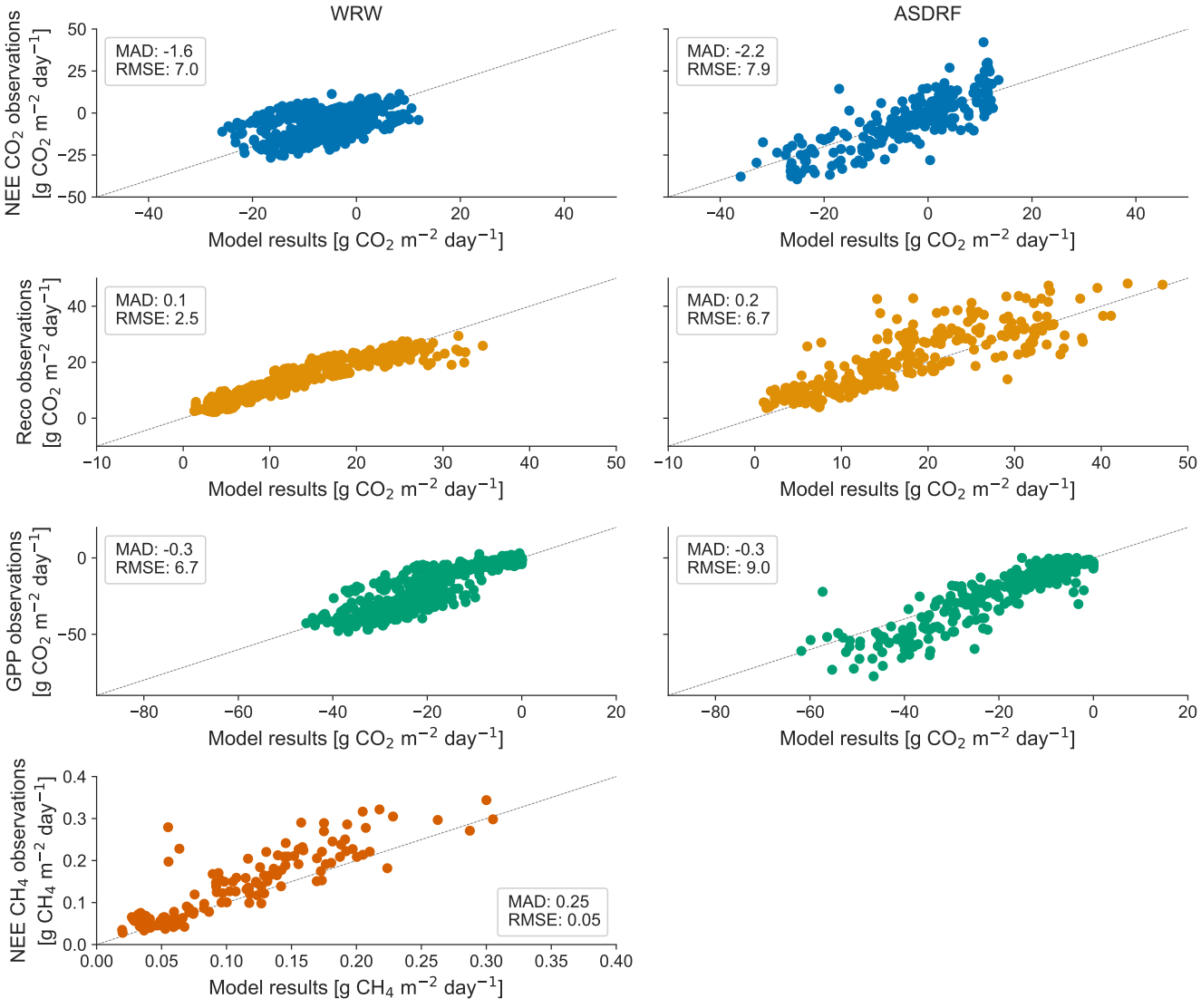

Figure 3. The model reproduces observed daily fluxes. The mean absolute deviation (MAD) and root mean square error (RMSE) are provided in the legend. Fluxes are plotted for validation-period days where observational data are available.

With respect to $\mathrm{NEE_{CO_2}}$, the MAD (-1.6 and -2.2 g CO_2 m^{-2} day^{-1} at the Weerribben and Assendelft sites, respectively) was modest relative to the magnitude of observed fluxes. However, the RMSE (7 and 7.9 g CO_2 m^{-2} day^{-1} at the Weerribben and Assendelft sites, respectively) was larger than the mean observed daily $\mathrm{NEE_{CO_2}}$ flux at the two sites, which shows that the model uncertainty in representing GPP and Reco, do not compensate for each other but are perpetuated in the $\mathrm{NEE_{CO_2}}$ estimates.

https://doi.org/10.5194/egusphere-2026-2450
Preprint. Discussion started: 26 June 2026

The performance of the model to simulate CH_4 emissions was evaluated at the Weerribben site. The model estimated CH_4 fluxes with skill at the Weerribben site (MAD: 0.25 g CH_4 m^{-2} day^{-1}, RMSE: 0.05 g CH_4 m^{-2} day^{-1}), capturing both seasonal dynamics and overall variability. However, spring emission peaks in 2024, a particularly wet year were underestimated. This indicates that either CH_4 production may be insufficiently sensitive to changing temperature or water level fluctuations, or that CH_4 transport was not sufficiently sensitive to increasing belowground CH_4 concentrations, or a combination of the two. Half hourly observations show particularly strong diurnal patterns at the Weerribben site, suggesting a strong sensitivity to vegetation activity (Buzacott et al., 2024). Plant-mediated transport dominated simulated CH_4 pathways at the Weerribben site indicating vegetation productivity is strongly coupled to CH_4 emissions (Fig. 4). Overall, the model (0.11±0.06 g CH_4 m^{-2} day^{-1}) did a good job of reproducing the observed (0.14±0.08 g CH_4 m^{-2} day^{-1}) mean CH_4 flux and standard deviation.

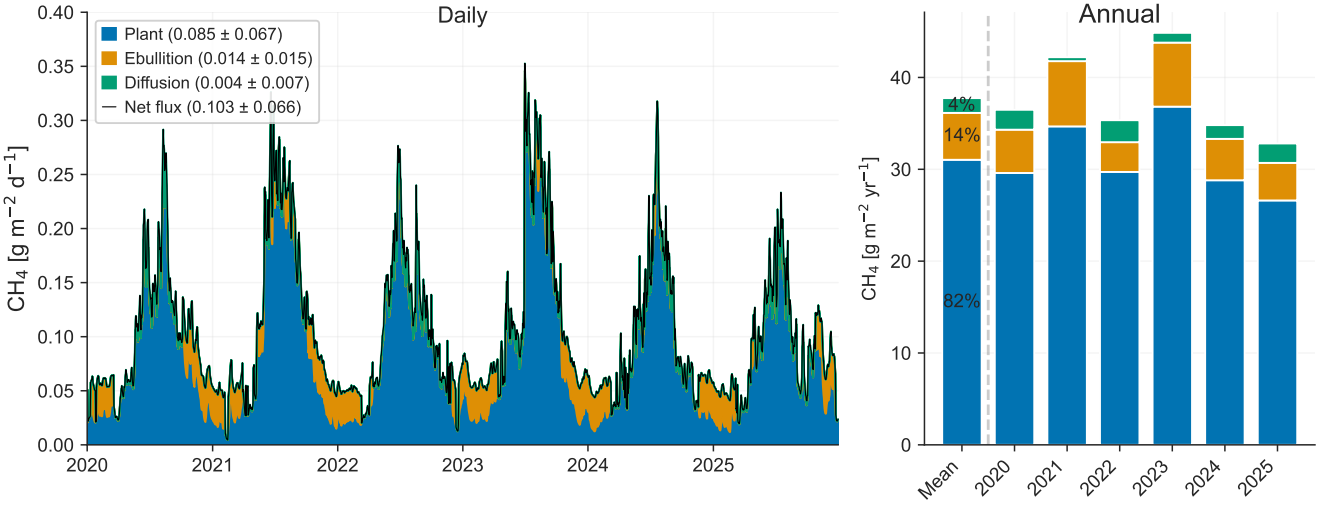

Figure 4. Simulated CH_4 transport pathways at the Weerribben site. Left: time series of daily CH_4 fluxes showing contributions from plant transport, ebullition, and diffusion, and the resulting net surface flux. Means and standard deviations shown in the legend are calculated over the plotted period. Right: annual summed CH_4 emissions separated by transport pathway. The "Mean" shows the multi-year average contribution, with percentages indicating their relative importance in controlling total emissions.

Trends estimated, using both observed and simulated fluxes, indicate that the Weerribben site is becoming an increasing sink of atmospheric CO_2, while simultaneously an increasing source of atmospheric CH_4. Combining NEE_{CO_2}, NEE_{CH_4}, and off-site CO_2 emissions from harvested biomass, showed that the Weerribben is carbon-neutral, on average, when calculated using a 100-year GWP (Fig. 5). Despite not being a source of atmospheric CH_4, the Assendelft functions as a net CO_2 source when including offsite annual CO_2 emissions from harvested biomass, where both observations and simulations indicate that the site is an increasing CO_2 source over time.

Overall, Peatland-VU v3.0 demonstrates robust skill in reproducing daily to seasonal CO_2 and CH_4 fluxes across two contrasting peatland sites, where model performance was strongest for GPP and Reco. However, uncertainties in these components

https://doi.org/10.5194/egusphere-2026-2450
Preprint. Discussion started: 26 June 2026

propagated into NEE, particularly at the more intensively managed Assendelft site, since RECO and GPP are cancelling each other out leading to relatively low NEE values. Small uncertainties in RECO and GPP lead to high uncertainties in NEE. Differences in observational techniques, site management, and unrepresented processes such as the effect of fertilisation on vegetation growth, partly explain differencec in site-specific performance. It is important to keep in mind that two different measurement techniques/practices were undertaken at the two sites: automated chamber measurements were performed at the Assendelft site and EC measurements were performed at the Weerribben site. Automatic chamber measurements have a distance advantage of capturing microscale flux measurements that are specific to the microecosystem. However, EC measurements are typically less heterogeneous due to their landscape scale footprint and therefore, are generally more easily captured by the model. The addition of synthetic fertilisers at the Assendelft site may also impact vegetation growth rates, but is not accounted for in the model. Nevertheless, the model successfully reproduces patterns in CO_2 and CH_4 emissions, supporting its applicability for simulating GHG dynamics in both restored and managed peatlands.

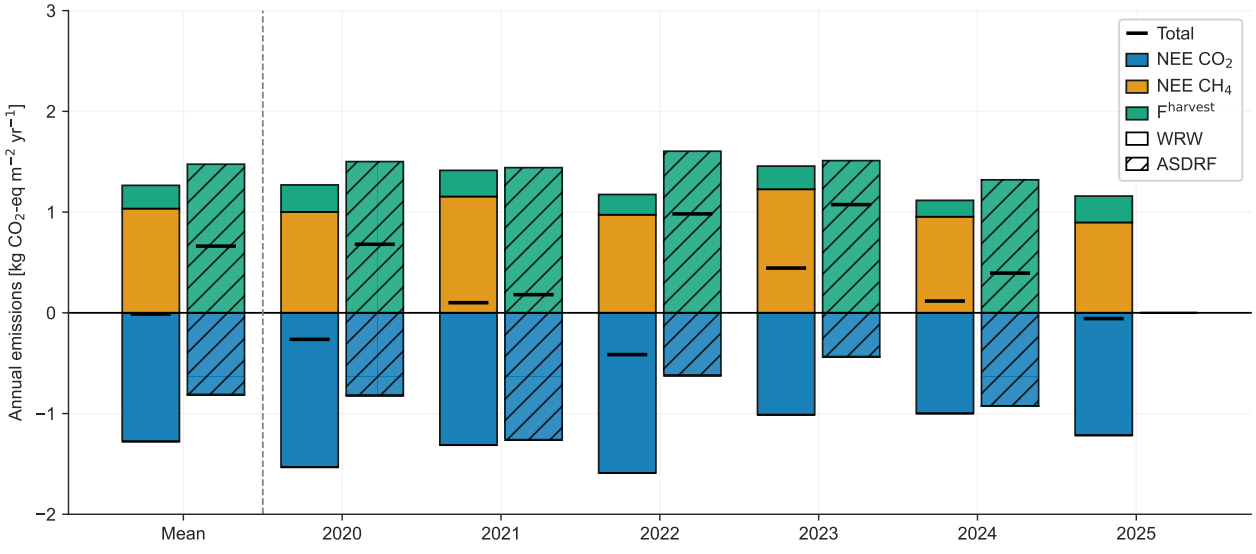

Figure 5. Simulated mean and annual CO_2 and CH_4 emissions including decomposition from harvest. Methane emissions were calculated using a 100 year GWP of 27.9. Horizontal black lines indicate the annual sum.

5.2 Testing of model sensitivity

We test the sensitivity of the model in response to several input parameters and environmental forcings at the Assendelft and Weerribben sites.

5.2.1 Sensitivity of photosynthesis and autotrophic respiration modules

Given the central role of plant productivity and growth in driving ecosystem carbon dynamics, we first assess the sensitivity of the two NPP modules, BIOME3 and Shaver (Fig. 6). Modifications to the inputs of the NPP modules influence almost

https://doi.org/10.5194/egusphere-2026-2450
Preprint. Discussion started: 26 June 2026

all processes within Peatland-VU v3.0. This system-wide response is expected given the central role of photosynthesis and autotrophic respiration in controlling carbon inputs and internal cycling.

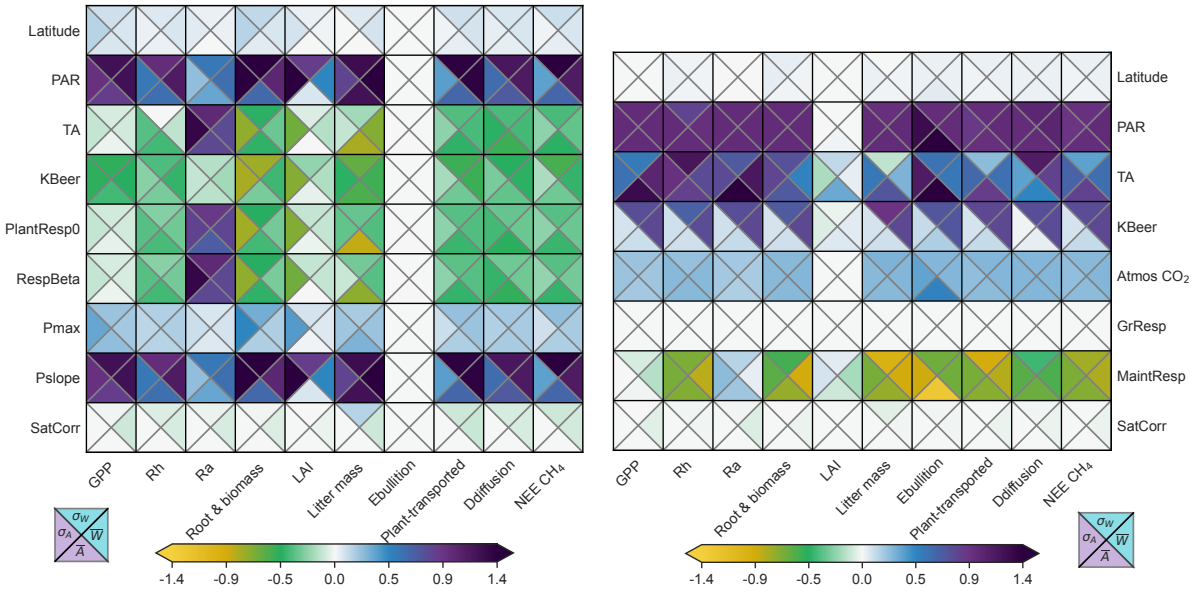

Figure 6. The sensitivity of the Shaver (left) and BIOME3 (right) production modules to environmental and parameter inputs at the Assendelft and Weerribben sites. A positive number indicates that increasing the value of the parameter leads to an increase in the value of the output variable. The lower and left triangles represent results for the Assendelft site, whereas the upper and right triangles represent results for the Weerribben site. Sensitivity of the magnitude of modelled outputs is shown in the lower and right triangles, while sensitivity of model variability is shown in the left and upper triangles.

Rising temperature, radiation, and atmospheric CO_2 concentration are well documented to enhance GPP, Ra, and Rh, provided the system is not water-, nutrient-, or otherwise limited (Medlyn et al., 2011). In both the Shaver and BIOME3 NPP modules, PAR showed positive relationships with all model output variables, consistent with expectations as increased radiation stimulates photosynthesis, biomass accumulation (which results in enhanced carbon transfer to below ground carbon pools), heterotrophic respiration, and CH_4 production. In the BIOME3 module, air temperature (TA) and atmospheric CO_2 concentration (Atmos CO_2) positively influenced all carbon pools and fluxes. However, the effects of Atmos CO_2 may be overestimated without including the effects of nutrient limitation. In contrast, while autotrophic respiration is temperature-sensitive in the Shaver module, GPP is not directly related to temperature nor are the effects of atmospheric CO_2 fertilisation represented. Latitude influences day length in both the BIOME3 and Shaver modules and therefore affects calculations of photosynthesis and autotrophic respiration. Increasing latitude enhanced GPP and autotrophic respiration in the Shaver module but had negligible effects on these fluxes in the BIOME3 module, contrary to expectations that variability of productivity would increase at higher latitudes. Consequently, although both modules broadly reproduce expected responses to radiation, the absence of

https://doi.org/10.5194/egusphere-2026-2450
Preprint. Discussion started: 26 June 2026

temperature and atmospheric CO_2 sensitivities in the Shaver module may limit its applicability for long-term climate change simulations (Rogers et al., 2017). These effects could be considered in considered in future model versions.

The Shaver module was developed on the premise that both autotrophic respiration and GPP are correlated with LAI and therefore use parameters that fit equations of the relationships between LAI, GPP, and autotrophic respiration . The outcome of this is that PlantResp0 and RespBeta are input parameters used to estimate autotrophic respiration and Pmax and Pslope are input parameters used to estimate GPP. PlantResp0 and RespBeta have positive relationships with Ra. Pslope and Pmax have positive relationships with GPP where, the effect of Pslope is greater than the effect of Pmax. Increasing maintenance respiration (MaintResp) rates in the BIOME3 module led to higher autotrophic respiration but reduced root and aboveground biomass, indicating that higher metabolic costs limit carbon available for growth. In contrast, varying the growth respiration parameter (GrResp) had little effect on autotrophic respiration or biomass.

Many wetland species close their stomata in the initial days after flooding, reducing photosynthetic capacity (Chen et al., 2005). The flooding correction parameter (SatCorr) showed limited effects on GPP and related processes at the Weerribben site and no effect at Assendelft, likely because water tables at Assendelft did not reach levels that triggered the SatCorr response. While consistent with empirical observations, future model developments could represent these processes more explicitly, such as stomatal closure during flooding or reduced GPP due to oxygen limitation in roots (Lindenberger et al., 2025).

We observed divergent behaviour in response to the light interception parameter (KBeer) between modules, reflecting different definitions of light limitation. In BIOME3, KBeer governs canopy light interception via the Beer-Lambert law, whereas in Shaver it controls the curvature of the light-response function and thus photosynthetic efficiency. These differences highlight the need to clearly document parameter definitions in both production modules and suggest that future developments could benefit from harmonising the treatment of light extinction to improve comparability and parameter transferability.

5.2.2 Sensitivity of allocation and senescence modules

Here, we assess the sensitivity of key parameters governing biomass allocation, senescence, and phenology (Fig. 7). Carbon allocation varies between plant types, seasons, and according to resource availability (Metcalfe et al., 2011). In the Peatland-VU model, allocation is governed by parameters regulating biomass partitioning and canopy development. The LAICarbonFraction parameter determines carbon allocation to leaves, where higher values reduced leafy biomass, inversely affecting productivity and system outputs. Similarly, the ShootsFactor parameter partitions NPP between above- and belowground growth and also plays a role in estimating LAI. We observed a positive relationship between ShootsFactor and total biomass at the Weerribben site and converse relationship at the Assendelft site, possibly due to differing rates of senescence and harvest (mowing) or constraints caused by maximum LAI. The initial biomass parameter (BioMass) did not influence long-term carbon cycling. Further developing explicit carbon allocation to plant organs could improve the representation of NPP in the model, and increase the value of later developing the nitrogen cycle and nitrogen limitation (Stocker et al., 2025).

Senescence is a key driver of heterotrophic respiration and CH_4 substrate availability, however, observations are often hard to gather, relative to those related to growth and productivity (Randerson et al., 2009). Parameters governing plant senescence and biomass retention directly regulate the transfer of carbon from living biomass to litter pools. The biomass senescence

https://doi.org/10.5194/egusphere-2026-2450
Preprint. Discussion started: 26 June 2026

parameter (BiomassSenescence), determines the fraction of biomass that dies each day, negatively affects total biomass, whilst increasing litter mass. The MinBiomass parameter, which restricts biomass loss to litter and the maximum amount of biomass that can be harvested, shoed a positive relationship with the magnitude of total biomass as higher thresholds retain more living biomass whilst reducing variability. Increases to daily root mortality (i.e. RootSenescence parameter) produced, as expected, a negative effect on total root and shoot biomass. Increasing the amount of litter transferred to the litter SOM pool by increasing Litfrac decreases the litter mass, as expected. Explicit representation of processes accelerating or triggering senescence could improve the model's capacity to simulate decomposition and carbon storage (Ruehr et al., 2023).

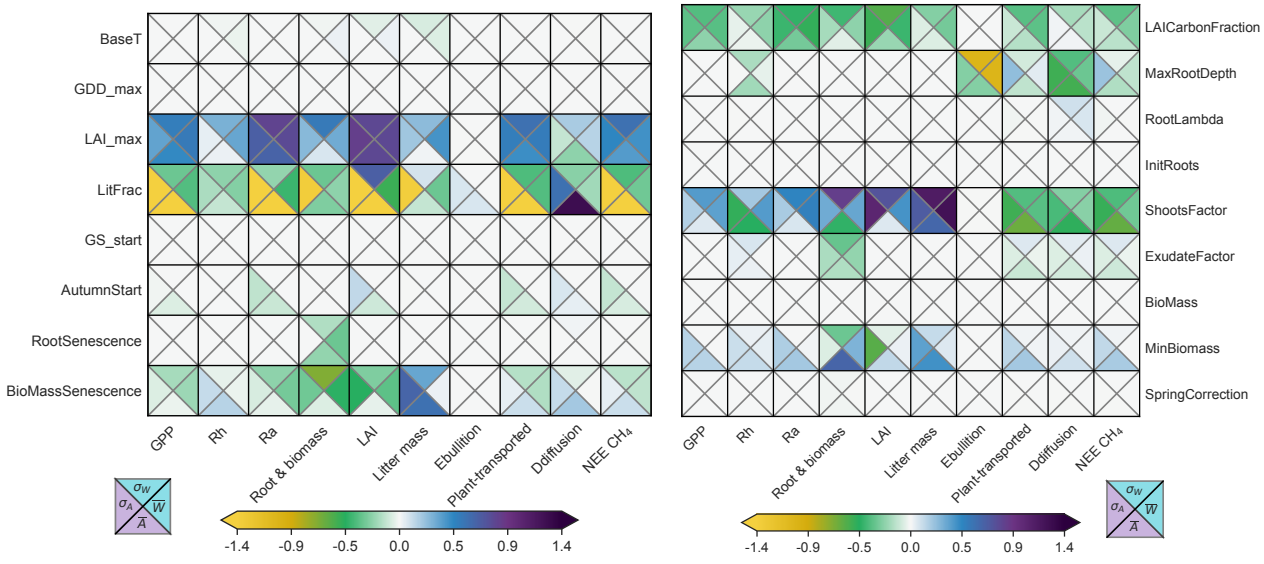

Figure 7. Sensitivity of plant growth and mortality modules to environmental drivers and model parameters.

Plant phenology, the annually recurring sequence of plant developmental stages, is largely photoperiod dependent, where its timing is shifting with climate change (Piao et al., 2019). In the Peatland-VU model, the parameters that control the duration of the growing season and timing of leaf senescence (AutumnStart and GS_start), hold potential to affect litter and aboveground biomass dynamics. A later AutumnStart reduced LAI and autotrophic respiration, while a later GS_start did not play a detectable role. The LAI_max parameter, sets an upper bound on canopy leaf area where higher values enable greater light interception, positively feeding back into GPP, plant respiration, and biomass. BaseT affects GDD accumulation, where increasing BaseT, decreases the daily thermal increment, and therefore LAI development. The maximum GDD parameter (GDD_max) determines the threshold for full leaf expansion but showed limited influence. Overall, the phenology module responded reliably, however, to allow the growing season to move with climate variability, the GDD module could be further adapted to determine the timing of the growing season start and end depending on factors such as seasonal temperature, precipitation, or GDD (Peaucelle et al., 2019).

https://doi.org/10.5194/egusphere-2026-2450
Preprint. Discussion started: 26 June 2026

Plant roots play critical roles in ecosystem dynamics where belowground biomass can exceed aboveground biomass (Iversen et al., 2015). In the Peatland-VU model, several parameters control the initialisation and vertical distribution of roots, with implications for belowground carbon cycling rather. The InitRoots parameter sets initial root mass across soil layers but does not influence long-term biomass after spin-up. The RootLambda parameter, which determines the exponential distribution of roots with depth, had limited impact on overall model function but slightly increased CH_4 diffusion, suggesting the root architecture can impact CH_4 transport, consistent with observations (Määttä and Malhotra, 2024). The MaxRootDepth parameter influences the vertical root profile, where increasing the values of this parameter, decreased heterotrophic respiration and decreased the magnitude of CH_4 emissions at both sites but increased the variability in CH_4 emissions at the Assendelft site. This is consistent with observations, where increased maximum rooting depth has been shown to increase both CH_4 production and oxidation, leading to a net decrease in CH_4 emissions (Määttä and Malhotra, 2024). The ExudateFactor parameter governs the carbon allocation to exudates, at the expense of roots. Therefore, increasing this parameter reduces root biomass, as expected. The SpringCorrection parameter represents enhanced exudation during the growing season but had limited effects on model outputs. Overall, the root parameters primarily influenced SOM inputs, and CH_4 production and transport pathways.

Overall, the allocation and senescence modules behaved in line with ecological expectations where shifting to more dynamic phenology and senescence modules could increase the models capacity to emulate the impacts of climate change on the growing season, heterotrophic respiration and carbon storage.

5.2.3 Sensitivity of decomposition modules

Decomposition of SOM varies tremendously as a function of the structure and chemical composition of the organic matter being decomposed (here, represented by the base decomposition rate), the abiotic environment in which decomposition is occurring (e.g. temperature, moisture, and aeration which are represented here as environmental corrections), and the degree to which the decomposing substrate is exposed to heterotrophs, both microbial and faunal (implicitly represented through aerobic and anaerobic partitioning). Here we assess the sensitivity of the SOM decomposition module to parameters and environmental forcings (Fig. 8). In Sect. 5.2.4, we assess the Q10 and Arrhenius temperature sensitivity modules. Across simulations, we found the Kdecay, Cfrac, HalfSatPoint, and KLitter constants to be most influential over Rh.

The capacity of SOM to decompose is represented by the base decomposition rate (Kdecay) which represents differences in the structure and chemical composition of the SOM that either aid or hinder microbial decomposition (Robertson et al., 2000). Increasing Kdecay for the peat and humus pools increased both the magnitude and variability of heterotrophic respiration and CH_4. The impact on heterotrophic respiration is straightforward because these pools constitute a large fraction of total soil carbon and therefore strongly influence heterotrophic respiration. The fractions of total decomposed SOM transferred to dead microbial biomass and humus remain fixed, and therefore a higher peat or humus decomposition rate increases the absolute amount of carbon converted to (dead) microbial SOM, which is more readily available for subsequent respiration and methanogenesis than the original peat or humus pools, leading to enhanced CH_4. In contrast, increasing the Kdecay rates of other SOM pools did not noticeable affect heterotrophic respiration which may also reflect the relative size of the SOM pools (Fig. SC3). However, CH_4 emissions decreased for litter and roots and microbial SOM pools, indicating that accelerated decomposition

https://doi.org/10.5194/egusphere-2026-2450
Preprint. Discussion started: 26 June 2026

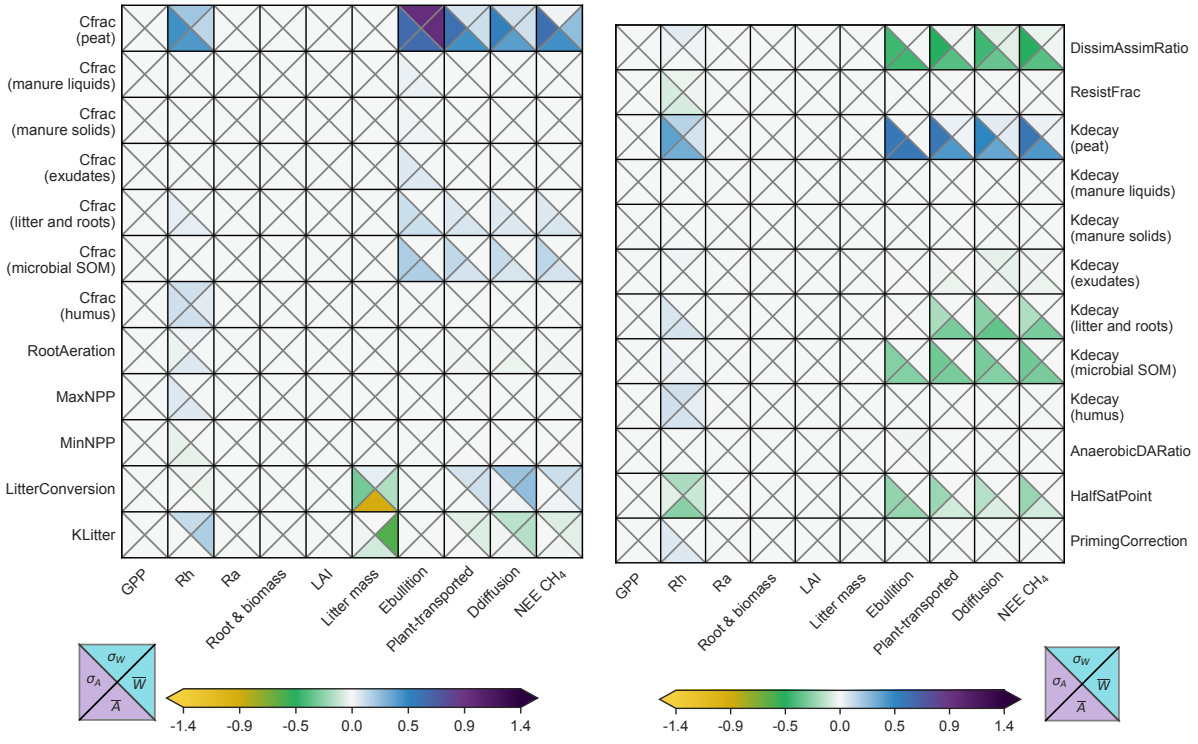

Figure 8. The sensitivity of SOM decomposition modules to environmental drivers and model parameters.

reduced the availability of labile substrates supporting methanogenesis. The rate of mineralisation of saturated SOM layers is determined by the Kanaerobic decay constants which did not lead to detectable impacts on heterotrophic respiration, likely due to the relatively small contribution of the anaerobic soil layers to heterotrophic respiration (Fig. SC4).

Living microorganisms drive the global biogeochemical cycle, yet dead microbial biomass is often overlooked despite continuing to contribute to biogeochemical cycling, and functioning as one of the largest SOM pools on Earth (Sokol et al., 2022). The parameters AnaerobicDARatio and DissimAssimRatio regulate the fraction of anaerobic and aerobic SOM converted to dead microbial biomass, where larger numbers lead to less converted SOM. Within the tested perturbation range, AnaerobicDARatio did not produce a detectable response, likely reflecting the small contribution of anaerobic SOM to heterotrophic respiration. DissimAssimRatio showed a converse relationship with CH_4 at the Assendelft site only, reducing both the magnitude and variability. This indicates that increasing DissimAssimRatio reduced easily decomposable substrate (exudates) available for CH_4 production, indicated by reduced CH_4 fluxes. A larger effect observed at the Assendelft site is likely due to a larger aerobic zone, leading to greater aerobic decomposition and reduced carbon available for CH_4 production. These results highlight the role of microbial turnover in regulating substrate availability and CH_4 dynamics.

Increasing the proportion of carbon stored in resistant pools decreases soil respiration. The parameter ResistFrac, which controls the fraction of SOM cycled into resistant material (humus), did not produce a detectable impact on either heterotrophic

https://doi.org/10.5194/egusphere-2026-2450
Preprint. Discussion started: 26 June 2026

respiration or CH_4 within the tested parameter bounds. The absence of a clear model response may be due to relatively small size of the humus pool relative to overall SOM.

Soil organic carbon content is highly coupled to the contributing plant matter, where natural and semi-natural systems tend to have high carbon contents relative to croplands, an important factor separating croplands grown on degraded peat soils from croplands grown on mineral soils (Reinsch et al., 2025). Cfrac, which sets the initial carbon content of the SOM pools, shows the expected positive relationship with CH_4 and to a lesser extent, Rh, confirming that initial substrate availability drives persistent differences in fluxes.

Several parameters are in place to slow or enhance decomposition due to dryness, wetness, pH, C/N ratio, priming. Both HalfSatPoint and C/N constants led to impacts on SOM pools that led to impacts on R_h fluxes. A low HalfSatPoint value increased sensitivity of the system to moisture, decreasing Rh, as expected. The KPeatCN1 (reference C/N ratio) and KPeatCN2 (slope of relative decrease of decomposition rate constant) parameters provide bounds on mineralization based on site-specific C/N ratios, limiting decomposition rates in the presence of very high or low C/N values, consistent with nutrient feedbacks or botanic origin influencing decomposition efficiency. Increasing KPeatCN1 enhanced CH_4 emissions, while increasing KPeatCN2 suppresses CH_4 emissions, consistent with nutrient feedbacks influencing decomposition efficiency. Parameters accounting for the affects of soil matric potential (MatricPotThres1 and MatricPotThres2) and soil dryness (DrynessCorrection1 and DrynessCorrection2) did not lead to effects at either site (Fig. C4). The parameters, PrimingCorrection, MaxNPP and MinNPP, control the extent that priming effects of decomposition and did not lead to detectable impacts. The RootAeration parameter can change the decomposition sensitivity to a dense root system, decreasing the efficiency of SOM decomposition, did not lead to a detectable relationship with R_h or CH_4 production. Future modelling efforts may look at increasing the sensitivity of environmental corrections. And also consider the impacts of root respiration on Rs.

The rate of litter being transferred from the surface litter layer to belowground SOM, LitterConversion, led to an inverse relationship with litter mass, as expected. Increased CH_4 cycling indicates that more substrate is available. The initial litter pool size, LitterLayer, did not lead to persistent impacts, indicating that it plays a limited role on longterm model behaviour. The KLitter parameter, representing the decomposition rate constant of surface litter, inversely affects litter mass as expected, potentially increasing Rh. Reduced CH_4 emissions suggest that increasing this parameter can lead to a decrease in substrate available for methanogenesis, as expected.

5.2.4 Sensitivity of temperature sensitivity module

Temperature sensitivity of SOM decomposition is a key control on peatland carbon cycling (Qin et al., 2019). Here, we show that both the the Q10 and Arrhenius modules produced reliable responses to perturbations of both environmental forcings and input parameters (Fig. 9). We found that the reference temperature, TS, and peat Q10 values led to the largest impacts on Rh.

Changes in TS showed a correlating relationship with both R_h and CH_4 fluxes due to amplified decomposition and mineralisation at warmer temperatures, as expected. Interestingly the variability of heterotrophic respiration was impacted more than the magnitude, when using the Arrhenius module, indicating that seasonal amplitude increased, as found in other studies. The

https://doi.org/10.5194/egusphere-2026-2450
Preprint. Discussion started: 26 June 2026

Assendelft was more sensitive to changing TS when using the Q10 module, which is to be expected as dryer soils are more sensitive to temperature change.

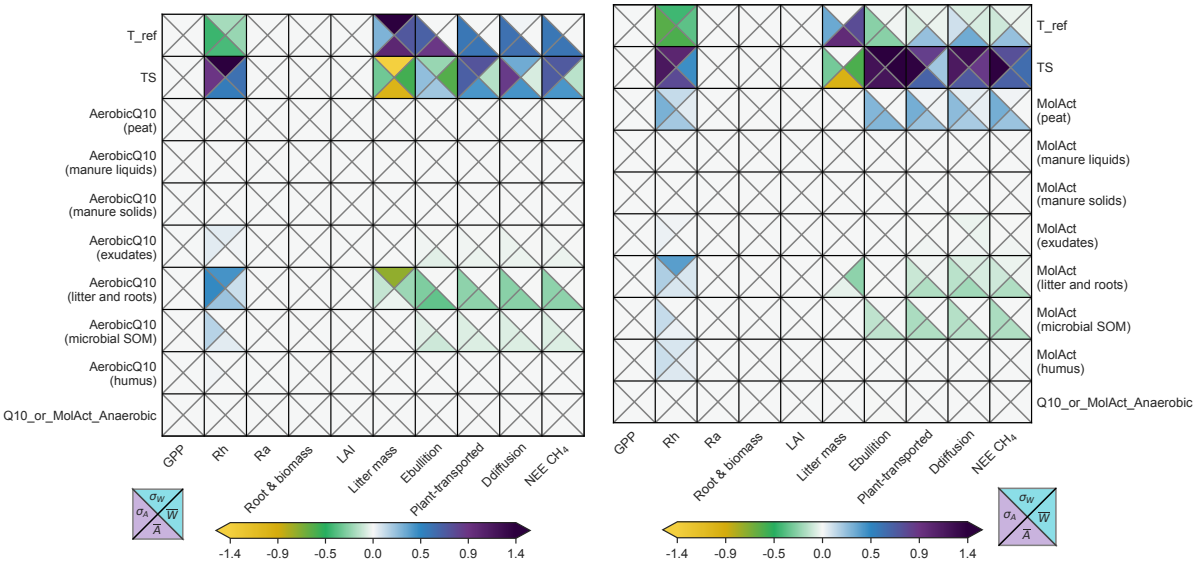

Figure 9. The sensitivity of the Q10 (left) and Arrhenius (right) temperature sensitivity SOM decomposition modules to environmental drivers and model parameters.

In the Arrhenius module, the temperature sensitivity is driven by the molecular activation energy parameter (MolAct) assigned to each SOM pool. Similarly, in the Q10 formulation, Q10 values impact the temperature sensitivity of heterotrophic respiration. Higher MolAct values increased heterotrophic respiration across all pools. Both Q10 and MolAct values are assigned to each SOM pool, where the litter and roots and microbial SOM pools were most sensitive to changing Q10 and MolAct values. In the Arrhenius module, the peat and humus SOM pools were also found to be sensitive to changing MolAct values. The Q10Anaerobic and MolAct anaerobic parameters represent the temperature sensitivity of anaerobic SOM layers. Varying these parameters did not produce detectable impacts, likely because the anaerobic SOM pools are relatively small and contribute little to total heterotrophic respiration. Reaction rate ratios (Fig. 10) calculated using the variable Q10 and MolAct values used in the sensitivity analysis closely match compiled global peat incubation data (Dehaen et al., 2025).

The reference temperature is linked to the decomposition rate constants, where decomposition rates decreases with lower temperatures and increases with higher temperatures. In both the Arrhenius and Q10 modules, increasing the reference temperature decreased Rh, as the daily thermal anomaly decreases, reducing the rate of decomposition.

Notably, both modules impacted heterotrophic respiration and CH_4 fluxes, where enhanced heterotrophic respiration often depleted substrates available for methanogenesis, reflecting competitive microbial dynamics observed in saturated soils (Ritson et al., 2021; Hu et al., 2024). While both the Q10 and Arrhenius modules both simulated plausible responses to changing temperatures, differences were observed between the modules. Both Q10 and Arrhenius formulations impose a monotonically

https://doi.org/10.5194/egusphere-2026-2450
Preprint. Discussion started: 26 June 2026

increasing temperature response, which neglects the presence of an optimum (typically around 30-40°C) and fails to capture the decline in process rates that may occur at either higher and lower temperatures (Schipper et al., 2014). These findings highlight the importance of the chosen temperature response function when projecting heterotrophic respiration under warming scenarios and across climate gradients (Ise et al., 2008; Davidson and Janssens, 2006; Kirschbaum, 2006).

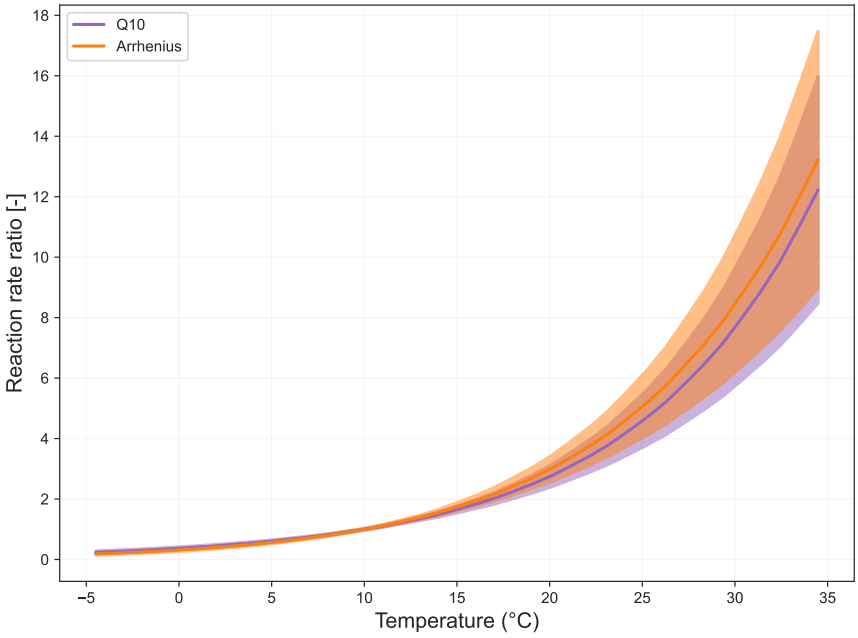

Figure 10. Variation of peat Q10 and Arrhenius reaction rate ratios. A synthetic temperature dataset is used to evaluate the temperature sensitivity functions based on the Q10 and MolAct parameter ranges applied in the sensitivity analysis.

5.2.5 Sensitivity of CH_4 module

This CH_4 subroutine calculates CH_4 production and oxidation across soil layers for a given timestep, based on environmental conditions like soil temperature and water saturation, as well as model parameters. It distinguishes between aerobic and anaerobic zones, and simulates carbon flow as CH_4 and CO_2. Here we assess the affects of all inputs into the CH_4 module (Fig. 11). Ecosystem CH_4 emissions are difficult to model due to the complex and highly heterogeneous array of interacting small and large scale processes (Lippmann et al., 2024; Chang et al., 2021).

Methane emissions respond strongly to changes in the groundwater level where shallower (higher) WTD leads to increased magnitude of CH_4 emissions as expected but with decreased variability.

Temperature is a dominant driver of net wetland CH_4 emissions due to its role driving both methanogenesic and methanotrophic activity, amongst other indirect feedbacks (Knox et al., 2021; Hu et al., 2024). Increasing TS increased the magnitude and variability of CH_4 emissions. In the model, methanogenesis follows a Q10 formulation defined by MethaneQ10 and MethaneTRef, where MethaneTRef is the temperature at which the baseline production rate is specified. Increasing

https://doi.org/10.5194/egusphere-2026-2450
Preprint. Discussion started: 26 June 2026

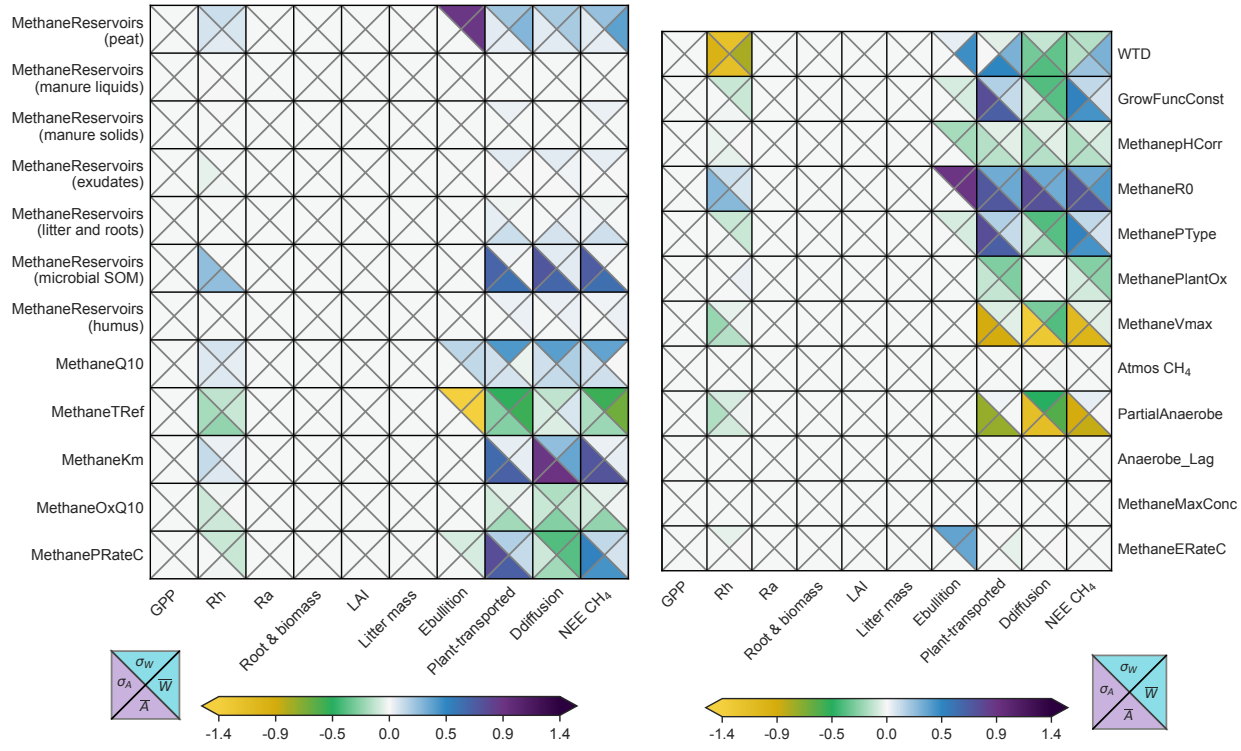

Figure 11. The sensitivity of the CH_4 module to environmental and parameter inputs.

MethaneQ10 led to higher surface CH_4 emissions at the Assendelft site, reflecting amplified production at elevated temperatures but more variable emissions at the Weerribben site which may be due to the high WTD where TS plays less of a driving role. In contrast, increasing MethaneTRef reduced net CH_4 emissions by decreasing effective temperature sensitivity at prevailing site temperatures. This response reflects a structural property of the formulation because MethaneTRef and the associated rate constant are coupled.

Key parameters influencing methanogenesis include MethaneR0, MethanepHCorr, MethaneQ10, MethaneTref, AnaerobeLagFactor and PartialAnaerobe. MethaneR0, the base methanogenic rate, is positively correlated with CH_4 emissions, as expected. MethanepHCorr showed a negative relationship with surface CH_4 emissions. The role of this parameter is to correct for the pH sensitivity of methanogenesis. Increasing this parameter, decreases CH_4 production where maximum production occurs at pH 7. Delayed activation of anaerobic microbes after resaturation (Estop-Aragonés et al., 2013) is represented by the parameter, AnaerobeLagFactor, but was not found to impact CH_4 emissions. The parameter, PartialAnaerobe, represents the sensitivity of aerobic CH_4 production to water filled pore space. Its effect on net CH_4 emissions is site-specific where there parameter had a negative correlation with CH_4 emissions at the Assendelft site and a negative but muted affect at the Weerribben site. The fraction of each SOM pool accessible to methanogenesis (MethaneReservoirs), influences both CH_4 production and substrate turnover where the peat, microbial SOM, and litter and roots SOM pools showed most sensitivity.

https://doi.org/10.5194/egusphere-2026-2450
Preprint. Discussion started: 26 June 2026

Aerobic CH_4 oxidation is a key control on net CH_4 emissions where the impact of environmental conditions are further governed by parameters describing enzymatic kinetics and sensitivity to the environmental changes (Walter and Heimann, 2000; Walter et al., 2001). In aerobic conditions, CH_4 is oxidized following Michaelis-Menten enzyme kinetics using the parameters MethaneKm, MethaneVmax, and MethaneOxQ10. The parameter MethaneKm (the half-saturation constant) positively correlates with CH_4 emissions, as higher Km reduces oxidation efficiency at low concentrations. The MethaneVmax parameter, represents the maximum oxidation rate impacting methanotrophic capacity, and showed a negative correlation with surface CH_4 emissions, as expected. The parameter, MethaneOxQ10, is the Q10 value for methanotrophic activity. Increasing this value, decreases surface CH_4 emissions, as expected. Together, these results highlight the strong but context-dependent role of methanotrophic kinetics and soil aeration in regulating surface CH_4 emissions across peatland sites.

Plant-mediated transport through aerenchyma provides an efficient pathway for CH_4 to bypass aerobic soil layers and prevails as the dominant CH_4 emission pathway in many wet systems (Ueyama et al., 2023; Bansal et al., 2020). Methane which is transported through plant tissues via aerenchyma is dependent on the MethanePRateC, MethanePType, MethanePlantOx, and GrowFuncConst parameters (Walter and Heimann, 2000; Walter et al., 2001). MethanePRateC and MethanePType control the amount of plant transported CH_4 where both parameters play a correlating role with plant-mediated transport. MethanePlantOx represents the fraction of CH_4 that is oxidised in the root tips as CH_4 enters the plant's root from the soil, increasing this parameter, decreases surface CH_4 emissions. The capacity of the aerenchyma pathway to transport CH_4 gas is determined by LAI and GrowFuncConst, where GrowFuncConst showed a correlating relationship with plant-mediated transport, thereby decreasing CH_4 emissions transported by ebullition or diffusion. Instead of using the MethanePlantOx parameter, it may be possible to include a relationship between CH_4 oxidation at the root tip and the diameter of the root tip in future model developments. Similarly, a relationship between GrowFuncConst and stem diameter could also be used to make these parameters more closely relate to observed plant traits and shift the parameters towards observed of evidence based meanings. Linking these transport and oxidation parameters more explicitly to measurable plant traits, such as root tip or stem diameter, could improve both the mechanistic realism and empirical interpretability of plant-mediated CH_4 fluxes in peatland models.

In addition to biological controls, physical transport processes such as ebullition and diffusion strongly regulate the release of CH_4 from wetland soils to the atmosphere (Ueyama et al., 2023; Villa et al., 2021). The occurrence of ebullition and diffusion are dependent on the MethaneERateC, MethaneMaxConc and MethaneAir parameters. MethaneERateC is the ebullition rate constant, where increasing this increases the amount of ebullition, only evident at the Weerribben site where high WTD perists. MethaneMaxConc is the threshold for ebullition to occur. Changes were not detected in these runs, signalling that large changes to this threshold parameter may be required. The sensitivity analysis shows that initial CH_4 concentrations (InitMethane) did not hold a legacy effect in the model (Fig. SC5). The atmospheric CH_4 concentration (at the land surface), represented by the Atmos CH_4 parameter, influences diffusion between the atmosphere and the soil layer. Higher atmospheric CH_4 lowers the soil-to-air gradient, decreasing CH_4 emitted by diffusion. However, impacts were not observed in these sensitivity assessments. Together, these parameters determine the balance between episodic ebullition and continuous diffusive exchange, exerting a first-order control on the timing and magnitude of surface CH_4 emissions.

https://doi.org/10.5194/egusphere-2026-2450
Preprint. Discussion started: 26 June 2026

Overall, these results indicate that while the CH_4 module captures first-order CH_4 dynamics, introducing explicit microbial process representation would substantially improve its robustness, interpretability, and mechanistic congruence in CH_4-producing environments. For example, explicit living pools of methanogenic and methantrophic microorganisms are missing from the model and such representation could be the first step towards mechanistic representation of microorganisms, which are particularly important in CH_4 producing environments (Bahram et al., 2022).

The sensitivity of CH_4 emissions to changes in photosynthesis and autotrophic respiration related parameters discussed above (Sect. 5.2.1) reveals strong feedbacks within the model structure. These sensitivity results highlight that future model developments to improve the representation of photosynthesis and autotrophic respiration in response to environmental change, can substantially improve CH_4 emissions and the skill of the model overall (Li et al., 2016; Gao et al., 2025).

5.2.6 Sensitivity to land use management

Drained peatlands are subject to a range of land management practices. Although the Peatland-VU model does not yet include a full nitrogen cycle, the effects of harvest, manure, and grazing on CO_2 and CH_4 fluxes are represented. Where the timing of grazing and harvest showed substantial impacts (Fig. 12).

The grazing period is defined by two contrasting controls: biomass is removed (Grazed_frac) and manure is added (ManurefromGrazing) due to grazing. A later grazing onset (start) was associated with reduced CH_4 and R_h, whereas delaying the end of grazing increased both, reflecting the dominant effect of manure deposition and fresh substrate supply during the grazing period. As expected, the amount of biomass lost to grazing (GrazeFrac) showed a negative relationship with LAI. Increased manure inputs from grazing, allowed greater labile carbon available for heterotrophic respiration, methanogenesis and enhanced CH_4 emissions at the Weerribben site. One off manure additions did not lead to detectable effects.

Overall, variation of the harvest parameters produced comparatively modest effects where the timing of harvests led to a larger impact than the amount of harvest. The timing of harvest (HarvestDay) showed a negative relationship with biomass stocks and productivity, indicating that earlier harvests led to higher mean daily GPP, biomass and rootmass over the analysis period, possibly reflecting a longer effective regrowth period following early-season biomass removal. Whilst the other harvest parameters, HarvFrac, HarC, RecovT and HarvestLitter may impact fluxes subsequent harvest events but did not produce detectable effects on simulation mean fluxes.

Regarding the decomposition of the harvest pools, parameters primarily influenced the temporal variability of emissions rather than their overall magnitude. Increasing the fast decomposition rate ($k_{\mathrm{harvest,fast}}$) led to a strong increase in variability, while the effect of the slow pool ($k_{\mathrm{harvest,slow}}$) was similar but less pronounced. In contrast, increasing the fraction of material allocated to the slow pool ($\mathrm{harvest\_slow\_partition}$) reduced variability, reflecting a shift towards more gradual decomposition. Overall, harvest pool dynamics regulate the timing of emissions rather than their cumulative flux.

5.2.7 Sensitivity of soil profile

The soil physical or mechanistic state is built from the number and depths of soil horizons and detailed information describing the soil quality and structure. For each soil horizon the C/N ratio, dry bulk density (DBD), total SOM fraction (PercOrg),

https://doi.org/10.5194/egusphere-2026-2450
Preprint. Discussion started: 26 June 2026

respective SOM pool fractions (InitRes), pH, clay (ClayFraction) and sand (SandFraction) fractions, a freezing curve constant (FreezingCurve), pF values (pFVal), and Van Genuchten parameters are prescribed (Fig. SC6).

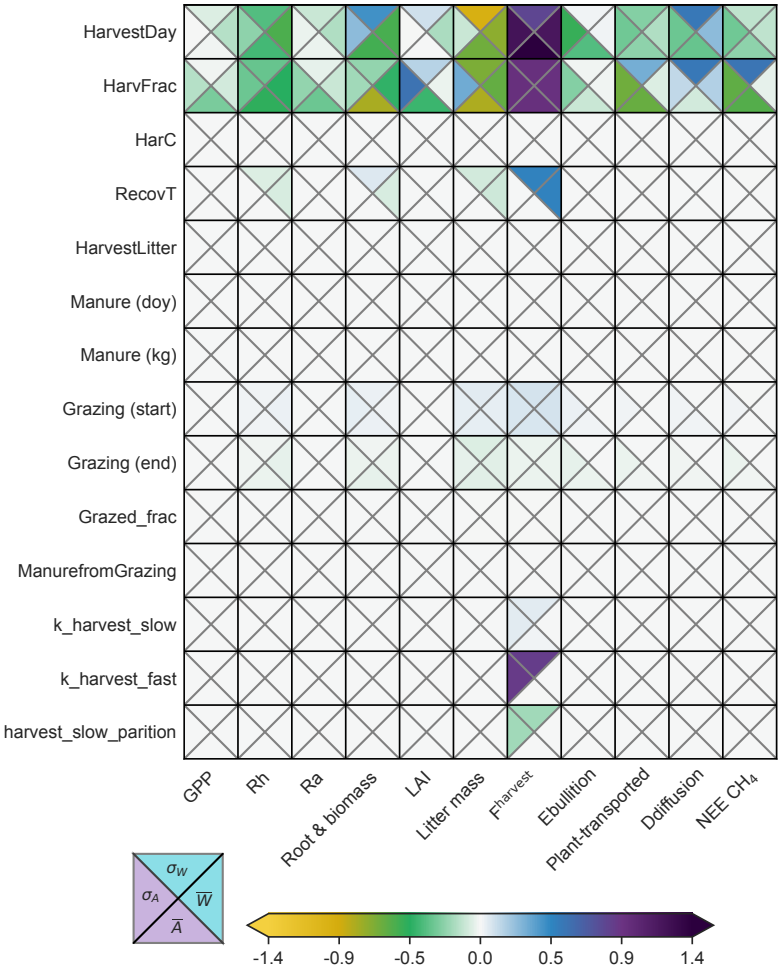

Figure 12. The sensitivity of harvest, manure, and grazing modules to environmental and parameter inputs.

Of the initial respective SOM pool fractions (InitRes), the fraction of the total SOM peat that is peat, showed the largest legacy effect on heterotrophic respiration and CH_4 emissions. The pH values (Layer_pH) played a role on heterotrophic respiration and CH_4 emissions, particularly in the upper and lower horizons (1, 2 and 5). The total SOM fraction (PercOrg) only impacted CH_4 emissions in the deepest horizon. Variations to the C/N ratio (CNRatio), DBD, clay and sand fractions, pF values, and freezing curve did not show lasting impacts on the magnitude or variability of model outputs, beyond the model spin-up, and within the tested parameter bounds.

The parameters used in the Van Genuchten relationship (theta_r_pF, theta_s_pF, alpha_pF_pF, n_pF, l_pF) which define the soil water retention curve and thus the relationship between soil moisture and matric potential were also tested. We found

https://doi.org/10.5194/egusphere-2026-2450
Preprint. Discussion started: 26 June 2026

that theta_s_pF, alpha_pF, and n_pF led to impacts on heterotrophic respiration and CH_4. The effects of alpha_pF and n_pF were concentrated in the upper horizons, where small changes in water retention strongly affect oxygen availability and thus aerobic-anaerobic partitioning. In contrast, theta_s_pF influenced fluxes across all horizons, reflecting its role in setting overall soil moisture storage and therefore the extent and persistence of anaerobic conditions. In contrast, theta_r_pF and l_pF, which control residual water content and pore connectivity/tortuosity respectively, showed little effect, likely because they primarily influence the extremes of the moisture range or hydraulic conductivity rather than the mid-range soil moisture conditions that govern aerobic-anaerobic partitioning in this model.

5.2.8 Sensitivity of soil thermal modules

Here, we report on the efficacy of the new analytical soil thermal model and then discuss the sensitivity of three soil thermal modules to environmental driver, TS, and input parameters. The classical thermal module was calibrated against the in situ soil temperature profile at the Assendelft site, achieving high agreement shown by a concordance correlation coefficient > 0.98 (van den Berg et al., 2026). A comparison of the three soil thermal modules shows that the seasonal sinusoidal formulation captures the mean seasonal variation but fails to reproduce extreme warm and cold periods (Fig. SC8). In contrast, the new analytical diffusion module effectively captures temperature extremes, but may overestimate the efficiency of heat propagation downwards through the soil column.

Surface soil temperature (TS) exerted a strong control on simulated soil thermal profiles, although the response differed across the three thermal modules (Fig. SC7). In all thermal modules, increases in TS propagated through the soil profile, leading to warmer conditions. However, the response diverged between sites and formulations. While all modules showed sensitivity to the surface TS at Weerribben, only the classic explicit heat transport module responded consistently across both sites. The initial thermal profile (Tdepth and initial SoilTemp) did not lead to large effects in any thermal model. Increasing the time lag parameter (ThermTime_lag) increased the soil temperature profile whereas the vertical dampening parameter (ThermDamp_lag) did not lead to detectable effects on magnitude or variability in the analytical thermal diffusion module.

Within the classic module, both vegetation insulation (VegTScalingFactor) and the depth of the simulated thermal domain (MaxDepthHeat) impacted the thermal profile. Increasing MaxDepthHeat at the Weerribben site led to enhanced ebullitive CH_4 fluxes at the surface likely due to enhanced production in deeper soil layers. Similarly, increasing VegTScalingFactor substantially raised soil temperatures at both sites, leading to higher CH_4 emissions and R_h, as well as enhanced transfer of litter into deeper SOM pools. Notably, VegTScalingFactor showed a strong influence on the variability of fluxes than on their mean magnitude. Parameters associated with snow processes (MaxSnowdepth, SnowMeltrate, DayMaxSnowdepth) did not produce detectable effects, despite the occurrence of sub-zero air temperatures at both sites, suggesting a limited role of snow insulation under the simulated conditions. These results highlight that the choice of thermal module can substantially influence model behaviour and should be aligned with the intended application.

https://doi.org/10.5194/egusphere-2026-2450
Preprint. Discussion started: 26 June 2026

5.2.9 Sensitivity of water table module

The internal groundwater table module (Fig. 13) is primarily controlled by the minimum groundwater depth (MinGW), evaporation, and drainage spacing (DrainageDist). The parameters, RunoffThreshold, WatertableInit, Ksat, and DrainLevel did not lead to large impacts on the WTD or subsequent feedbacks. Evaporation is regulated by the evaporation constant (EvapCorrection), correction for pooled water (OpenWaterFactor), correction due to vegetation (CropFactor). Increasing MinGW raised water table depth at the Assendelft site but had little effect at Weerribben. Lower EvapCorrection values, reduced evaporation, and increased both the height and variability of the water table. Increasing the CropFactor parameter, increased evaporation which lowered the water table and reduced its variability. Increasing the OpenWaterFactor parameter, increased evaporation which decreased the water table depth at Assendelft only. Increasing precipitation (PR) raised the WTD, increased the soil moisture values and net CH_4 fluxes while decreasing heterotrophic respiration at the Assendelft site. Increasing evapotranspiration (ET) lowered the water table whilst increasing WTD variability with comparable results for soil moisture and decreased net CH_4 emissions.

https://doi.org/10.5194/egusphere-2026-2450
Preprint. Discussion started: 26 June 2026

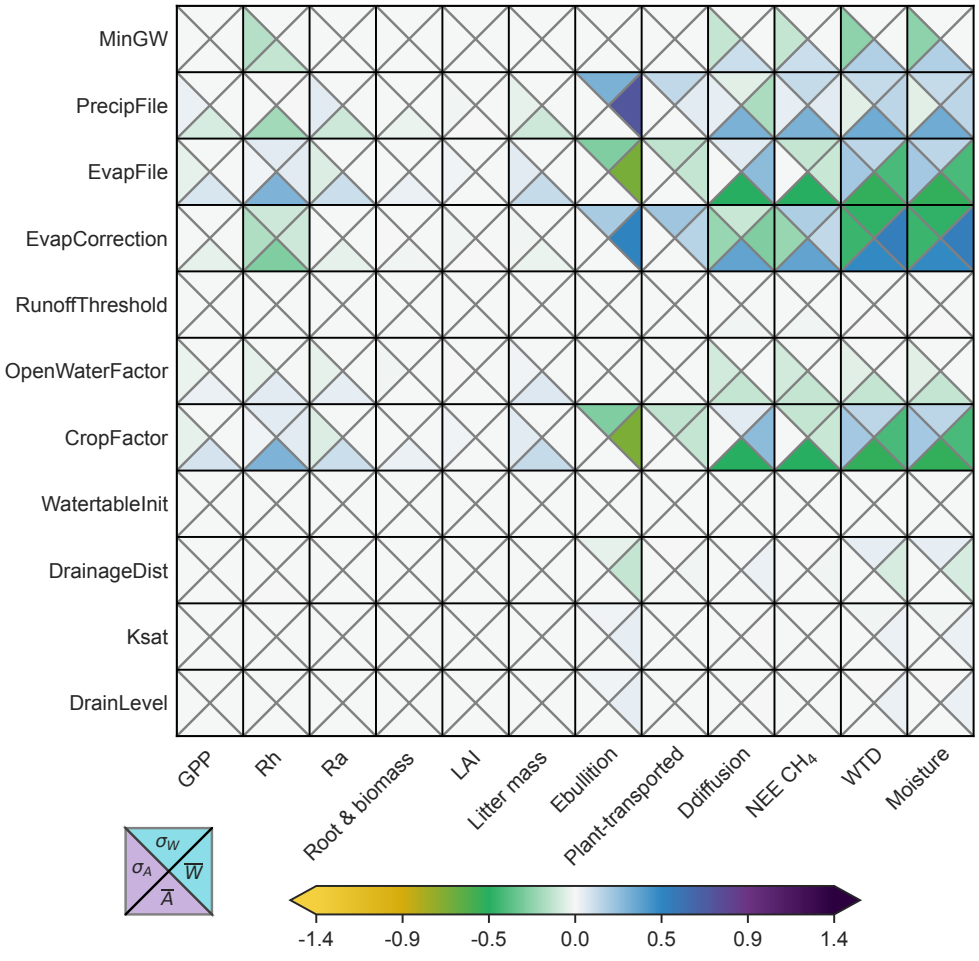

Figure 13. The sensitivity of the water table module.

6 Conclusions

This study investigated the interplay of environmental controls, plant-soil interactions, and parameter sensitivities in shaping carbon cycling within the Peatland-VU v3.0 model. Peatland-VU v3.0 demonstrates a consistent ability to reproduce observed patterns and magnitudes of GPP, Reco, $\mathrm{NEE}_{\mathrm{CO_2}}$, and $\mathrm{NEE}_{\mathrm{CH_4}}$ fluxes across two contrasting peatland systems. As expected, the production and autotrophic respiration modules exert strong control over model behaviour, reflecting their central role in ecosystem functioning. The model provides a useful framework for exploring greenhouse gas dynamics across drained and natural peatlands, and for evaluating management interventions aimed at reducing emissions and restoring ecosystem function. While many expected ecosystem responses are captured, several areas for improvement remain, including the implementation of mechanistic microbial processes, a full Farquhar photosynthesis scheme, a fully dynamic phenology module, incorporation

https://doi.org/10.5194/egusphere-2026-2450
Preprint. Discussion started: 26 June 2026

of a complete nitrogen cycle, and improved representation of peat development. The site-specific nature of the model serves as a framework for accessible integration of emergent processes, while remaining computationally efficient on standard hardware and readily transferable to new sites. This study has highlighted both the strengths of the model and key avenues for future development. The Peatland-VU v3.0 model therefore represents a useful tool for both applied peatland management and the development of process-based understanding under changing environmental conditions.

Code and data availability. A frozen copy of the code and the input files used to produce the results used in the model validation are available from a zenodo repository (https://doi.org/10.5281/zenodo.19816805, Lippmann et al. (2026)). Updated versions of both the code and model input files are available in the repository (bitbucket.org/peatland_modellers/peatland-vu-public).

Author contributions. Model developments: KvH, MvdB, TJRL equally contributed. Model parametrisation: MvdB, TJRL, KvH. Preparation of flux and input data: MvdB, VB. Wrote the original manuscript and performed all analysis: TJRL. All authors reviewed the draft manuscript. Overall concept and development of study: TJRL, MvdB, KvH, YvdV. Secured funding: YvdV.

Competing interests. The authors declare no competing interests are present.

Acknowledgements. We warmly thank Jim Boonman, Corrine van Huissteden, Alex Buzacott, Bart Kruijt and all those involved in the collection of field data. TJRL was supported by Horizon Europe AVENGERS (101081322). All authors were supported by Netherlands Research Program on Greenhouse gas dynamics in Peatlands and organic soils (NOBV), funded by the Dutch Ministry of Agriculture, Nature and Food Quality.

https://doi.org/10.5194/egusphere-2026-2450
Preprint. Discussion started: 26 June 2026

Appendix A: Overview of model inputs

Table A1. Environmental forcings

Driver	Unit	Resolution	Requirement
Air temperature	°C	daily	Either air or soil temperature is required
Soil temperature	°C	daily	Either air or soil temperature is required
PAR	umol m^{-2} s^{-1}	daily	Either PAR or total daily radiation is required for the calculation of GPP
Total daily radiation	J m^{-2}	daily	Either PAR or total daily radiation is required for the calculation of GPP
Water table	m below surface	daily	Optional.
Soil moisture	m^3 m^{-3}	daily	Optional.
Atmospheric CO_2	ppm	yearly	Optional. Used to calculate NPP by Haxeltine and Prentice (1996) only.
Snow depth	m	daily	Optional.
NPP	kg C m^{-2} day^{-1}	daily	Instead of calculating GPP and plant respiration, NPP values can also be provided as input.
Precipitation	mm	daily	Necessary if calculating WTD
Evapotranspiration	mm	daily	Necessary if calculating WTD

Table A2. Land management forcings

Driver	Unit
Harvest day of year	day number
Harvest dates	DD/MM/YY
Fraction of biomass harvested	-
Grazing (start)	day of year
Grazing (end)	day of year
Grazing (manure added)	kg day^{-1}
Grazing (biomass lost)	kg day^{-1}
Manure (day)	day of year
Manure (kg)	kg

https://doi.org/10.5194/egusphere-2026-2450
Preprint. Discussion started: 26 June 2026

Table A3. Soil forcings

Soil property	Unit	Description
C/N ratio	gC/gN	C/N ratio for each soil horizon
DBD	kg m^{-3}	Dry bulk density of each soil horizon
Horizons	-	Depth of soil horizons
Initial OM fraction	-	Initial fraction of OM found in each SOM reservoir in each soil horizon
Total OM	%	Percentage of total dry weight that is OM for each horizon
pH	pH	pH of each horizon
Soil horizons	-	Number of soil horizons
Sand fraction	-	Fraction of each soil horizon that is sand
Clay fraction	-	Fraction of each soil horizon that is clay
pF curve	m^3 m^{-3}	pF curve per soil horizon
pF potential	log cm H_2O	Soil moisture potential for each soil horizon

Appendix B: Existing model processes

B1 Photosynthesis and autotrophic respiration

The calculation of C3 photosynthesis, leaf respiration, and net primary production (NPP) follows a modified implementation of the primary production module introduced in PV v2.0 (Mi et al., 2014), itself adapted from the BIOME3 equilibrium biosphere model (Haxeltine and Prentice, 1996). The approach assumes that both photosynthetic carbon uptake and leaf respiration are governed by the activity of Rubisco-associated processes in chloroplasts. Photosynthesis is calculated using stomatal conductance and Rubisco activity:

$$\mathrm{GPP}(t) = \frac{J_E(t) + J_C(t) - \sqrt{(J_E(t) + J_C(t))^2 - 4 \cdot J_E(t) \cdot J_C(t)}}{20 \cdot WSF(t)} \tag{B1}$$

where J_E [kg C m^{-2} day^{-1}] is the light-limited rate of photosynthesis determined by photosynthetically active radiation (PAR), and J_C [kg C m^{-2} day^{-1}] is the rate constrained by Rubisco activity.

R_a is calculated as:

$$R_a(t) = R_a^{\mathrm{leaf}}(t) + \frac{R_a^{\mathrm{growth}}(t)}{T_{year}} + \frac{\int_z^0 R_a^{\mathrm{root}}(t)dz}{T_{year}} \tag{B2}$$

R_{leaf} [kg C m^{-2} day^{-1}] and R_{root} [kg C m^{-3} day^{-1}] correspond to leaf and root respiration, respectively. The factor T_{year} converts the original BIOME3 annual respiration terms (R^a_{root} and R^a_{growth}) to daily values. Total daily root respiration is calculated from root growth distributed across the soil profile according to the prescribed root distribution.

$$R_a^{\mathrm{leaf}}(t) = b \cdot V_m(t) \tag{B3}$$

https://doi.org/10.5194/egusphere-2026-2450
Preprint. Discussion started: 26 June 2026

where, b [-] is the leaf respiration coefficient, and V_m [kg C m^{-2} day^{-1}] represents the maximum daily rate of net photosynthesis.

$$J_E(t) = C_1(t) \cdot \mathrm{FPAR}(t) \cdot \mathrm{PAR}(t) \tag{B4}$$

where J_E [kg C m^{-2} day^{-1}] is the light-limited photosynthetic rate, C_1 [kg mol^{-1}] is a model coefficient defined below, FPAR [-] is the fraction of incoming PAR intercepted by vegetation, and PAR [mol m^{-2} day^{-1}] denotes incoming photosynthetically active radiation.

$$C_1(t) = \frac{p_i - \Gamma}{pi + \Gamma} \cdot C_{\mathrm{mass}} \cdot \phi_c(t) \cdot \phi_T(t) \cdot \alpha_a \cdot \alpha \tag{B5}$$

where α [-] denotes the intrinsic quantum efficiency for CO2 uptake (0.08), α_a [-] is a scaling factor (0.5), and $C\mathrm{mass}$ [kg mol^{-1}] is the molar mass of carbon (0.012 kg mol^{-1}). Furthermore, p_i [Pa] represents the intercellular CO_2 partial pressure and Γ [Pa] is the CO_2 compensation point.

ϕ [-] is calculated:

$$\phi_(t) = TFL(t) \cdot TFH(t) \tag{B6}$$

where, TFL [-] and TFH [-] represent temperature stress factors for low and high temperatures, respectively:

$$TFL(t) = \frac{1}{1 + e^{T1 \cdot (T2 - T(t))}}, \tag{B7}$$

$$TFH(t) = 1 - 0.01 \cdot e^{T3 \cdot (TA(t) - TA_{\max})} \tag{B8}$$

where, T1 [°C $^{-1}$], T2 [°C $^{-1}$], T3 [°C $^{-1}$] are constants:

$$T1 = \frac{2 \cdot \ln(1/0.99 - 1)}{T_{MinPhoto} - T_{\min}}, \tag{B9}$$

$$T2 = \frac{\ln(0.99/0.01)}{2 \cdot T_{MinPhoto} + T_{maxopt}}, \tag{B10}$$

$$T3_p = \frac{\ln(0.99/0.01)}{T_{MaxPhoto} - T_{maxopt}} \tag{B11}$$

J_C [kg C m^{-2} day^{-1}] describes the Rubisco limited rate of photosynthesis:

$$J_C(t) = C_2 \cdot V_m(t) \tag{B12}$$

C_2 [-] is a dimensionless coefficient defined below, and V_m [kg C m^{-2} day^{-1}] denotes the maximum attainable daily rate of net photosynthesis.

$$V_m(t) = \frac{\mathrm{FPAR}(t) \cdot \mathrm{PAR}(t)}{b} \cdot \frac{C_1}{C_2} \cdot (s(t) \cdot (2 \cdot \theta - 1) - \sigma(t) \cdot (2 \cdot s(t) \cdot \theta - C_2)) \tag{B13}$$

https://doi.org/10.5194/egusphere-2026-2450
Preprint. Discussion started: 26 June 2026

σ [-] is defined by the equations below, s [kg C m^{-2}] is obtained from Eq. SB15, and θ [-] is the co-limitation constant, set to 0.7.

$$\sigma(t) = \sqrt{1 - \frac{C_2 - s(t)}{C_2 - \theta \cdot s(t)}} \tag{B14}$$

$$s(t) = \frac{Rr}{DL(t)} \tag{B15}$$

DL [day^{-1}] corresponds to the photoperiod (day length).

$$C_2 = \frac{p_i - \gamma}{p_i + KC \cdot KCC} \tag{B16}$$

γ [-] is a dimensionless constant set to 0.7. The variable O_2 [Pa] represents the oxygen partial pressure, while K_C [Pa] is the Michaelis constant for CO2 (30 Pa). The coefficient KCC [-] is determined using Eq. SB17.

$$KCC = \frac{O_2}{K0} + 1 \tag{B17}$$

$K0$ [Pa] is the Michaelis constant for O_2 and has value 0.03, O_2 [Pa] represents the partial pressure of oxygen and has value 20,900.

$$\Gamma = \frac{O_2}{2 \cdot \tau} \tag{B18}$$

τ [-] is a dimensionless parameter describing Rubisco specificity for CO_2 relative to O_2, and has a value of 2,600.

$$pi = \Gamma \cdot pa \tag{B19}$$

p_a [Pa] denotes the atmospheric partial pressure of CO_2, while γ [-] is a dimensionless constant equal to 0.7.

B2 Carbon allocation

Plant growth is partitioned between above-ground and below-ground tissues using a fixed shoot-to-root allocation scheme. As the formation of leaves and shoots constitutes a major resource demand, both shoot and root production are derived from NPP using prescribed allocation fractions. The fractions assigned to shoot and root growth sum to one, such that total NPP is conserved. Growth is therefore calculated according to:

$$SM(t) = RS \cdot NPP(t) \tag{B20}$$

SM [kg C m^{-2} day^{-1}] represents the rate of shoot growth and RS [-] defines the allocation ratio between shoot and root production. The size of the living above-ground biomass pool (Eq. B21) is determined by the balance between shoot production (Eq. B20) and biomass losses through senescence to the litter layer:

$$\frac{\delta}{\delta t} CB(t) = SM(t) - BS(t) \cdot CB(t) \tag{B21}$$

where, BS [day^{-1}] represents the fraction of above-ground biomass littered each day and is set to KL [day^{-1}] during Autumn for deciduous plants.

https://doi.org/10.5194/egusphere-2026-2450
Preprint. Discussion started: 26 June 2026

B3 Root growth

The representation of roots follows the soil discretisation used by the model, with root mass and root distribution allocated across layers based on their depth and physical characteristics. Soil organic matter pools are likewise distributed vertically through the profile. The production of new roots (R_d) is then calculated from NPP using a fixed allocation relationship between shoot and root growth:

$$Rd(t,z) = (1 - RS) \cdot NPP(t) \cdot f(z) \tag{B22}$$

where $1 - RS$ represents the proportion of growth allocated to roots, and $f(z)$ [m^{-1}] describes the vertical root distribution between the soil surface and the prescribed maximum rooting depth (MRD). Both root biomass and root density decline exponentially with depth and are constrained to the rooting zone defined by MRD.

$$\int_{-MRD}^{0} f(z)dz = 1 \tag{B23}$$

$$\frac{\delta}{\delta t} RM(t,z) = Rd(t,z) - RX(t,z) - RDR(t,z) \tag{B24}$$

where RM [kg C m^{-3}] is the root mass, while RDR [kg C m^{-3} day^{-1}] describes the loss of root biomass through root senescence. In the model, root exudates (RX, Eq. B25) are parameterised as a prescribed fraction of root production (R_d):

$$RX(t,z) = Rd(t,z) \cdot f(KSP_{(DoY)}) \cdot REX(t) \tag{B25}$$

where DoY corresponds to the day of year, REX [-] is a unitless factor governing root exudation, and $f(KSP)$ [-] is a parameter-dependent modifier that can be applied to simulate elevated spring exudation. Root turnover is calculated from the existing root biomass and the prescribed senescence coefficient:

$$RDR(t,z) = RM(t,z) \cdot RSX \tag{B26}$$

where RSX [day^{-1}] is the first-order rate constant governing root senescence.

B4 Biomass senescence

During the growing season, a constant turnover of biomass is calculated, representing senescence due to age or damage:

$$Fs(t) = AB \cdot dt \tag{B27}$$

During autumn and winter, the rate of aboveground living biomass senescence is calculated as a function of changing LAI Eq. B28. Decreased LAI leads to increased litterfall.

$$Fs(t) = \frac{LAI_{(t-1)} - LAI(t)}{LAI_{(t-1)}} \tag{B28}$$

Aboveground biomass is then re-calculated:

$$Ba = Sb_{(t-1)} \cdot (1 - Fs(t)) \tag{B29}$$

https://doi.org/10.5194/egusphere-2026-2450
Preprint. Discussion started: 26 June 2026

B5 Litter addition and decomposition

Carbon released from senescing above-ground biomass is added to the litter pool (Eq. B30).

$$\frac{\delta}{\delta t}LL(t) = LLp(t) - LLl(t) - LLd(t) \tag{B30}$$

where,

$$LLp(t) = BS \cdot CB(t) \tag{B31}$$

$$LLl(t) = \frac{TA_{(t)}}{KT} \cdot LC \cdot LL(t) \tag{B32}$$

$$LLd(t) = LL(t) \cdot e^{keL} \tag{B33}$$

LL_p [kg C m^{-2} day^{-1}] corresponds to litter production and LL_l [kg C m^{-2} day^{-1}] denotes the transfer of litter carbon to the soil SOM pool. During autumn, the senescence parameter for deciduous vegetation, BS [day^{-1}], is set equal to K_L [day^{-1}]. The parameter LC [day^{-1}] defines the proportion of litter converted to SOM each day. Temperature effects are referenced to K_T [°C], with T_A [°C] representing daily air temperature. No litter decomposition is assumed to occur when T_A is below freezing. The term ke_L [kg C m^{-2} day^{-1}] describes the environmentally adjusted litter decomposition flux.

B5.1 Resistant SOM priming sensitivity

Enhanced decomposition of resistant SOM occurs upon addition of easily decomposable material. Increased microbial activity due to the increased availability of easily decomposable compounds can also lead to enhanced decomposition of resistant SOM. For this reason, the decomposability of the resistant SOM reservoirs (i.e. peat and humus) is dependent on the amount of root growth:

$$fprim(t,z) = 1 + rm(t,z) \cdot fgrow(t) \cdot fspring \tag{B34}$$

where, fprim [-] is the SOM decomposition sensitivity to fresh root growth, fspring [-] is a spring correction constant, fgrow [-] represents a root growth factor, and rm [kg C m-2] represents the root mass.

$$fgrow(t) = \frac{NPP(t) - minpp}{manpp - minpp} \tag{B35}$$

NPP [kg C m-2 day-1] is the net primary productivity, manpp [kg C m-2 day-1] and minpp [kg C m-2 day-1] represent the constants for the maximum and minimum NPP.

B5.2 SOM decomposition sensitivity to soil aeration

For the effect of soil dryness, we assumed a linear decrease of fm from 1.0 to 0.2 between pF 2.7 and pF 4.2 (wilting point). For the effect of soil moisture on aeration we apply a linear relation of the aeration factor on soil water content, which lets fae decline from 1 to 0 between a pore water saturation from 80% to 100%.

$$fae(t,z) = 1 - \frac{(1 - pF2) * (MP_{(z)} - pF1)}{pF3 - pF2} \tag{B36}$$

https://doi.org/10.5194/egusphere-2026-2450
Preprint. Discussion started: 26 June 2026

where, fae [-] represents the correction factor for soil aridity, pF1 [-], pF2 [-], and pF3 [-] are pF constants, and MP [-] represents the matric potential correction.

B5.3 SOM decomposition sensitivity to soil moisture

$$fm(t,z) = \frac{sm(t,z)}{2 \cdot sc(1 - rm(t,z) \cdot rac)} \tag{B37}$$

where, fm [1/kg C m-2] represents the sensitivity of SOM decomposition to soil moisture, sm [-] represents the fraction of water filled pore space, sc [-] represents the soil moisture constant, and rac [-] represents the root aeration constant.

B5.4 SOM decomposition sensitivity to soil pH

$$fpH_{(z)} = \frac{1}{1 + e^{-2.5(pH_{(z)} - 5)}} \tag{B38}$$

where, pH represents the soil pH and fpH represents the sensitivity of SOM decomposition to soil pH.

B6 Methane

B6.1 Methane oxidation

Microbial oxidation of CH_4 can occur in both aerobic and anaerobic soil layers, where microbial activity (methanotrophy) is also dependent on soil temperature:

$$Rox(t,z) = \frac{MethaneV_max \cdot C_{CH_4}((t,z))}{MethaneKm + C_{CH_4}} \cdot MethaneOxQ10^{\frac{TA(t,z) - TA_{mean}}{10}} \tag{B39}$$

where, MethaneV_max [µmol day^{-1}], MethaneKm [µmol], MethaneOxQ10 [-] are constants. C_{CH_4} denotes the CH_4 concentration.

B6.2 Plant-mediated transport

Plant-mediated CH_4 transport is controlled by two main processes. The first is the size and vertical distribution of the root system, which determine the capacity of CH_4 to enter plant tissues. Larger root biomass and deeper rooting profiles provide a greater interface for CH_4 uptake from the soil. During transport through the oxic rhizosphere surrounding root tips, a portion of the CH_4 can be oxidised before entering the plant (Ström et al., 2005). This process is represented by the dimensionless oxidation parameter $PlOx$ (Eq. B41).

The second control is the efficiency with which CH_4 is transported through plant tissues and released to the atmosphere. This transport capacity is associated with the development of aerenchyma, which provides low-resistance pathways for gas movement.

$$Qpl(t,z) = -cP \cdot vP \cdot \mathrm{LAI}(t) \cdot f((z)) \cdot C_{CH_4,t,z} \tag{B40}$$

https://doi.org/10.5194/egusphere-2026-2450
Preprint. Discussion started: 26 June 2026

The dimensionless parameter vP [-] characterises the effectiveness of the vegetation in conducting CH_4 through above-ground tissues. Qpl [μM m^{-3} day^{-1}] is the rate of plant-mediated CH4 transport, cP [m^{-2} day^{-1}] is a rate constant with a value of 0.24, $f(z)$ [m^{-1}] denotes the exponential root distribution (Eq. B23), and CCH_4 [μM m^{-3}] is the CH_4 concentration. Integrating the transport rate over the rooting zone yields the net plant-mediated CH_4 flux at the surface:

$$Fpl(t) = \int_{MRD}^{0} \left[Qpl(t,z) \cdot (1 - PlOx)\right] dz \tag{B41}$$

where Fpl [μM m^{-2} day^{-1}] represents the total CH_4 flux transported through vegetation to the atmosphere.

B6.3 Methane diffusion

The transport of CH_4 gas through soil is an outcome of plant mediated transport (described above), ebullition (described below), and molecular diffusion. The amount of gas transported by molecular diffusion is largely determined by the soil's porosity and moisture. It is also possible for atmospheric CH_4 to enter the soil column through molecular diffusion.

Molecular diffusion is calculated through air filled pore space is calculated using Fick's first law:

$$Fdiff_{t,z} = -D_{CH_4,z} \cdot \frac{\delta}{\delta z} C_{CH_4,t,z} \tag{B42}$$

where $Fdiff_{t,z}$ [μM m^2 day^{-1}] represents the CH_4 flux due to molecular diffusion and D [-] is the CH_4 diffusion coefficient at depth z. The coefficient is calculated using the Penman approach with a tortuosity factor of 0.66:

$$D_{CH_4,z} = D_i \cdot 0.66 \cdot f_{coarse} \tag{B43}$$

where D_i equals 1.728 m^2 day^{-1} in aerated soil and 1.728×10^{-4} m^2 day^{-1} under saturated conditions (Walter and Heimann, 2000). The factor f_{coarse} [-] accounts for the proportion of coarse pore space available for gaseous diffusion (Walter and Heimann, 2000). Methane concentrations are defined at layer midpoints, while diffusion coefficients are evaluated at the boundaries between adjacent layers. The following lower boundary condition is applied:

$$\frac{\delta}{\delta z} C_{CH_4,t,z=nsoil} = 0 \tag{B44}$$

and the upper boundary condition:

$$\frac{\delta}{\delta z} C_{CH_4,t,z=u+0.04m} = C_{atm} \tag{B45}$$

where, u is either the WL or the soil surface, C_{atm} is the atmospheric CH_4 concentration (0.076 μ M) Walter and Heimann (2000).

https://doi.org/10.5194/egusphere-2026-2450
Preprint. Discussion started: 26 June 2026

B6.4 Methane ebullition

Methane gas bubbles can bypass this microbial sink due to their rapid rise through the saturated water column leading to an enhanced CH_4 flux to the atmosphere:

$$Feb(t) = \int_{z=nsoil}^{WL(t)} Qeb(t,z)dz \tag{B46}$$

where F_{eb} [μM m^{-2} day^{-1}] denotes the surface ebullition flux and $nsoil$ [m] defines the lower boundary of the simulated soil profile. When the water table is located at or above the soil surface, the ebullitive CH_4 is released directly to the atmosphere. Under unsaturated surface conditions, CH_4 transported upward by ebullition is instead transferred to the uppermost saturated-unsaturated soil layer and added to the CH_4 pool of the lowest unsaturated soil layer.

$$Qeb(t,z) = -k_m \cdot f(C_{CH_4}) \cdot (C_{CH_4,t,z} - MethaneMaxConc) \tag{B47}$$

where k_m [day^{-1}] is an empirical rate constant equal to 1/24. The function $f(C_{CH_4})$ is a threshold function that takes a value of 1 when the CH4 concentration, CCH_4, exceeds the threshold concentration C_{thresh} and 0 otherwise. Consequently, ebullition is only activated when CH_4 concentrations are greater than the prescribed maximum concentration, $MethaneMaxConc$. For soil layers located above the water table, Qeb is assumed to be zero.

Table B1. Soil organic matter pools represented by the model, their respective rates of aerobic decomposition (k), and their contributing sources.

SOM pool	k (Weerribben)	k (Assendelft)	Source
Peat	0.01	0.01706	Inert carbon from all other SOM pools
Liquid manure	-	-	Manure additions from model inputs
Solid manure	-	-	Manure additions from model inputs
Root exudates	3.0	2.56089	Root exudation as a fraction of root growth
Litter and dead roots	0.2	0.17794	Above-ground biomass die off and root die off
Microbial biomass	0.3	0.30265	Old carbon transferred from the decomposition of litter & dead roots, root exudates, peat
Humus	0.02	0.02297	Old carbon transferred from the decomposition of litter & dead roots, root exudates, peat

https://doi.org/10.5194/egusphere-2026-2450
Preprint. Discussion started: 26 June 2026

Appendix C: Sensitivity testing

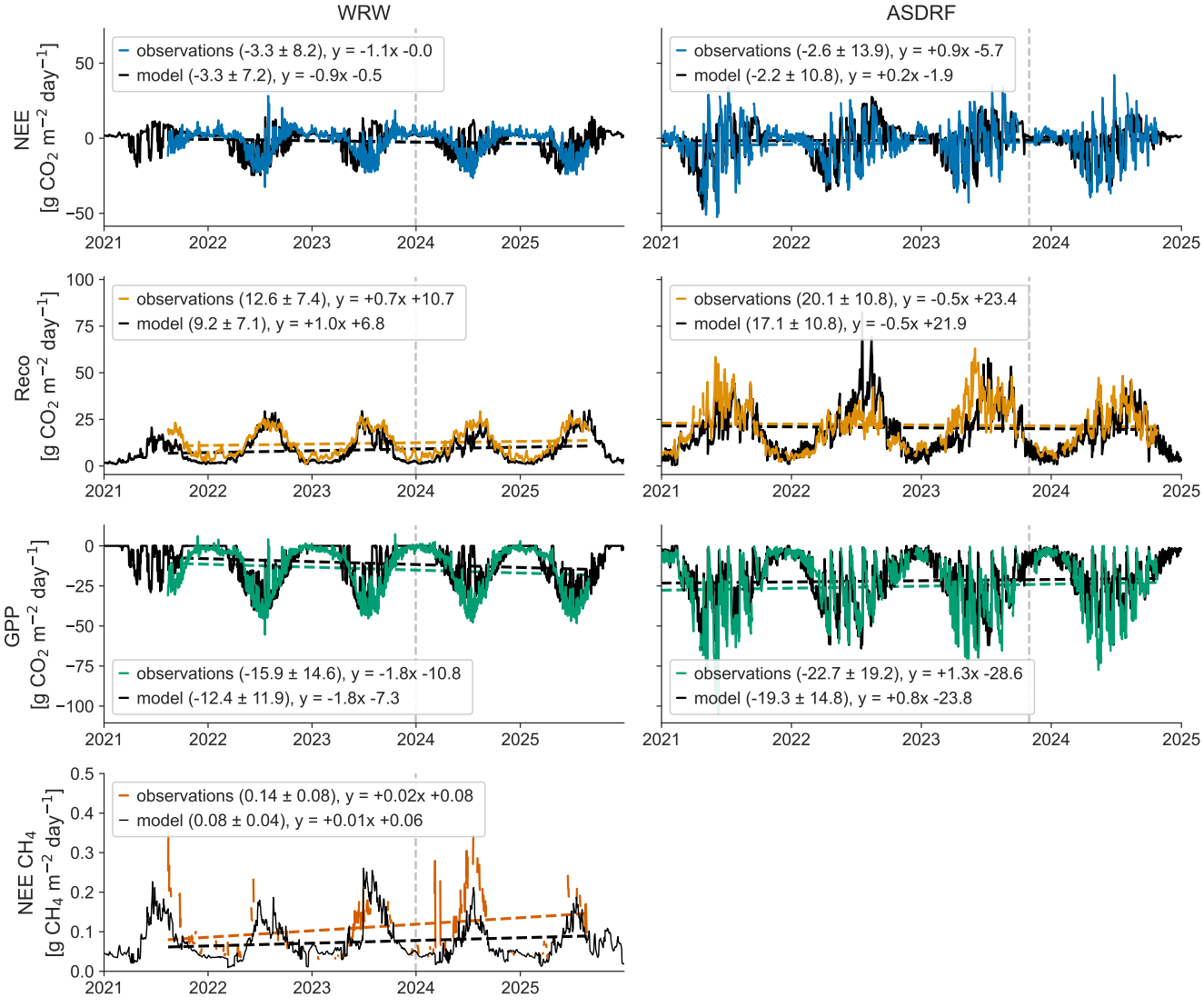

Figure C1. The model simulation results from the parameter sets used to evaluate the sensitivity of of the Shaver NPP, Arrhenius, phenology, CH_4, and SOM decomposition modules, as well as the soil profile.

https://doi.org/10.5194/egusphere-2026-2450
Preprint. Discussion started: 26 June 2026

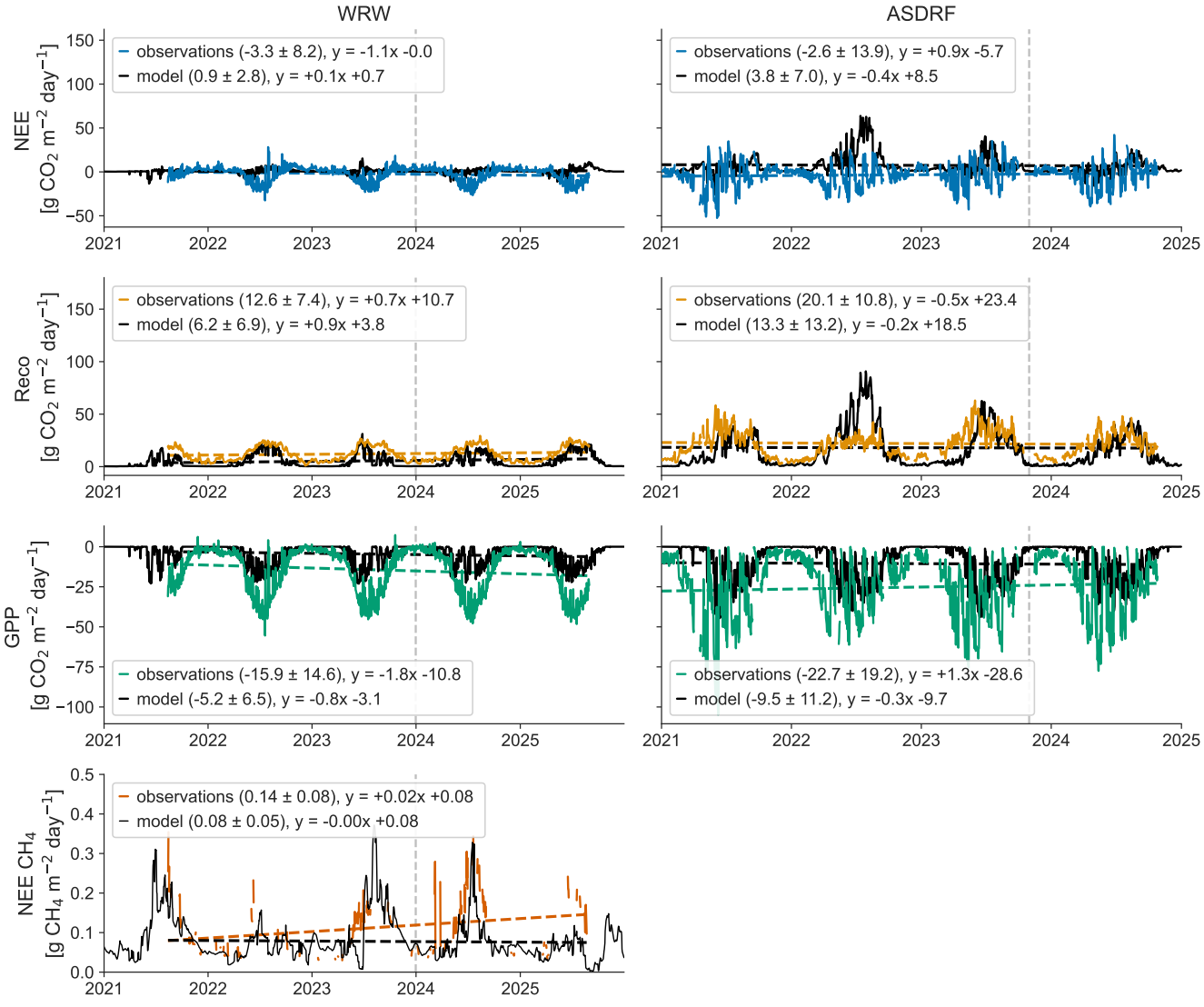

Figure C2. The model simulation results from the parameter sets used to evaluate the sensitivity of the BIOME3 NPP, Q10, CH_4, and management modules.

https://doi.org/10.5194/egusphere-2026-2450
Preprint. Discussion started: 26 June 2026

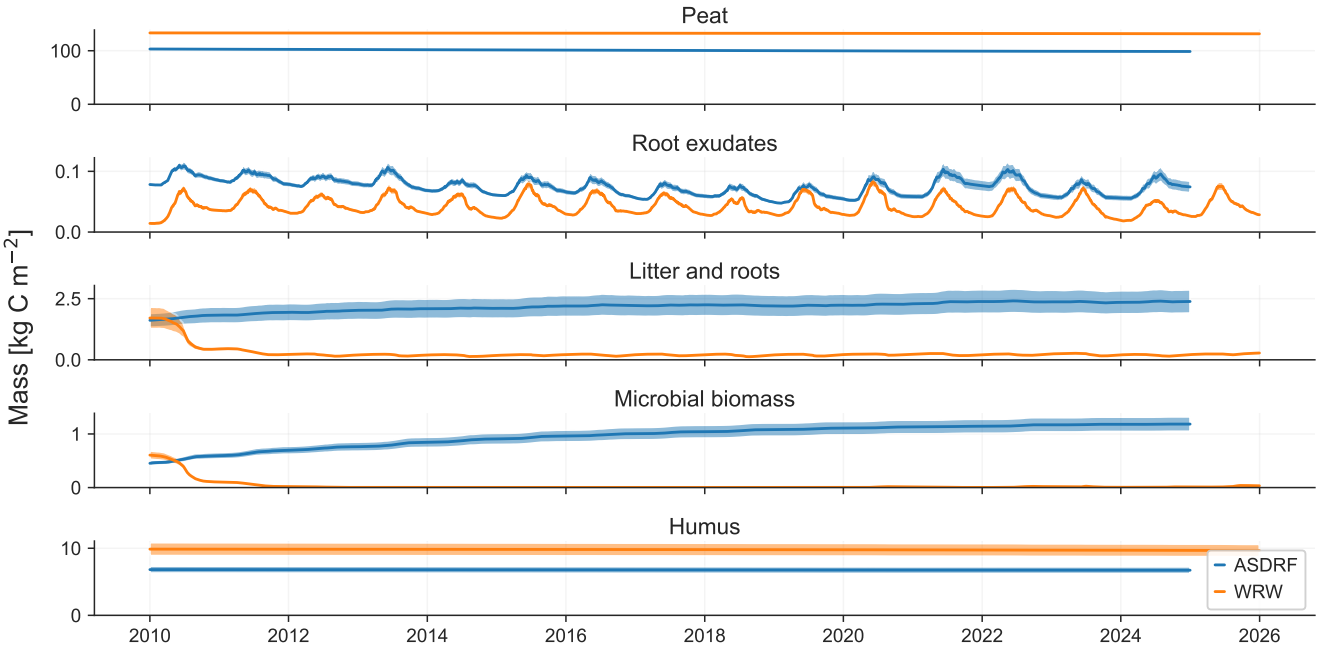

Figure C3. The stabilisation of the SOM pools. The sum (solid line) and standard deviation (shaded) of the mass of all soil layers is plotted for each SOM pool.

https://doi.org/10.5194/egusphere-2026-2450
Preprint. Discussion started: 26 June 2026

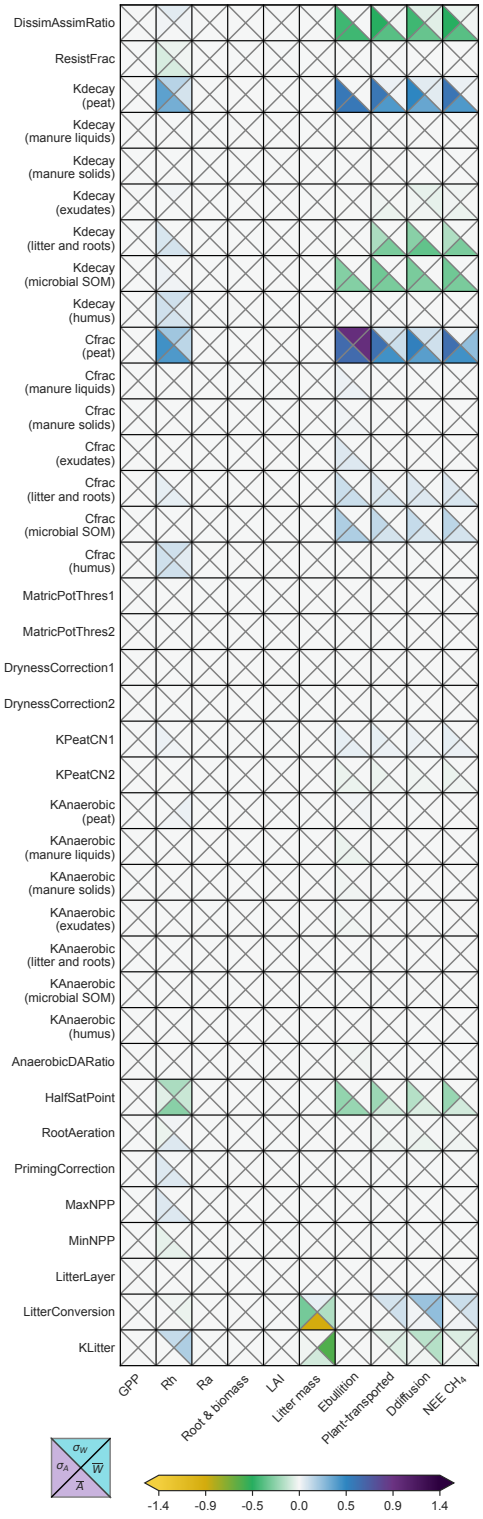

Figure C4. The sensitivity of all parameters within the SOM decomposition module to environmental and parameter inputs.

https://doi.org/10.5194/egusphere-2026-2450
Preprint. Discussion started: 26 June 2026

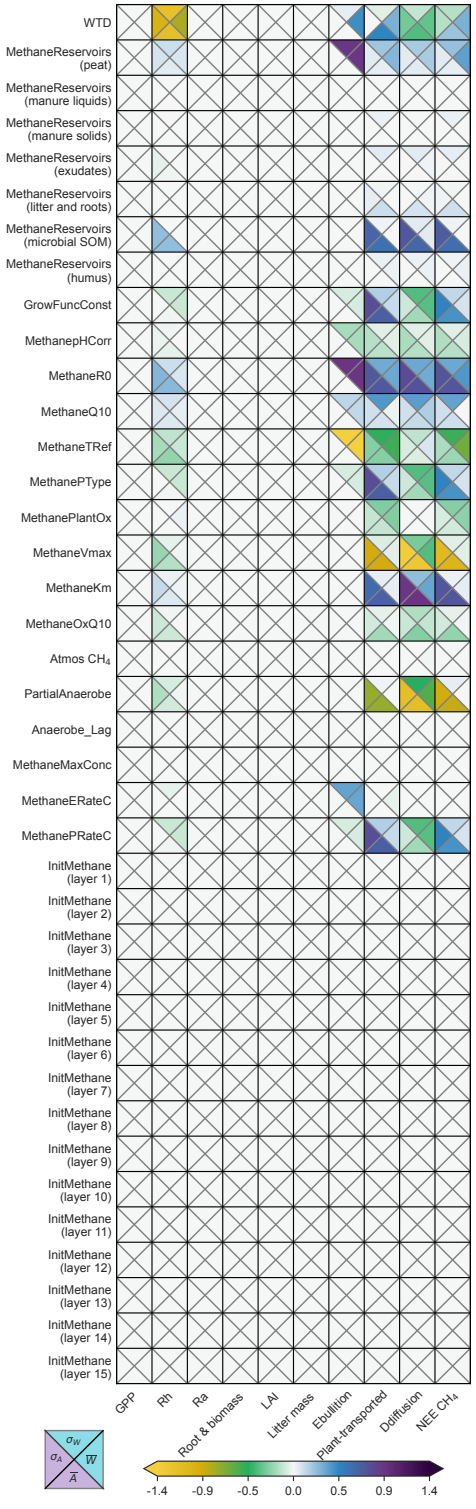

Figure C5. The sensitivity of all parameters within the CH_4 module to environmental and parameter inputs.

https://doi.org/10.5194/egusphere-2026-2450
Preprint. Discussion started: 26 June 2026

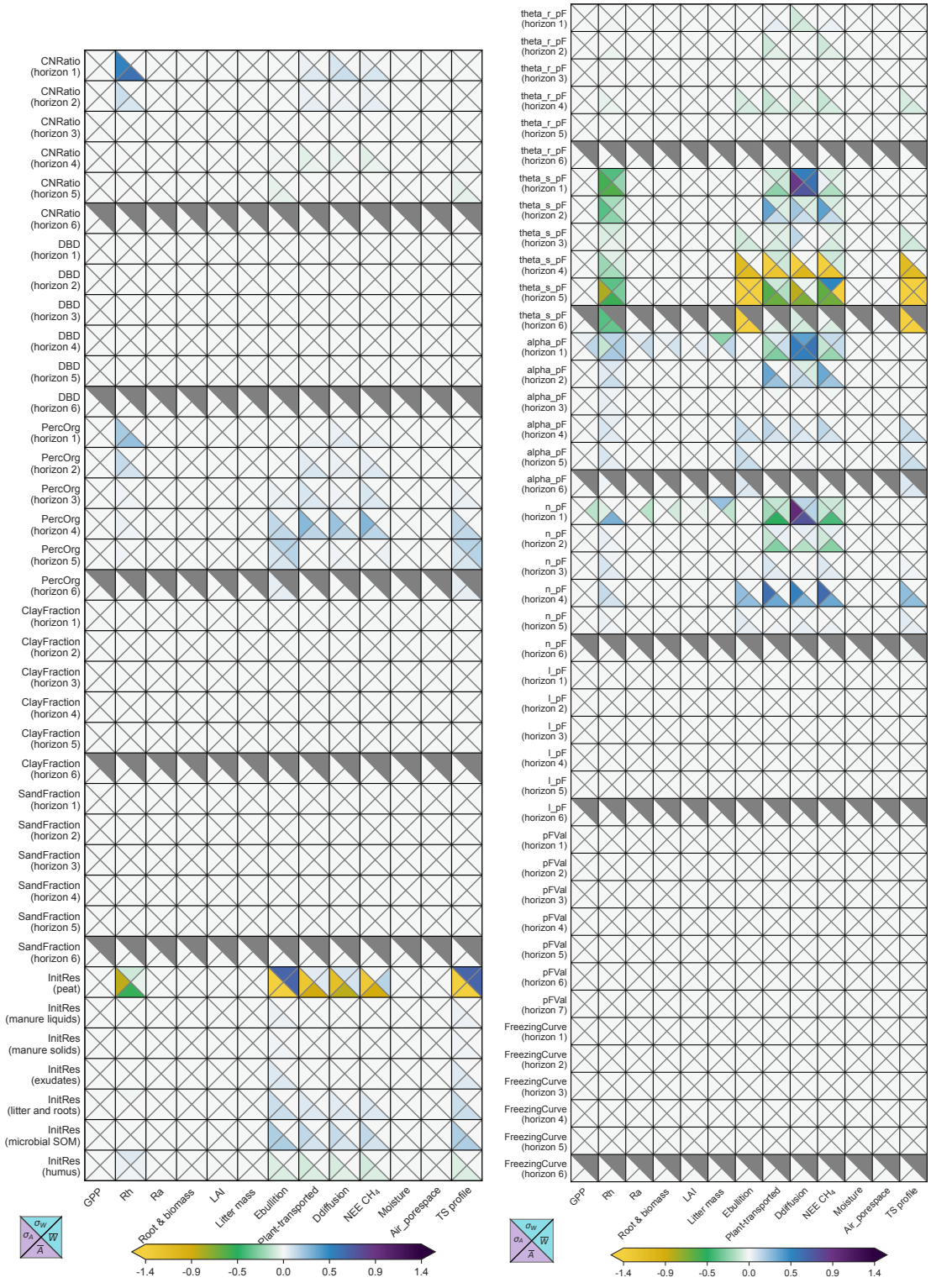

Figure C6. The sensitivity of the model to changing soil profile inputs. Grey indicates there was no input value for that soil horizon.

https://doi.org/10.5194/egusphere-2026-2450
Preprint. Discussion started: 26 June 2026

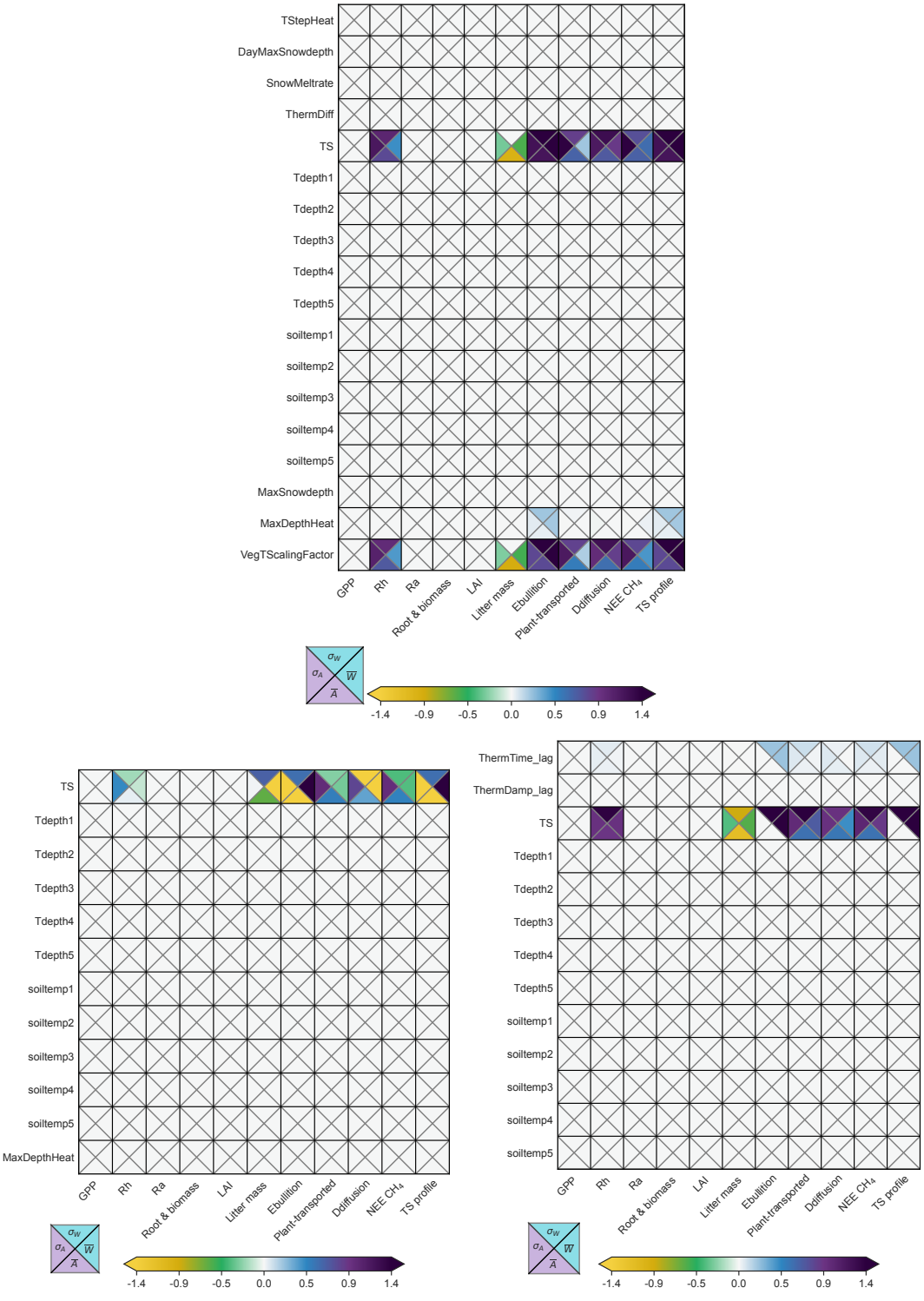

Figure C7. The sensitivity of the classic heat transport module (above), seasonal sinusoidal (bottom left) and the analytical thermal diffusion module (bottom right).

https://doi.org/10.5194/egusphere-2026-2450
Preprint. Discussion started: 26 June 2026

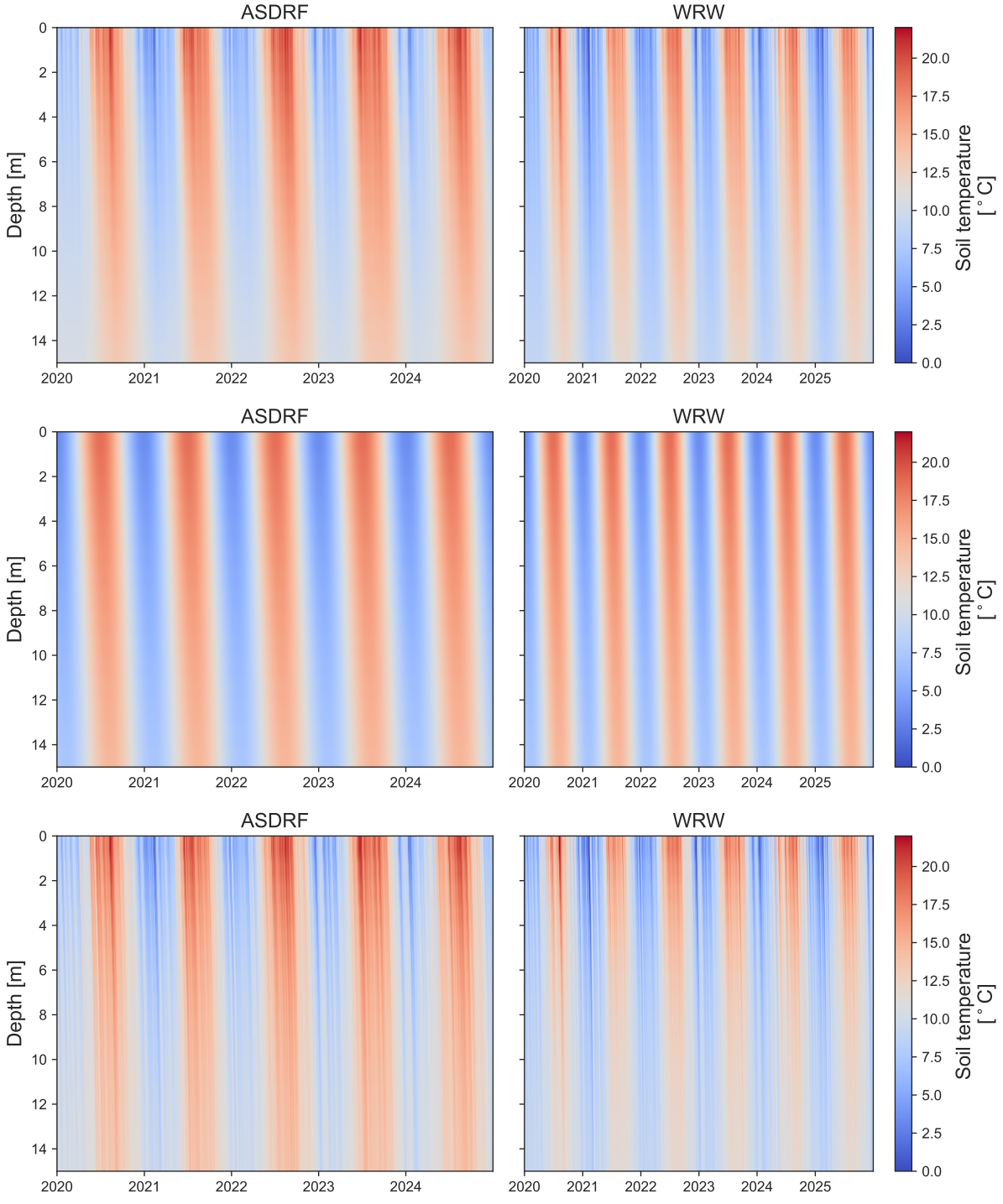

Figure C8. The soil temperature profile estimated using the classical heat transport scheme (above), the seasonal sinusoidal (middle), and the analytical diffusion scheme (below).

https://doi.org/10.5194/egusphere-2026-2450
Preprint. Discussion started: 26 June 2026

References

Apers, S., De Lannoy, G. J., Baird, A. J., Cobb, A. R., Dargie, G. C., del Aguila Pasquel, J., Gruber, A., Hastie, A., Hidayat, H., Hirano, T., Hoyt, A. M., Jovani-Sancho, A. J., Katimon, A., Kurnain, A., Koster, R. D., Lampela, M., Mahanama, S. P., Melling, L., Page, S. E., Reichle, R. H., Taufik, M., Vanderborght, J., and Bechtold, M.: Tropical Peatland Hydrology Simulated With a Global Land Surface Model, Journal of Advances in Modeling Earth Systems, 14, 1–39, https://doi.org/10.1029/2021MS002784, 2022.

Bahram, M., Espenberg, M., Pärn, J., Lehtovirta-Morley, L., Anslan, S., Kasak, K., Kõljalg, U., Liira, J., Maddison, M., Moora, M., Niinemets, Ü., Öpik, M., Pärtel, M., Soosaar, K., Zobel, M., Hildebrand, F., Tedersoo, L., and Mander, Ü.: Structure and function of the soil microbiome underlying N2O emissions from global wetlands, Nature Communications, 13, 1–10, https://doi.org/10.1038/s41467-022-29161-3, 2022.

Bansal, S., Johnson, O. F., Meier, J., and Zhu, X.: Vegetation Affects Timing and Location of Wetland Methane Emissions, Journal of Geophysical Research: Biogeosciences, 125, https://doi.org/10.1029/2020JG005777, 2020.

Basile-Doelsch, I., Balesdent, J., and Pellerin, S.: Reviews and syntheses: The mechanisms underlying carbon storage in soil, Biogeosciences, 17, 5223–5242, https://doi.org/10.5194/bg-17-5223-2020, 2020.

Bond-Lamberty, B. and Thomson, A.: A global database of soil respiration data, Biogeosciences, 7, 1915–1926, https://doi.org/10.5194/bg-7-1915-2010, 2010.

Boonman, J., Hefting, M. M., Van Huissteden, C. J., Van Den Berg, M., Van Huissteden, J., Erkens, G., Melman, R., and Van Der Velde, Y.: Cutting peatland CO2 emissions with water management practices, Biogeosciences, 19, 5707–5727, https://doi.org/10.5194/bg-19-5707-2022, 2022.

Boonman, J., Harpenslager, S. F., van Dijk, G., Smolders, A. J., Hefting, M. M., van de Riet, B., and van der Velde, Y.: Redox potential is a robust indicator for decomposition processes in drained agricultural peat soils: A valuable tool in monitoring peatland wetting efforts, Geoderma, 441, 116 728, https://doi.org/10.1016/j.geoderma.2023.116728, 2024.

Budishchev, A., Mi, Y., van Huissteden, J., Belelli-Marchesini, L., Schaepman-Strub, G., Parmentier, F. J. W., Fratini, G., Gallagher, A., Maximov, T. C., and Dolman, A. J.: Evaluation of a plot-scale methane emission model using eddy covariance observations and footprint modelling, Biogeosciences, 11, 4651–4664, https://doi.org/10.5194/bg-11-4651-2014, 2014.

Buzacott, A. J., Kruijt, B., Bataille, L., van Giersbergen, Q., Heuts, T. S., Fritz, C., Nouta, R., Erkens, G., Boonman, J., van den Berg, M., van Huissteden, J., and van der Velde, Y.: Drivers and Annual Totals of Methane Emissions From Dutch Peatlands, Global Change Biology, 30, https://doi.org/10.1111/gcb.17590, 2024.

Campioli, M., Vicca, S., Luyssaert, S., Bilcke, J., Ceschia, E., Chapin, F. S., Ciais, P., Fernández-Martínez, M., Malhi, Y., Obersteiner, M., Olefeldt, D., Papale, D., Piao, S. L., Peñuelas, J., Sullivan, P. F., Wang, X., Zenone, T., and Janssens, I. A.: Biomass production efficiency controlled by management in temperate and boreal ecosystems, Nature Geoscience, 8, 843–846, https://doi.org/10.1038/ngeo2553, 2015.

Chang, K. Y., Riley, W. J., Knox, S. H., Jackson, R. B., McNicol, G., Poulter, B., Aurela, M., Baldocchi, D., Bansal, S., Bohrer, G., Campbell, D. I., Cescatti, A., Chu, H., Delwiche, K. B., Desai, A. R., Euskirchen, E., Friborg, T., Goeckede, M., Helbig, M., Hemes, K. S., Hirano, T., Iwata, H., Kang, M., Keenan, T., Krauss, K. W., Lohila, A., Mammarella, I., Mitra, B., Miyata, A., Nilsson, M. B., Noormets, A., Oechel, W. C., Papale, D., Peichl, M., Reba, M. L., Rinne, J., Runkle, B. R., Ryu, Y., Sachs, T., Schäfer, K. V., Schmid, H. P., Shurpali, N., Sonnentag, O., Tang, A. C., Torn, M. S., Trotta, C., Tuittila, E. S., Ueyama, M., Vargas, R., Vesala, T., Windham-Myers, L., Zhang, Z., and Zona, D.: Substantial hysteresis in emergent temperature sensitivity of global wetland CH4 emissions, Nature Communications, 12, https://doi.org/10.1038/s41467-021-22452-1, 2021.

https://doi.org/10.5194/egusphere-2026-2450
Preprint. Discussion started: 26 June 2026

Chen, H., Qualls, R. G., and Blank, R. R.: Effect of soil flooding on photosynthesis, carbohydrate partitioning and nutrient uptake in the invasive exotic Lepidium latifolium, Aquatic Botany, 82, 250–268, https://doi.org/10.1016/j.aquabot.2005.02.013, 2005.

Clerc, M.: From theory to practice in particle swarm optimization, in: Handbook of swarm intelligence: Concepts, Principles and Applications, pp. 3–36, Springer, 2011.

Clymo, R. S., Turunen, J., and Tolonen, K.: Carbon Accumulation in Peatland, Oikos, 81, 368, https://doi.org/10.2307/3547057, 1998.

Conrad, R.: Importance of hydrogenotrophic, aceticlastic and methylotrophic methanogenesis for methane production in terrestrial, aquatic and other anoxic environments: A mini review, Pedosphere, 30, 25–39, https://doi.org/10.1016/S1002-0160(18)60052-9, 2020.

Davidson, E. A. and Janssens, I. A.: Temperature sensitivity of soil carbon decomposition and feedbacks to climate change, Nature, 440, 165–173, https://doi.org/10.1038/nature04514, 2006.

Dehaen, E. M., Burke, E. J., Chadburn, S. E., Kaduk, J., Sitch, S., Smith, N. D., and Gallego-Sala, A. V.: Drivers of soil heterotrophic respiration in tropical peatlands: a review to inform peat carbon accumulation modelling, Frontiers in Geochemistry, 3, https://doi.org/10.3389/fgeoc.2025.1492386, 2025.

Estop-Aragonés, C., Knorr, K. H., and Blodau, C.: Belowground in situ redox dynamics and methanogenesis recovery in a degraded fen during dry-wet cycles and flooding, Biogeosciences, 10, 421–436, https://doi.org/10.5194/bg-10-421-2013, 2013.

Evans, C. D., Peacock, M., Baird, A. J., Artz, R. R., Burden, A., Callaghan, N., Chapman, P. J., Cooper, H. M., Coyle, M., Craig, E., Cumming, A., Dixon, S., Gauci, V., Grayson, R. P., Helfter, C., Heppell, C. M., Holden, J., Jones, D. L., Kaduk, J., Levy, P., Matthews, R., McNamara, N. P., Misselbrook, T., Oakley, S., Page, S. E., Rayment, M., Ridley, L. M., Stanley, K. M., Williamson, J. L., Worrall, F., and Morrison, R.: Overriding water table control on managed peatland greenhouse gas emissions, Nature, 593, 548–552, https://doi.org/10.1038/s41586-021-03523-1, 2021.

Faber, A. H., Kooijman, A. M., Brinkkemper, O., van der Plicht, J., and van Geel, B.: Palaeoecological reconstructions of vegetation successions in two contrasting former turbaries in the Netherlands and implications for conservation, Review of Palaeobotany and Palynology, 233, 77–92, https://doi.org/10.1016/j.revpalbo.2016.07.007, 2016.

Fisher, R. A. and Koven, C. D.: Perspectives on the Future of Land Surface Models and the Challenges of Representing Complex Terrestrial Systems, Journal of Advances in Modeling Earth Systems, 12, https://doi.org/10.1029/2018MS001453, 2020.

Gao, Y., Burke, E. J., Chadburn, S. E., Raivonen, M., Markkanen, T., Aurela, M., Flanagan, L. B., Fortuniak, K., Humphreys, E., Lohila, A., Li, T., Mammarella, I., Nevalainen, O., Nilsson, M. B., Pawlak, W., Tsuruta, A., Yang, H., and Aalto, T.: Assessing modelled methane emissions over northern wetlands by the JULES-HIMMELI model, Science of the Total Environment, 980, https://doi.org/10.1016/j.scitotenv.2025.179526, 2025.

Gremmen, T., van de Riet, B., van den Berg, M., Vroom, R., Weideveld, S., van Huissteden, K., Westendorp, P., and Smolders, F.: Natte teelten en veeteelt bij een verhoogd (grond)waterpeil in de veenweiden: de effecten van vernattingsmaatregelen op biogeochemie & broeikasgasemissies, Tech. rep., Vereniging Agrarisch Natuur- en Landschapsbeheer Water, Land & Dijken & Stichting Landschap Noord-Holland, Noord-Holland, 2022.

Haxeltine, A. and Prentice, C. I.: BIOME3: An equilibrium terrestrial biosphere model based on ecophysiological constraints, resource availability, and competition among plant functional types, Global Biogeochemical Cycles, 10, 693–709, https://doi.org/10.1029/96GB02344, 1996.

Heijmans, M. M., Mauquoy, D., Van Geel, B., and Berendse, F.: Long-term effects of climate change on vegetation and carbon dynamics in peat bogs, Journal of Vegetation Science, 19, 307–320, https://doi.org/10.3170/2008-8-18368, 2008.

https://doi.org/10.5194/egusphere-2026-2450
Preprint. Discussion started: 26 June 2026

Helbig, M., Waddington, J. M., Alekseychik, P., Amiro, B. D., Aurela, M., Barr, A. G., Black, T. A., Blanken, P. D., Carey, S. K., Chen, J., Chi, J., Desai, A. R., Dunn, A., Euskirchen, E. S., Flanagan, L. B., Forbrich, I., Friborg, T., Grelle, A., Harder, S., Heliasz, M., Humphreys, E. R., Ikawa, H., Isabelle, P. E., Iwata, H., Jassal, R., Korkiakoski, M., Kurbatova, J., Kutzbach, L., Lindroth, A., Löfvenius, M. O., Lohila, A., Mammarella, I., Marsh, P., Maximov, T., Melton, J. R., Moore, P. A., Nadeau, D. F., Nicholls, E. M., Nilsson, M. B., Ohta, T., Peichl, M., Petrone, R. M., Petrov, R., Prokushkin, A., Quinton, W. L., Reed, D. E., Roulet, N. T., Runkle, B. R., Sonnentag, O., Strachan, I. B., Taillardat, P., Tuittila, E. S., Tuovinen, J. P., Turner, J., Ueyama, M., Varlagin, A., Wilmking, M., Wofsy, S. C., and Zyrianov, V.: Increasing contribution of peatlands to boreal evapotranspiration in a warming climate, Nature Climate Change, 10, 555–560, https://doi.org/10.1038/s41558-020-0763-7, 2020.

Hemes, K. S., Chamberlain, S. D., Eichelmann, E., Knox, S. H., and Baldocchi, D. D.: A Biogeochemical Compromise: The High Methane Cost of Sequestering Carbon in Restored Wetlands, Geophysical Research Letters, 45, 6081–6091, https://doi.org/10.1029/2018GL077747, 2018.

Hendriks, D. M., van Huissteden, J., Dolman, A. J., and van Der Molen, M. K.: The full greenhouse gas balance of an abandoned peat meadow, Biogeosciences, 4, 411–424, https://doi.org/10.5194/bg-4-411-2007, 2007.

Hu, H., Chen, J., Zhou, F., Nie, M., Hou, D., Liu, H., Delgado-Baquerizo, M., Ni, H., Huang, W., Zhou, J., Song, X., Cao, X., Sun, B., Zhang, J., Crowther, T. W., and Liang, Y.: Relative increases in CH4 and CO2 emissions from wetlands under global warming dependent on soil carbon substrates, Nature Geoscience, 17, 26–31, https://doi.org/10.1038/s41561-023-01345-6, 2024.

Hu, J., VanZomeren, C. M., Inglett, K. S., Wright, A. L., Clark, M. W., and Reddy, K. R.: Greenhouse Gas Emissions Under Different Drainage and Flooding Regimes of Cultivated Peatlands, Journal of Geophysical Research: Biogeosciences, 122, 3047–3062, https://doi.org/10.1002/2017JG004010, 2017.

Huntzinger, D. N., Schaefer, K., Schwalm, C., Fisher, J. B., Hayes, D., Stofferahn, E., Carey, J., Michalak, A. M., Wei, Y., Jain, A. K., Kolus, H., Mao, J., Poulter, B., Shi, X., Tang, J., and Tian, H.: Evaluation of simulated soil carbon dynamics in Arctic-Boreal ecosystems, Environmental Research Letters, 15, https://doi.org/10.1088/1748-9326/ab6784, 2020.

Höglind, M., Oijen, M. V., Cameron, D., and Persson, T.: Process-based simulation of growth and overwintering of grassland using the BASGRA model, Ecological Modelling, 335, 1–15, https://doi.org/10.1016/j.ecolmodel.2016.04.024, 2016.

Ise, T., Dunn, A. L., Wofsy, S. C., and Moorcroft, P. R.: High sensitivity of peat decomposition to climate change through water-table feedback, Nature Geoscience, 1, 763–766, https://doi.org/10.1038/ngeo331, 2008.

Iversen, C. M., Sloan, V. L., Sullivan, P. F., Euskirchen, E. S., Mcguire, A. D., Norby, R. J., Walker, A. P., Warren, J. M., and Wullschleger, S. D.: The unseen iceberg: Plant roots in arctic tundra, New Phytologist, 205, 34–58, https://doi.org/10.1111/nph.13003, 2015.

Kala, J., Decker, M., Exbrayat, J. F., Pitman, A. J., Carouge, C., Evans, J. P., Abramowitz, G., and Mocko, D.: Influence of leaf area index prescriptions on simulations of heat, moisture, and carbon fluxes, Journal of Hydrometeorology, 15, 489–503, https://doi.org/10.1175/JHM-D-13-063.1, 2014.

Kirschbaum, M. U. F.: The temperature dependence of organic-matter decomposition - Still a topic of debate, Soil Biology and Biochemistry, 38, 2510–2518, https://doi.org/10.1016/j.soilbio.2006.01.030, 2006.

Knox, S. H., Sturtevant, C., Matthes, J. H., Koteen, L., Verfaillie, J., and Baldocchi, D.: Agricultural peatland restoration: Effects of land-use change on greenhouse gas (CO2 and CH4) fluxes in the Sacramento-San Joaquin Delta, Global Change Biology, 21, 750–765, https://doi.org/10.1111/gcb.12745, 2015.

Knox, S. H., Bansal, S., McNicol, G., Schafer, K., Sturtevant, C., Ueyama, M., Valach, A. C., Baldocchi, D., Delwiche, K., Desai, A. R., Euskirchen, E., Liu, J., Lohila, A., Malhotra, A., Melling, L., Riley, W., Runkle, B. R., Turner, J., Vargas, R., Zhu, Q., Alto, T., Fluet-

https://doi.org/10.5194/egusphere-2026-2450
Preprint. Discussion started: 26 June 2026

Chouinard, E., Goeckede, M., Melton, J. R., Sonnentag, O., Vesala, T., Ward, E., Zhang, Z., Feron, S., Ouyang, Z., Alekseychik, P., Aurela, M., Bohrer, G., Campbell, D. I., Chen, J., Chu, H., Dalmagro, H. J., Goodrich, J. P., Gottschalk, P., Hirano, T., Iwata, H., Jurasinski, G., Kang, M., Koebsch, F., Mammarella, I., Nilsson, M. B., Ono, K., Peichl, M., Peltola, O., Ryu, Y., Sachs, T., Sakabe, A., Sparks, J. P., Tuittila, E. S., Vourlitis, G. L., Wong, G. X., Windham-Myers, L., Poulter, B., and Jackson, R. B.: Identifying dominant environmental predictors of freshwater wetland methane fluxes across diurnal to seasonal time scales, Global Change Biology, 27, 3582–3604, https://doi.org/10.1111/gcb.15661, 2021.

Köster, E., Chapman, J. P., Barel, J. M., Korrensalo, A., Laine, A. M., Vasander, H. T., and Tuittila, E. S.: Water level drawdown makes boreal peatland vegetation more responsive to weather conditions, Global Change Biology, 29, 5691–5705, https://doi.org/10.1111/gcb.16907, 2023.

Leifeld, J., Klein, K., and Wüst-Galley, C.: Soil organic matter stoichiometry as indicator for peatland degradation, Scientific Reports, 10, 1–9, https://doi.org/10.1038/s41598-020-64275-y, 2020.

Li, T., Raivonen, M., Alekseychik, P., Aurela, M., Lohila, A., Zheng, X., Zhang, Q., Wang, G., Mammarella, I., Rinne, J., Yu, L., Xie, B., Vesala, T., and Zhang, W.: Importance of vegetation classes in modeling CH4 emissions from boreal and subarctic wetlands in Finland, Science of the Total Environment, 572, 1111–1122, https://doi.org/10.1016/j.scitotenv.2016.08.020, 2016.

Lindenberger, A., Rauch, H. P., Kasak, K., Stelzhammer, M., and von der Thannen, M.: Impact of various flood conditions on the CO2 ecosystem exchange as a component of floodplain grassland restoration, Ecological Engineering, 212, 107 489, https://doi.org/10.1016/j.ecoleng.2024.107489, 2025.

Lippmann, T. J., van Der Velde, Y., Heijmans, M. M., Dolman, H., Hendriks, D. M., and van Huissteden, K.: Peatland-VU-NUCOM (PVN 1.0): Using dynamic plant functional types to model peatland vegetation, CH4, and CO2 emissions, Geoscientific Model Development, 16, 6773–6804, https://doi.org/10.5194/gmd-16-6773-2023, 2023.

Lippmann, T. J., van der Velde, Y., Naudts, K., Hensgens, G., Vonk, J. E., and Dolman, H.: Simultaneous Hot and Dry Extreme-Events Increase Wetland Methane Emissions: An Assessment of Compound Extreme-Event Impacts Using Ameriflux and FLUXNET-CH4 Site Data Sets, Global Biogeochemical Cycles, 38, 1–20, https://doi.org/10.1029/2024GB008201, 2024.

Lippmann, T. J., van den Berg, M., and Huissteden, K. V.: Peatland-VU v3.0, https://doi.org/doi.org/10.5281/zenodo.19816805, 2026.

Loisel, J., Gallego-Sala, A. V., Amesbury, M. J., Magnan, G., Anshari, G., Beilman, D. W., Benavides, J. C., Blewett, J., Camill, P., Charman, D. J., Chawchai, S., Hedgpeth, A., Kleinen, T., Korhola, A., Large, D., Mansilla, C. A., Müller, J., van Bellen, S., West, J. B., Yu, Z., Bubier, J. L., Garneau, M., Moore, T., Sannel, A. B., Page, S., Väliranta, M., Bechtold, M., Brovkin, V., Cole, L. E., Chanton, J. P., Christensen, T. R., Davies, M. A., De Vleeschouwer, F., Finkelstein, S. A., Frolking, S., Gałka, M., Gandois, L., Girkin, N., Harris, L. I., Heinemeyer, A., Hoyt, A. M., Jones, M. C., Joos, F., Juutinen, S., Kaiser, K., Lacourse, T., Lamentowicz, M., Larmola, T., Leifeld, J., Lohila, A., Milner, A. M., Minkkinen, K., Moss, P., Naafs, B. D., Nichols, J., O'Donnell, J., Payne, R., Philben, M., Piilo, S., Quillet, A., Ratnayake, A. S., Roland, T. P., Sjögersten, S., Sonnentag, O., Swindles, G. T., Swinnen, W., Talbot, J., Treat, C., Valach, A. C., and Wu, J.: Expert assessment of future vulnerability of the global peatland carbon sink, Nature Climate Change, 11, 70–77, https://doi.org/10.1038/s41558-020-00944-0, 2021.

Määttä, T. and Malhotra, A.: The hidden roots of wetland methane emissions, Global Change Biology, 30, 1–23, https://doi.org/10.1111/gcb.17127, 2024.

Medlyn, B. E., Duursma, R. A., and Zeppel, M. J.: Forest productivity under climate change: A checklist for evaluating model studies, Wiley Interdisciplinary Reviews: Climate Change, 2, 332–355, https://doi.org/10.1002/wcc.108, 2011.

https://doi.org/10.5194/egusphere-2026-2450
Preprint. Discussion started: 26 June 2026

Metcalfe, D. B., Fisher, R. A., and Wardle, D. A.: Plant communities as drivers of soil respiration: Pathways, mechanisms, and significance for global change, Biogeosciences, 8, 2047–2061, https://doi.org/10.5194/bg-8-2047-2011, 2011.

Metzger, C., Nilsson, M. B., Peichl, M., and Jansson, P. E.: Parameter interactions and sensitivity analysis for modelling carbon heat and water fluxes in a natural peatland, using CoupModel v5, Geoscientific Model Development, 9, 4313–4338, https://doi.org/10.5194/gmd-9-4313-2016, 2016.

Mi, Y., van Huissteden, J., Parmentier, F. J., Gallagher, A., Budishchev, A., Berridge, C. T., and Dolman, A. J.: Improving a plot-scale methane emission model and its performance at a northeastern Siberian tundra site, Biogeosciences, 11, 3985–3999, https://doi.org/10.5194/bg-11-3985-2014, 2014.

Moore, T. R., Large, D., Talbot, J., Wang, M., and Riley, J. L.: The Stoichiometry of Carbon, Hydrogen, and Oxygen in Peat, Journal of Geophysical Research: Biogeosciences, 123, 3101–3110, https://doi.org/10.1029/2018JG004574, 2018.

Müller, J. and Joos, F.: Committed and projected future changes in global peatlands-continued transient model simulations since the Last Glacial Maximum, Biogeosciences, 18, 3657–3687, https://doi.org/10.5194/bg-18-3657-2021, 2021.

Nungesser, M. K.: Modelling microtopography in boreal peatlands: Hummocks and hollows, Ecological Modelling, 165, 175–207, https://doi.org/10.1016/S0304-3800(03)00067-X, 2003.

Pan, Y., Birdsey, R. A., Fang, J., Houghton, R., Kauppi, P. E., Kurz, W. A., Phillips, O. L., Shvidenko, A., Lewis, S. L., Canadell, J. G., Ciais, P., Jackson, R. B., Pacala, S. W., McGuire, A. D., Piao, S., Rautiainen, A., Sitch, S., and Hayes, D.: A large and persistent carbon sink in the world's forests, Science, 333, 988–993, https://doi.org/10.1126/science.1201609, 2011.

Pärn, J., Thayamkottu, S., Öpik, M., Bahram, M., Tedersoo, L., Espenberg, M., Davison, J. A., Kasak, K., Maddison, M., Niinemets, Ü., Ostonen, I., Soosaar, K., Sohar, K., Zobel, M., and Mander, Ü.: Soil moisture and microbiome explain greenhouse gas exchange in global peatlands, Scientific Reports, 15, 1–9, https://doi.org/10.1038/s41598-025-92891-z, 2025.

Peaucelle, M., Ciais, P., Maignan, F., Nicolas, M., Cecchini, S., and Viovy, N.: Representing explicit budburst and senescence processes for evergreen conifers in global models, Agricultural and Forest Meteorology, 266-267, 97–108, https://doi.org/10.1016/j.agrformet.2018.12.008, 2019.

Petrescu, A. M., van Huissteden, J., Jackowicz-Korczynski, M., Yurova, A., Christensen, T. R., Crill, P. M., Bäckstrand, K., and Maximov, T. C.: Modelling CH4 emissions from arctic wetlands: Effects of hydrological parameterization, Biogeosciences, 5, 111–121, https://doi.org/10.5194/bg-5-111-2008, 2008.

Petrescu, A. M., van Beek, L. P., van Huissteden, J., Prigent, C., Sachs, T., Corradi, C. A., Parmentier, F. J., and Dolman, A. J.: Modeling regional to global CH4 emissions of boreal and arctic wetlands, Global Biogeochemical Cycles, 24, 1–12, https://doi.org/10.1029/2009GB003610, 2010.

Piao, S., Liu, Q., Chen, A., Janssens, I. A., Fu, Y., Dai, J., Liu, L., Lian, X., Shen, M., and Zhu, X.: Plant phenology and global climate change: Current progresses and challenges, Global Change Biology, 25, 1922–1940, https://doi.org/10.1111/gcb.14619, 2019.

Qin, S., Chen, L., Fang, K., Zhang, Q., Wang, J., Liu, F., Yu, J., and Yang, Y.: Temperature sensitivity of SOM decomposition governed by aggregate protection and microbial communities, Tech. Rep. 7, ISSN 23752548, https://doi.org/10.1126/sciadv.aau1218, 2019.

Qiu, C., Ciais, P., Zhu, D., Guenet, B., Peng, S., Petrescu, A. M. R., Lauerwald, R., Makowski, D., Gallego-Sala, A. V., Charman, D. J., and Brewer, S. C.: Large historical carbon emissions from cultivated northern peatlands, Science Advances, 7, 1–11, https://doi.org/10.1126/sciadv.abf1332, 2021.

Raivonen, M., Mäkiranta, P., Lohila, A., Juutinen, S., Vesala, T., and Tuittila, E. S.: A simple CO2 exchange model simulates the seasonal leaf area development of peatland sedges, Ecological Modelling, 314, 32–43, https://doi.org/10.1016/j.ecolmodel.2015.07.008, 2015.

https://doi.org/10.5194/egusphere-2026-2450
Preprint. Discussion started: 26 June 2026

Randerson, J. T., Hoffman, F. M., Thornton, P. E., Mahowald, N. M., Lindsay, K., Lee, Y. H., Nevison, C. D., Doney, S. C., Bonan, G., Stöckli, R., Covey, C., Running, S. W., and Fung, I. Y.: Systematic assessment of terrestrial biogeochemistry in coupled climate-carbon models, Global Change Biology, 15, 2462–2484, https://doi.org/10.1111/j.1365-2486.2009.01912.x, 2009.

Reinsch, S., Lebron, I., de Jonge, L. W., Weber, P. L., Norgaard, T., Arthur, E., Gomes, L., Pesch, C., Konstantinos, K., Zalidis, G., Epelde, L., Romic, M., Romic, D., Zovko, M., Reljic, M., Heikkinen, J., Feeney, C., Bentley, L., Levy, P., Vanguelova, E., Panagos, P., Schneider, F., Ahrens, B., Leifeld, J., Hugelius, G., Emmett, B. A., Cosby, B. J., Brentegani, M., Tandy, S., Thomas, A., van Soest, M. A., and Robinson, D. A.: The Fraction of Carbon in Soil Organic Matter as a National-Scale Soil Process Indicator, Global Change Biology, 31, https://doi.org/10.1111/gcb.70572, 2025.

Ritson, J. P., Alderson, D. M., Robinson, C. H., Burkitt, A. E., Heinemeyer, A., Stimson, A. G., Gallego-Sala, A., Harris, A., Quillet, A., Malik, A. A., Cole, B., Robroek, B. J., Heppell, C. M., Rivett, D. W., Chandler, D. M., Elliott, D. R., Shuttleworth, E. L., Lilleskov, E., Cox, F., Clay, G. D., Diack, I., Rowson, J., Pratscher, J., Lloyd, J. R., Walker, J. S., Belyea, L. R., Dumont, M. G., Longden, M., Bell, N. G., Artz, R. R., Bardgett, R. D., Griffiths, R. I., Andersen, R., Chadburn, S. E., Hutchinson, S. M., Page, S. E., Thom, T., Burn, W., and Evans, M. G.: Towards a microbial process-based understanding of the resilience of peatland ecosystem service provisioning – A research agenda, Science of the Total Environment, 759, https://doi.org/10.1016/j.scitotenv.2020.143467, 2021.

Robertson, G. P., Paul, E. A., and Harwood, R. R.: Greenhouse gases in intensive agriculture: Contributions of individual gases to the radiative forcing of the atmosphere, Science, 289, 1922–1925, https://doi.org/10.1126/science.289.5486.1922, 2000.

Rogers, A., Medlyn, B. E., Dukes, J. S., Bonan, G., von Caemmerer, S., Dietze, M. C., Kattge, J., Leakey, A. D., Mercado, L. M., Niinemets, Ü., Prentice, I. C., Serbin, S. P., Sitch, S., Way, D. A., and Zaehle, S.: A roadmap for improving the representation of photosynthesis in Earth system models, https://doi.org/10.1111/nph.14283, 2017.

Ruehr, S., Keenan, T. F., Williams, C., Zhou, Y., Lu, X., Bastos, A., Canadell, J. G., Prentice, I. C., Sitch, S., and Terrer, C.: Evidence and attribution of the enhanced land carbon sink, Nature Reviews Earth and Environment, 4, 518–534, https://doi.org/10.1038/s43017-023-00456-3, 2023.

Schapendonk, A. H. C. M., Stol, W., Kraalingen, D. W. G. V., and Bouman, B. A. M.: LINGRA, a sink/source model to simulate grassland productivity in Europe, Tech. rep., 1998.

Schipper, L. A., Hobbs, J. K., Rutledge, S., and Arcus, V. L.: Thermodynamic theory explains the temperature optima of soil microbial processes and high Q10 values at low temperatures, Global Change Biology, 20, 3578–3586, https://doi.org/10.1111/gcb.12596, 2014.

Shaver, G. R., Street, L. E., Rastetter, E. B., van Wijk, M. T., and Williams, M.: Functional convergence in regulation of net CO2 flux in heterogeneous tundra landscapes in Alaska and Sweden, Journal of Ecology, 95, 802–817, https://doi.org/10.1111/j.1365-2745.2007.01259.x, 2007.

Silva, M. P., Healy, M. G., and Gill, L.: Reviews and syntheses: A scoping review evaluating the potential application of ecohydrological models for northern peatland restoration, Biogeosciences, 21, 3143–3163, https://doi.org/10.5194/bg-21-3143-2024, 2024.

Sokol, N., Blazewicz, S., Hestrin, R., Marschmann, G., Brodie, E., Nicolas, A., Hungate, B., Stone, B., Koch, B., Foley, M., and Zablocki, O.: Life and death in the soil microbiome: how ecological processes influence biogeochemistry, Nature Reviews Microbiology, 20, 415–430, 2022.

Stocker, B. D., Dong, N., Perkowski, E. A., Schneider, P. D., Xu, H., de Boer, H. J., Rebel, K. T., Smith, N. G., Van Sundert, K., Wang, H., Jones, S. E., Prentice, I. C., and Harrison, S. P.: Empirical evidence and theoretical understanding of ecosystem carbon and nitrogen cycle interactions, New Phytologist, 245, 49–68, https://doi.org/10.1111/nph.20178, 2025.

https://doi.org/10.5194/egusphere-2026-2450
Preprint. Discussion started: 26 June 2026

Ström, L., Mastepanov, M., and Christensen, T. R.: Species-specific effects of vascular plants on carbon turnover and methane emissions from wetlands, Biogeochemistry, 75, 65–82, https://doi.org/10.1007/s10533-004-6124-1, 2005.

Tolunay, D., Kowalchuk, G. A., Erkens, G., and Hefting, M. M.: Aerobic and anaerobic decomposition rates in drained peatlands: Impact of botanical composition, Science of the Total Environment, 930, 172 639, https://doi.org/10.1016/j.scitotenv.2024.172639, 2024.

Ueyama, M., Knox, S. H., Delwiche, K. B., Bansal, S., Riley, W. J., Baldocchi, D., Hirano, T., McNicol, G., Schafer, K., Windham-Myers, L., Poulter, B., Jackson, R. B., Chang, K. Y., Chen, J., Chu, H., Desai, A. R., Gogo, S., Iwata, H., Kang, M., Mammarella, I., Peichl, M., Sonnentag, O., Tuittila, E. S., Ryu, Y., Euskirchen, E. S., Göckede, M., Jacotot, A., Nilsson, M. B., and Sachs, T.: Modeled production, oxidation, and transport processes of wetland methane emissions in temperate, boreal, and Arctic regions, Global Change Biology, 29, 2313–2334, https://doi.org/10.1111/gcb.16594, 2023.

van den Berg, M., Gremmen, T. M., Vroom, R. J., van Huissteden, J., Boonman, J., van Huissteden, C. J., van Der Velde, Y., Smolders, A. J., and van De Riet, B. P.: A case study on topsoil removal and rewetting for paludiculture: effect on biogeochemistry and greenhouse gas emissions from Typha latifolia, Typha angustifolia, and Azolla filiculoides, Biogeosciences, 21, 2669–2690, https://doi.org/10.5194/bg-21-2669-2024, 2024.

van den Berg, M., Jacobus, v. H., Lippmann, T. J., Boonman, J., van de Craats, D., Buzacott, A. J., Keuskamp, J. A., and van der Velde, Y.: Contrasting effect of peat loss and net ecosystem carbon loss to water table changes in drained peat grasslands, using the PEATLAND-VU model, Journal of Geophysical Research: Biogeosciences, Under revi, 2026.

van der Velde, Y., Temme, A. J., Nijp, J. J., Braakhekke, M. C., van Voorn, G. A., Dekker, S. C., Dolman, A. J., Wallinga, J., Devito, K. J., Kettridge, N., Mendoza, C. A., Kooistra, L., Soons, M. B., and Teuling, A. J.: Emerging forest–peatland bistability and resilience of European peatland carbon stores, Proceedings of the National Academy of Sciences of the United States of America, 118, https://doi.org/10.1073/pnas.2101742118, 2021.

van Huissteden, J., van den Bos, R., and Marticorena Alvarez, I.: Modelling the effect of water-table management on CO2 and CH4 fluxes from peat soils, Geologie en Mijnbouw/Netherlands Journal of Geosciences, 85, 3–18, https://doi.org/10.1017/S0016774600021399, 2006.

van Huissteden, J., R. Petrescu, A. M., D. Hendriks, D. M., and Rebel, K. T.: Sensitivity analysis of a wetland methane emission model based on temperate and arctic wetland sites, Biogeosciences, 6, 3035–3051, https://doi.org/10.5194/bg-6-3035-2009, 2009.

Villa, J. A., Ju, Y., Yazbeck, T., Waldo, S., Wrighton, K. C., and Bohrer, G.: Ebullition dominates methane fluxes from the water surface across different ecohydrological patches in a temperate freshwater marsh at the end of the growing season, Science of the Total Environment, 767, 144 498, https://doi.org/10.1016/j.scitotenv.2020.144498, 2021.

Walter, B. P. and Heimann, M.: A process-based, climate-sensitive model to derive methane emissions from natural wetlands: Application to five wetland sites, sensitivity to model parameters, and climate, Global Biogeochemical Cycles, 14, 745–765, https://doi.org/10.1029/1999GB001204, 2000.

Walter, B. P., Heimann, M., and Matthews, E.: Modeling modern methane emissions from natural wetlands 2. Interannual variations 1982-1993, Journal of Geophysical Research Atmospheres, 106, 34 207–34 219, https://doi.org/10.1029/2001JD900164, 2001.

Wang, Y., Calanca, P., and Leifeld, J.: Sources of nitrous oxide emissions from agriculturally managed peatlands, Global Change Biology, 30, 1–13, https://doi.org/10.1111/gcb.17144, 2024.

Xu, J., Morris, P. J., Liu, J., and Holden, J.: PEATMAP: Refining estimates of global peatland distribution based on a meta-analysis, Catena, 160, 134–140, https://doi.org/10.1016/j.catena.2017.09.010, 2018.

https://doi.org/10.5194/egusphere-2026-2450
Preprint. Discussion started: 26 June 2026

Yu, Z., Loisel, J., Brosseau, D. P., Beilman, D. W., and Hunt, S. J.: Global peatland dynamics since the Last Glacial Maximum, Geophysical Research Letters, 37, 1–5, https://doi.org/10.1029/2010GL043584, 2010.